2018

IMPLICATIONS OF MODULATING GLACIERS AND SNOW COVER IN MONGOLIA

Caleb Gikai Pan

IMPLICATIONS OF MODULATING GLACIERS AND SNOW COVER IN MONGOLIA

By

CALEB GIKAI PAN

M.S. Geography, University of Montana, Missoula, MT, 2013
B.S. Geography, Appalachian State University, Boone, NC, 2010

Dissertation

presented in partial fulfillment of the requirements
for the degree of

Doctor of Philosophy
in Systems Ecology

The University of Montana
Missoula, MT

December 2018

Approved by:

Scott Whittenburg, Dean of The Graduate School
Graduate School

Dr. John S. Kimball, Chair
Department of Ecosystem and Conservation Sciences

Dr. Brady Allred
Department Ecosystem and Conservation Sciences

Dr. Sarah J. Halvorson
Department of Geography

Dr. Peter B. Kirchner
Department of Ecosystem and Conservation Sciences

Dr. Hugh Robinson
Department of Ecosystem and Conservation Sciences

ABSTRACT

Pan, Caleb, G., Ph.D., December 2018 *Systems Ecology*

Implications of modulating glaciers and snow cover in Mongolia

Chairperson: Dr. John. S. Kimball

Mongolia's cryosphere (glaciers and snow cover) drives ecosystem services and in turn, supports emerging economies in the water-restricted country. However, as Mongolia experiences long-term drought conditions and an increase in annual air temperatures at twice the global rate, the potential adverse effects of the changing cryosphere during a period of climate uncertainty will have cascading implications to water availability and economic development. Using several data sources and methods, I partitioned my dissertation into two components to determine the hydrologic and economic implications of modulations in Mongolia's cryosphere. The first component is an examination of glacier recession in Mongolia's Altai Mountains, where I identified the major drivers of glacier recession and the role of glaciers in the regional hydrology. In the second component we created novel techniques to detect snowmelt events and to determine their role in large annual livestock mortality across Mongolia.

In chapter 2 we identified a rate of glacier recession of 6.4 ± 0.4 km^2 yr^{-1} from 1990-2016, resulting in an overall decrease in glacier area of 43%, which were comparable to rates of recession in mountain ranges across Central Asia. In chapter 3 we found that glaciers contributed up to 22% of the regional hydrology in the glaciated Upper Khovd River Basin (UKRB) and glacier melt contributions began to decrease after 2016, suggesting an overall depletion of accumulation zones. In chapter 4, we developed a novel approach to detect snow melt events in Alaska, USA – due to its high satellite coverage, climate monitoring network, and previous existing studies – and produced a gridded geospatial data product. In chapter 5, we expanded on the novel methods developed in chapter 4 to determine the spatio-temporal role of snowmelt events on large annual livestock mortality in Mongolia. Results showed strong correlations between snowmelt events and mortality in the southern Gobi during the fall and the central and western regions during the spring. As Mongolia continues to develop climatically vulnerable economic industries, future modulations in Mongolia's cryosphere will likely decrease regional water-availability and amplify annual livestock mortality.

ACKNOWLEDGEMENTS

I wish to thank Dr. John Kimball for advising this dissertation and contributing his wealth of experience and knowledge to my development as a scientist. I would also like to thank my committee members, Drs. Brady Allred, Sarah J. Halvorson, Peter B. Kirchner, and Hugh Robinson. Thank you all so much for your guidance and patience. As a sidenote – thanks to Peter for his time during countless and lengthy, yet productive, discussions over the phone. During my time as a PhD student I was fortunate to work with several talented individuals, many of whom contributed to this work including; Ulrich Kamp, Lucas Menzel, Munkhdavaa Munkhjargal, Nathaniel Robinson, Michael Walther, Avirmed Dashtseren, Jinyang Du, and Youngwook Kim.

I acknowledge support through many grants and fellowships including the Montana Space Grant Consortium, Fulbright, German Academic Exchange Program, National Park Service Southwest Alaska Network and the NASA Arctic Boreal Vulnerability Experiment (ABoVE) (NNX15AT74A).

Lastly, I am very lucky for the unconditional love and support from my family and friends during this wild adventure.

TABLE OF CONTENTS

Chapter 1

1.1 Introduction

Mongolia is a semi-arid, sparsely populated country in the heart of the Asian landmass and has an economy comprised of industries including livestock production, mining, and agriculture that are highly susceptible to slight fluctuations to both water resources and climate change. Recent work has shown significant changes in Mongolia's climate system, trending towards drier and warmer weather (Hessl *et al* 2018, Li *et al* 2015, Batima *et al* 2005). Additional research has identified that the rapid decrease in lake levels across the country over the past 40 years is largely attributed to water extractions from mining and other land use practices coupled with increased aridity (Tao *et al* 2015). Mongolia's economic vulnerabilities to climatic conditions are also manifested in the country's extensive livestock population, such that during periods of drought coupled with anomalous climate conditions, annual livestock die-offs can extend into the millions (Fernández-giménez *et al* 2016).

Fluctuations in Mongolia's glaciers and snow cover are understudied but can provide important contributions to our greater knowledge of recent climate change, current and future water availability and an understanding of potential adverse effects to national livestock populations.

Dynamic fluctuations in Earth's cryosphere are one of the best natural proxies to global climate change – ranging from daily changes in snow cover to slower changes over decades and centuries in glaciers that provide excellent indicators of climatic variability (Oerlemans 2005, Zemp *et al* 2015). Globally scaled, snow and ice cover at high latitudes enhance surface albedo to create poleward temperature gradients, helping to move heat and energy through atmospheric and oceanic circulations (Mcconnell 2005). However, recent observations of reduced snowcover and sea-ice extent along with increased temperatures interact to create a positive feedback - amplifying the rate of increase in surface air temperature over time by reducing surface insolation and increasing the amount of absorbed solar energy (Serreze and Francis 2006, Derksen and Brown 2012, Stroeve *et al* 2007).

In addition to being an important governor of the global energy budget, Earth's cryosphere fills a critical niche in global, regional, and local hydrologic cycles and water

resources (Zemp *et al* 2013). For large regional watersheds like the Ob, Lena, Indus, or Amu Darya, snowmelt is the dominant contributor to regional runoff (Alford et al. 2013, Oshima et al 2018). However, in closer proximity to the watershed headwaters, the dominant contributor to runoff transitions from snow to glaciers, particularly in semi-arid environments where summer precipitation is uncommon and sporadic (Viviroli *et al* 2007, Racoviteanu *et al* 2013). Regardless, snow and glacier melt runoff is critical for downstream populations ranging from large metropolitan centers to small mountain communities (Bolch *et al* 2012, Lutz *et al* 2012). But recently, amplified warming at higher elevations has made the timing and reliability of glacier and snow melt more unpredictable with changing melt durations (Kim *et al* 2012, Dietz *et al* 2014), rain-on-snow (ROS) events (Beniston and Stoffel 2016), and an overall reduction in glacier area (Zemp et al. 2015).

Snow cover processes, including melt events or ROS events, can also have adverse effects on ungulate populations (Loe *et al* 2016, Berger *et al* 2018). These events can occur after a brief period of warm weather increases the liquid water content (LWC) of the snowpack and accumulates between the snow and vegetation/surface interface where it freezes into a substantial layer of ice when temperatures return to below freezing. This layer of ice creates an effective barrier between the ungulate and their feed and can often result in large animal die-offs (Grenfell and Putkonen 2008). In Mongolia, these icing events are colloquially referred to as the *tumer dzud* or *iron winter disaster* which refers to large livestock die-offs that resulted from the development of thick ice lenses from snow melt (Allison 2017).

1.2 Scientific Goals, Questions and Objectives

The goal of this dissertation is to contribute to our greater knowledge of Mongolia's evolving cryosphere to determine how such changes will manifest and to inform socio-economic development across Mongolia. To address the above goal, this dissertation asks the following questions; 1) How are amplified temperatures affecting glacier extent across Mongolia and what roles do extrinsic and intrinsic factors contribute to glacier areal extent? 2) What is the role of glacier-melt runoff in the regional hydrology of western Mongolia? 3) How effective are remote sensing platforms at

detecting snowmelt or rain-on-snow (ROS) events across the mid to high-latitudes? 4) What is the role of anomalous snowmelt events influencing large livestock mortality across Mongolia?

The following dissertation objectives address the research questions. 1) To advance cryosphere research in the high and mid-latitudes and the potential socio-economic impacts of modulations to the regional cryosphere under environmental and land use change. 2) Provide non-governmental organizations (NGOs), government institutes, and international development groups (e.g. World Bank, Asian Development Bank) with: i) a grounded understanding of the future potential of glacier-melt runoff as a water resource as Mongolia transitions to water-intensive industries, and ii) a scientific understanding of the spatiotemporal variability in climatic contributors to livestock die-off events in Mongolia for a more effective determination in the distribution of aid relief during such events. 3) Provide the cryosphere community with two publicly available datasets i) a multi-temporal glacier inventory derived from satellite optical remote sensing and can be downloaded from the Global Land Ice Measurements from Space (GLIMS) Program (www.glims.org) and ii) a satellite based ROS record for Alaska archived at the Oak Ridge National Laboratory (ORNL) through the NASA Distributed Active Archive Center (DAAC).

1.3 Outline

This dissertation is partitioned into two components. In the first component, I address changes in the glaciers of the Altai Mountains of western Mongolia using satellite optical-infrared remote sensing. I then applied an ice ablation model to assess the contribution of glacier melt to regional hydrology. The second component of the dissertation examines modulations in snow melt events across Mongolia using satellite passive microwave remote sensing. Next, I determine the role of snow melt events in annual livestock mortality across Mongolia. These components comprise the following four chapters and are the result of multiple publications or subject to peer-review.

In Chapter 2 (Pan *et al* 2017), I assess the changes in glacier area and number in western Mongolia at multiple time intervals from 1990 to 2016 and regressed these changes to extrinsic and intrinsic conditions to determine the regional governors of

glacier recession. Using optical remote sensing from the recently launched Landsat 8 Operational Land Imager (OLI) and Sentinel 2-A MultiSpectral Instrument (MSI), I created a new satellite derived glacier inventory from Kamp and Pan, 2015; resulting in a coherent glacier record for 1990, 2000, 2010, and 2016. I then used the new glacier satellite record coupled with a digital elevation model to characterize the intrinsic properties of the glaciers including, the equilibrium line altitude (ELA), maximum, minimum, and range elevations, aspect, slope, and latitude. Extrinsic factors, including seasonal mean temperature and seasonal precipitation, were derived by creating a homogenized climate time series from six regional long-term climate stations. Correlation analysis showed that summer temperature had the highest correlation during periods of the greatest rates of glacier recession, particularly from 1990 to 2000 and 2010 to 2016. Aspect showed the greatest control on glacier recession relative to other intrinsic factors, but minimum elevation was also important. The rates of glacier recession in Mongolia compared well to other rates of glacier recession in continental climates which were all elevated when compared to rates of recession in maritime climates.

In Chapter 3 (Pan *et al.* submitted), I contextualize the importance of glaciers to the hydrologic regime in western Mongolia by first estimating the amount of glacier-melt runoff to the Upper Khovd River Basin (UKRB) from 1990 to 2016 using a simple ice ablation model coupled with glaciological and hydrographic data. Model outputs determined that glaciers contributed 12% to the local hydrological runoff during the summer months of 2016. To simulate conditions of below and above normal temperatures, the ice ablation model was operated using an ablation gradient of ± 0.1 m water equivalent (w.e.) During periods of amplified temperatures, glacier-melt can contribute up to 15% of the total runoff. Model simulations suggest that earlier estimations of glacier-melt over-estimated the importance of glaciers to the regional hydrology at the national scale (Dashdeleg 1983). However, within the headwaters of glaciated watersheds, such as the UKRB, glacier-melt runoff is a critical component of the ecologic and hydrologic systems.

In Chapter 4 (Pan *et al* 2018), I introduce a satellite data-driven algorithm to detect anomalous ROS events across Alaska, USA from 2003-2016. This chapter presents a new gridded ROS data record derived by fusing the Moderate-resolution

Imaging Spectroradiometer (MODIS) snow cover extent product (MOD10A1) with vertically (V) and horizontally (H) polarized passive microwave (PM) brightness temperature (T_b) retrievals at 19 and 37 GHz from the Advanced Microwave Scanning Radiometer (AMSR) mapped to a 6 km EASE-GRID projection. Detected ROS events were validated using a two-tiered approach. Tier-1 corroborated human observed ROS and in situ climate observations in Fairbanks, AK with satellite detected ROS events and produced an overall agreement between 75-100%. The second tier created temperature dependent variables as precipitation proxies from 53 long-term climate stations across Alaska. These proxies included a ratio between minimum and maximum temperature, a ratio between dew point and average temperature, and wet bulb temperature. Using these proxies, satellite detected ROS events were screened using thresholds that did not meet the conditions defined by the precipitation proxies and resulted in an overall accuracy of 86%.

We included Alaska in this dissertation to serve as a study domain to test and develop our initial ROS algorithm. As a study domain, Alaska provides high spatial and temporal coverage of polar-orbiting sensors and available data necessary for validation including; dense long-term climate monitoring networks, human observed ROS observations, and previous studies for which to compare results (Wang *et al* 2016, Semmens *et al* 2013, Wilson *et al* 2013). Regional similarities include large temperate conifer forests in northern Mongolia and the Alaska interior and both regions have observed winter time icing events that have contributed to ungulate mortality (Berger *et al* 2018, Allison 2017). Key differences exist in snow cover retrievals influenced by Alaska's wet maritime relative to Mongolia's semi-arid climate with deep and dry soils which should create favorable ROS retrievals.

In Chapter 5 (Pan *et al.* submitted), I apply the algorithm developed in Chapter 4 to determine and quantify the role of snow melt events on anomalously high annual livestock mortality across Mongolia. In this chapter I detected anomalous snowmelt events and subsequently examined their trends from 2003-2016. An analysis of the resulting seasonal patterns identified that snow melt events were more frequent in the southern Gobi Desert during the fall and more common in the western and central regions of Mongolia during the spring. An increasing trend in fall melt events was also identified

in certain regions, which may indicate an increase in intermittent snow cover and a reduction in persistent snow cover. I next created climate time-series for each provincial unit in Mongolia including winter temperature, normalized difference vegetation index (NDVI), and snow cover duration (SCD), in addition to seasonal melt events. The climate time-series were then used in a generalized linear model (GLM) framework to quantify how much variance in livestock mortality each climate driver explained. The GLM outputs indicated that anomalous seasonal melt events explained 18-34% of the total variance in annual livestock mortality, predominantly in the western and central regions. Winter temperature was found to be the leading driver of annual livestock mortality followed by an unseasonably low NDVI.

In Chapter 6, the results of the prior chapters (2-5) are summarized and discussed relative to the dissertation objectives as well as future potential directions of scientific inquiry.

1.4 References

Batima P, Natsagdorj L, Gombluudev P and Erdenetsetseg B 2005 Observed Climate Change in Mongolia *AIACC Work. Pap.* 25

Beniston M and Stoffel M 2016 Rain-on-snow events, floods and climate change in the Alps: Events may increase with warming up to 4C and decrease thereafter *Sci. Total Environ.* **571** 228–36 Online: http://dx.doi.org/10.1016/j.scitotenv.2016.07.146

Berger J, Hartway C, Gruzdev A and Johnson M 2018 Climate Degradation and Extreme Icing Events Constrain Life in Cold-Adapted Mammals *Sci. Rep.* **8** 1156 Online: http://www.nature.com/articles/s41598-018-19416-9

Bolch T, Kulkarni A, Kääb A, Huggel C, Paul F, Cogley J G, Frey H, Kargel J S, Fujita K, Scheel M, Bajracharya S and Stoffel M 2012 The State and Fate of Himalayan Glaciers *Science (80-.).* **336** 310–4

Cohen J L, Furtado J C, Barlow M A, Alexeev V A and Cherry J E 2012 Arctic warming, increasing snow cover and widespread boreal winter cooling *Environ. Res. Lett.* **7** 014007 Online: http://stacks.iop.org/1748-9326/7/i=1/a=014007?key=crossref.b774aafc53389f43a9e3492e8a36e8b1

Cohen J, Screen J A, Furtado J C, Barlow M, Whittleston D, Coumou D, Francis J, Dethloff K, Entekhabi D, Overland J and Jones J 2014 Recent Arctic amplification and extreme mid-latitude weather *Nat. Geosci.* **7** 627–37 Online: http://dx.doi.org/10.1038/ngeo2234

Dietz A J, Conrad C, Kuenzer C, Gesell G and Dech S 2014 Identifying changing snow cover characteristics in central Asia between 1986 and 2014 from remote sensing data *Remote Sens.* **6** 12752–75

Fernández-giménez M E, Venable N H, Angerer J, Fassnacht S R, Reid R S and Khishigbayar J 2016 Exploring Linked Ecological and Cultural Tipping Points in Mongolia *Anthropocene* **17** 46–69 Online: http://dx.doi.org/10.1016/j.ancene.2017.01.003

Grenfell T C and Putkonen J 2008 A method for the detection of the severe rain-on-snow event on Banks Island, October 2003, using passive microwave remote sensing *Water Resour. Res.* **44** 1–9

Hahn, Allison H 2017 Mongolian Dzud: threats to and protection of Mongolia's herding communities *Assoc. Asian Stud.* **22**

Hessl A E, Anchukaitis K J, Jelsema C, Cook B, Byambasuren O, Leland C, Nachin B, Pederson N, Tian H and Hayles L A 2018 Past and future drought in Mongolia *Sci. Adv.* **4** 1–8

Kim Y, Kimball J S, Zhang K and McDonald K C 2012 Satellite detection of increasing Northern Hemisphere non-frozen seasons from 1979 to 2008: Implications for regional vegetation growth *Remote Sens. Environ.* **121** 472–87 Online: http://dx.doi.org/10.1016/j.rse.2012.02.014

Li Z, Chen Y, Li W, Deng H and Fang G 2015 Potential impacts of climate change on vegetation dynamics in Central Asia *J. Geophys. Res. Atmos.* **120** 345–56

Loe L E, Hansen B B, Stien A, Albon S D, Bischof R, Carlsson A, Irvine R J, Meland M, Rivrud I M, Ropstad E, Veiberg V and Mysterud A 2016 Behavioral buffering of extreme weather events in a high-Arctic herbivore *Ecosphere* **7** 1–13

Lutz A F, Droogers P, Immerzeel W W and Bank A D 2012 Climate Change Impact and Adaptation on the Water Resources in the Amu Darya and Syr Darya River Basins **31**

Mcconnell J R 2005 198: Role and Importance of Cryospheric *Encycl. Hydrol. Sci.* 1–6

Oerlemans J 2005 Extracting a Climate Signla from 169 Glacier Records *Science (80-.).* **308** 675–7

Oshima K, Ogata K, Park H and Tachibana Y 2018 Influence of atmospheric internal variability on the long-term Siberian water cycle during the past 2 centuries *Earth Syst. Dyn.* **9** 497–506

Pan C G, Kirchner P, Kimball J S, Kim Y and Du J 2018 Rain-on-snow events in Alaska, and their frequency and distribution from satellite observations *Environ. Res. Lett.*

Pan C G, Pope A, Kamp U, Dashtseren A, Walther M and Syromyatina M V. 2017 Glacier recession in the Altai Mountains of Mongolia in 1990–2016 *Geogr. Ann. Ser. A, Phys. Geogr.* **0** 1–19 Online:

https://www.tandfonline.com/doi/full/10.1080/04353676.2017.1407560

Racoviteanu A E, Armstrong R and Williams M W 2013 Evaluation of an ice ablation model to estimate the contribution of melting glacier ice to annual discharge in the Nepal Himalaya *Water Resour. Res.* **49** 5117–33

Semmens K A, Ramage J, Bartsch A and Liston G E 2013 Early snowmelt events: Detection, distribution, and significance in a major sub-arctic watershed *Environ. Res. Lett.* **8**

Tao S, Fang J, Zhao X, Zhao S, Shen H, Hu H, Tang Z, Wang Z and Guo Q 2015 Rapid loss of lakes on the Mongolian Plateau. *Proc. Natl. Acad. Sci. U. S. A.* **112** 2281–6 Online: http://www.pnas.org/content/112/7/2281.short

Tedesco M, Brodzik M, Armstrong R, Savoie M and Ramage J 2009 Pan arctic terrestrial snowmelt trends (1979-2008) from spaceborne passive microwave data and correlation with the Arctic Oscillation *Geophys. Res. Lett.* **36** 1–6

Viviroli D, Dürr H H, Messerli B, Meybeck M and Weingartner R 2007 Mountains of the world, water towers for humanity: Typology, mapping, and global significance *Water Resour. Res.* **43** 1–13

Wang L, Toose P, Brown R and Derksen C 2016 Frequency and distribution of winter melt events from passive microwave satellite data in the pan-Arctic, 1988-2013 *Cryosphere* **10** 2589–602

Wilson R R, Bartsch A, Joly K, Reynolds J H, Orlando A and Loya W M 2013 Frequency, timing, extent, and size of winter thaw-refreeze events in Alaska 2001-2008 detected by remotely sensed microwave backscatter data *Polar Biol.* **36** 419–26

Zemp M, Frey H, Gärtner-Roer I, Nussbaumer S U, Hoelzle M, Paul F, Haeberli W, Denzinger F, Ahlstrøm A P, Anderson B, Bajracharya S, Baroni C, Braun L N, Càceres B E, Casassa G, Cobos G, Dàvila L R, Delgado Granados H, Demuth M N, Espizua L, Fischer A, Fujita K, Gadek B, Ghazanfar A, Hagen J O, Holmlund P, Karimi N, Li Z, Pelto M, Pitte P, Popovnin V V., Portocarrero C A, Prinz R, Sangewar C V., Severskiy I, Sigurdsson O, Soruco A, Usubaliev R and Vincent C 2015 Historically unprecedented global glacier decline in the early 21st century *J. Glaciol.* **61** 745–62

Zemp M, Thibert E, Huss M, Stumm D, Rolstad Denby C, Nuth C, Nussbaumer S U, Moholdt G, Mercer A, Mayer C, Joerg P C, Jansson P, Hynek B, Fischer A, Escher-Vetter H, Elvehøy H and Andreassen L M 2013 Reanalysing glacier mass balance measurement series *Cryosphere* **7** 1227–45

CHAPTER 2
Glacier Recession in the Altai Mountains of Mongolia from 1990–2016

Corresponding publication:

Pan, C.G., Pope, A., Kamp, U., Walther, M., Avirmed, D. (2017). Glacier recession in the Altai Mountains of Mongolia 1990-2016. *Geografiska Annaler, A: Physical Geography*. DOI:10.1080/04353676.2017.1407560

2.1 Abstract

Relatively little is known about glaciers in the continental climates of North Asia and even less is known about the glaciers of the Mongolian Altai. In an attempt to fill this knowledge gap, we present a new satellite-derived glacier inventory for the Altai Mountains of Mongolia, using the recently launched Landat-8 OLI and Sentinel-2A MSI sensors to monitor glacier change from 1990-2016. We examine changes in climatic trends and glacier topomorphological parameters in conjunction with glacier fluctuations to determine governing controls over glacier recession in the Altai Mountains. Our glacier mapping results produced 627 debris-free glaciers with an area of 334.0 ± 42.3 km^2 as of 2016. These data were made available for download through the Global Land Ice Measurements from Space (GLIMS) initiative. A subsample of 206 glaciers that were mapped in 1990, 2000, 2010, and 2016 revealed that from 1990-2016, glacier area reduced by 43% at 6.4 ± 0.4 km^2 yr^{-1}. Glacier recession was greatest from 1990-2000 at a rate of 10.9 ± 0.8 km^2 yr^{-1}, followed by 2010-2016 at 4.4 ± 0.3 km^2 yr^{-1}. Rates of glacier recession were significantly correlated with intrinsic glacier parameters including mean, minimum and range elevations, mean slope and aspect. Furthermore, climate records indicated the warmest summer temperatures occurred during periods of high glacier recession.

2.2 Introduction

Glaciers are a keystone feature of terrestrial alpine ecosystems and have become one the best natural proxies for global climate change (Zemp et al. 2015; Oerlemans 2005). The global trend in retreat of glaciers in reaction to global climate change (IPCC, 2013) has implications for both ecological structure and function, and human development. A governor of ecological community composition, glacier sediment transported by melt runoff is an important input for both lentic and lotic aquatic ecosystem biodiversity (Muhlfeld et al. 2011; Brown, Hannah, and Milner 2007) and influences limitations on aquatic and terrestrial net primary productivity (Hodson et al., 2008). Glacier melt runoff is also an important water resource for downstream populations at scales ranging between small communities to large metropolitan centers (Lutz et al. 2014; T. Bolch et al. 2012).

Remotely sensed Earth observation satellites provide one of the most effective means to monitor changes in alpine glaciers, enabling global coverage of multispectral and optical images at moderate spatial resolution, an effective temporal resolution, and at limited costs (Raup et al., 2007; Bhambri & Bolch, 2009; Racoviteanu et al., 2009). Many studies have employed satellite images to inventory glaciers at a regional scale to detect changes in glacier area (Tennant et al., 2012; Chand & Sharma, 2015; Tielidze, 2016). One of the most widely applied sensors in the application of glacier monitoring is the Landsat series beginning in 1972, providing open access to a now 45-year record of global environmental change (Wulder et al., 2012; Pope et al., 2014). Two more recent satellites that provide images useful in glacier monitoring are Landsat 8 Operational Land Imager (OLI) (launched in 2013) (Roy et al. 2014) and Sentinel 2-A Multi-Spectral Instrument (MSI) (launched in 2015). These two new sensors are operating at a critical period as Landsat 5 was decommissioned in 2012 and Landsat 7 continues to suffer from a malfunctioning scan-line corrector (Frank Paul et al. 2016).

The glaciers of Mongolia are not well studied and have gained international attention only recently (Ganiushkin et al., 2015; Kamp & Pan, 2015; Syromyatina et al., 2015; Zhang et al., 2016, Walther et al., 2017). The Mongolian Altai is located within mid-latitudes of the North Asian landmass. Considering the majority of terrestrial alpine glaciers exist under some form of maritime influence, glaciers of North Asia and Mongolia are some of the few glaciers that exist in a continental climate (Baast, 1998). The objectives

of this paper are to: (1) map glaciers of the Mongolian Altai using the recently launched Landsat 8 OLI and Sentinel-2A MSI; (2) contribute new data to the previous glacier inventory created by Kamp & Pan (2015) to extend the glacier record for Mongolia; (3) analyze glacier change from 1990-2016 to understand the forces that contribute to glacier recession in the Mongolian Altai.

2.3 Study Area

2.3.1 Regional Context

The Altai Mountains form the border between Mongolia and China and trend from the northwest to the southeast for 1200 km before turning east and terminating in the Gobi Desert; they form the most extensive longitudinal mountain range in Central Asia, continuing into Russia to join the Russian Sayan Mountains (Figure 2.1). There are a number of isolated mountains greater than 4000 m a.s.l. within the Mongolian Altai with the highest elevations in the Tavan Bogd, where Khuiten Peak reaches a maximum elevation of 4374 m a.s.l. (Shinneman et al. 2010; Herren et al. 2013; Grunert, Lehmkuhl, and Walther 2000).

2.3.2 Previous Studies on Glaciers in the Altai Mountains

Long-standing glacier monitoring efforts in the Mongolian Altai do not exist, attributed in large part to the region's sparse population and limited infrastructure, making access to glaciers difficult. In spite of the challenges associated with glaciological methods in the Mongolian Altai, there have been a number of studies that used remotely sensed observations to monitor glacier changes. The majority of these studies focused on the glaciers of Tavan Bogd (Kadota & Gombo, 2007; Kadota et al., 2011; Krumwiede et al., 2014), Turgen Mountains (Lehmkuhl, 1999; Khrusky & Golubeva, 2008; Kamp et al., 2013), Tsambagarav Uul (Kadota et al., 2011), and Munkh Khairkhan (Krumwiede et al. 2014). A few studies examined glacier area within the entire Mongolian Altai (Selivanov, 1972; Devjatkin, 1981; Baast, 1998; Klinge, 2001; Enkhtaivan, 2006; Yabouki & Ohata, 2009; Kamp & Pan, 2015; Nuimura et al., 2015; Earl & Gardner, 2016). Within these studies, glacier mapping results were quite sporadic ranging in total glacier area from 300 km^2 (Devjatkin, 1981) to 659 km^2 (Baast, 1998). The discrepancy in these results is likely due to: (1) differing source data, (2) differing dates of source data, (3) author groups'

definition of ‘glacier’, (4) glacier mapping methodology, and (5) the spatial extent of ‘Mongolian Altai’. Only recently has the first satellite-derived systematic mapping and multi-temporal inventory of the Mongolian Altai been completed (Kamp & Pan, 2015). To the authors’ knowledge only two of the aforementioned studies mapped debris-covered glaciers in the Mongolian Altai. Aggregating the Russian and Mongolian Altai with the Russian Sayan Mountains, Earl & Gardner (2016) determined that debris-covered glaciers included 42 ± 4 km^2 (3.6%) of the total glacier area. Krumwiede et al. (2014) documented that in Tavan Bogd, the debris-covered area was 3.4 km^2 in 1989 and 2.9 km^2 in 2006.

2.4 Data and Methods

2.4.1 Satellite Data

In this study we employed Landsat 8 OLI and Sentinel-2A MSI imagery to generate a glacier inventory for the Mongolian Altai for 2016. Images for the new inventory were acquired from the USGS via its Global Visualization viewer (http://glovis.usgs.gov) (Table 2.1).

Both OLI and MSI possess sensor characteristics that are more advantageous to glacier mapping than earlier Landsat sensors. Improvements to radiometric resolution from 8 bit to 12 bit for OLI and a radiometric resolution of 12 bit for MSI sensors (Winsvold, Kääb, and Nuth 2016) has proven to be more effective at identifying glaciers within shadows (Kääb et al. 2016). The spatial resolution of OLI has remained at 30 m, whereas MSI has a spatial resolution of 10 m in the visible and Near-infrared (NIR) bands and a 20 m resolution moving into the Shortwave Infrared (SWIR). Possibly, the most important advantage for glacier mapping facilitated by these two new sensors is an unprecedented temporal coverage. In addition to OLI’s image acquisition rate of sixteen days, MSI acquires images every five days (at the equator). Combined, the synchronous operation of these two sensors greatly improves the annual acquisition of high-quality images with limited cloud cover at the end of the ablation season.

We used a 90 m SRTM v4.1 Digital Elevation Model (DEM) downloaded from the CGIAR CSI (www.cgiar-csi.org/data/srtm-90m-digital-elevation-database-v4-1) to characterize our glacier outlines with parameters including: mean, minimum, and elevation ranges, mean slope, and mean aspect. The vertical accuracy of the SRTM is spatially

variable, with the most significant errors originally existing in areas of steep topography. Voids have been filled with data from various DEM sources, greatly improving the overall quality of the SRTM (Frey & Paul, 2012).

2.4.2 Climate Data

The analysis of temperature and precipitation trends was performed on data from six publicly available climate stations within western Mongolia and the Russian Altai; data were acquired from the National Climatic Data Center (NCDC) (https://www.ncdc.noaa.gov/cdo-web/datatools/findstation). These stations ranged in elevation from 936 m a.s.l. in Ulaangom to 1759 m a.s.l. at Kosch Agach (Figure 2.1, Table 2.2). The geographic distribution of these stations is dispersed throughout the margins of the Altai Mountains, with the Ulgi station being the only one within the geographic center. The stations of Ulaangom, Khovd, and Omno Gobi are located at the transition between the desert steppes and the Altai Mountains, while Baitag and Kosch Agach are located at the Altai's southern and northern extents, respectively.

Climate data sets were used to examine fluctuations in temperature and precipitation in relation to changes in debris-free glacier area for the Mongolian Altai for the time periods 1990-2016, 1990-2000, 2000-2010, and 2010-2016. Due to the varying degree of elevation ranges, and temporal and spatial coverage, climate data from all six stations were aggregated to create a regional time series of precipitation and temperature trends. We homogenized the aggregated time series by extracting the monthly precipitation and temperature values from each station for a given month and year. The homogenization output a monthly mean value from all six stations. Trend coefficients were then extracted from linear regressions for both temperature and precipitation at seasonal and annual rates and for each time period (Bolch, 2007; Osmonov et al., 2013; Osipov & Osipova, 2014). Furthermore, it must be clarified that a glacier's response to climatic forcing can often manifest as a delayed response (Tennant et al. 2012) that can vary for different glaciers and different regions (Gardent et al. 2014). For this reason, in lieu of presenting climatic data for specific years, we present climatic trends for different periods.

2.4.3 Mapping Debris-free Glaciers

Glacier outlines for 1990, 2000, and 2010 were downloaded from the GLIMS database (www.glims.org). This multi-temporal inventory included a debris-free glacier area of 443 km^2 in 1990, 428 km^2 in 2000, and 371 km^2 in 2010 (Kamp & Pan, 2015). However, since in their original inventory Kamp & Pan (2015) were unable to map all glaciers in 1990 owing to significant cloud cover, they corrected the total glacier area for 1990 to 515 km^2 by including glacier outlines from 2000 in the 1990 inventory. As a result, the 1990 total glacier area represents only an estimated minimum that we here use in our glacier change analysis.

To retain glacier inventory integrity, we followed the same mapping approach as Kamp & Pan (2015). In their inventory, a NIR/SWIR band ratio was applied using a threshold of 2 (Bishop et al., 2004; Bhambri & Bolch, 2009;). Here, we applied the same band ratio using raw digital numbers (DNs) of NIR and SWIR bands (OLI5/OLI6 and MSI8/MSI11). However, we deviated from the original inventory by qualitatively determining scene-specific image thresholds (Table 2.1). The threshold was determined visually with the criteria to be as low as possible to include slightly dirty ice margins (F Paul et al. 2013). The average threshold was 1.5 for OLI images and 3.2 for MSI images. A 3 x 3 median filter was applied to band ratio thresholding results to remove misclassified isolated pixels before being converted to vector polygons. The polygons were aggregated, and a size threshold of 0.01 km^2 was applied. The glacier polygons were intersected with DEM-derived ice divides to segregate the entire debris-free glacier cover into individual glaciers (Tobias Bolch, Menounos, and Wheate 2010). After intersecting, the debris-free glaciers were manually edited to merge sliver polygons to larger adjacent glacier entities (Racoviteanu et al., 2009; Frey et al., 2012). Finally, we assigned each glacier outline either a GLIMSID from the previous inventory or a new GLIMSID (Raup et al. 2007).

2.4.3 Uncertainty and Error

Uncertainty and error in the mapping of debris-free ice can be manifested through several steps and processes. Addressing potential sources of uncertainty and error is critical as they can propagate through sequential steps and change detection analysis (A. E. Racoviteanu et al. 2015; F Paul et al. 2013). In our update of the glacier inventory, uncertainty and errors can potentially originate from: (1) the use of images with varying

spatial resolutions; (2) image threshold selection; (3) the misclassification of snowpack as ice; and (4) accuracy of the ice divides derived (Racoviteanu et al., 2009; Nuth et al., 2013).

We represented error as the residual error between the modeled and observed, which takes the following form:

$$E = \sqrt{E_i - \hat{E}_i^{\,2}} \qquad \text{(Eq.1)}$$

where E_i is the area of the glacier polygon and $\hat{E}_i$ is the glacier area determined by the pixel count multiplied by the image resolution. $\hat{E}_i$ is derived from a Perkal's epsilon band around each glacier outline and is buffered by the image resolution to represent a potential error within one pixel (Racoviteanu et al., 2009, 2015; Bolch et al., 2010). Analysis of glacier uncertainty has been documented to be <5% (Paul et al., 2013; Lynch et al., 2016). Our representation of uncertainty is a conservative assessment with values of 12.4% for 1990, 13.8% for 2000, 14.7% for 2010, and 12.6% for 2016.

2.5 Results

2.5.1 Updated Glacier Inventory

Our updated multi-temporal inventory resulted in 627 debris-free glaciers contributing to a total surface area of 334.0 ± 42.3 km^2 in 2016 (Table 2.3). In 2016, almost 60% of the glaciers were smaller than 0.125 km^2, and less than 2% were greater than 5.6 km^2; the mean glacier area was 0.53 km^2, the largest glacier area—that of the combined Potanin and Alexandra glaciers—was at 35.5 km^2. The minimum glacier elevation was 2708 m a.s.l., and the mean glacier elevation was 3449 m a.s.l. (Table 2.4).

2.5.2 Glacial Changes

2.5.2.1 Glacier Area Changes

From 1990-2016, the debris-free area of the 627 glaciers decreased by 181.0 ± 8.4 km^2 (35%); it decreased by 86.4 ± 3.3 km^2 (16.9%) from 1990-2000, 57.5 ± 2.2 km^2 (13.3%) from 2000-2010, and 66.5 ± 2.7 km^2 (18.1%) from 2010-2016. From 1990-2016, the rate of recession was 7.0 ± 0.3 km^2 yr^{-1}, with the highest rate of 11.1 ± 0.4 km^2 yr^{-1} for 2010-2016, followed by 8.6 ± 0.3 km^2 yr^{-1} for 1990-2000 and 5.8 ± 0.2 km^2 yr^{-1} for 2000-2010.

From henceforth, areal and topomorphological changes will be performed on a subsample of 206 glaciers. To be included in this subsample, a glacier was required to have been mapped and possess an area greater than 0.01 km^2 during all four time periods. It should also be noted that, if a glacier disintegrated into multiple parts, only the part that contained the GLIMSID remained within the subsample of 206. Glacier area in our subsample decreased by 43% from 1990-2016, 28% from 1990-2000, 11% from 2000-2010, and 10% from 2010-2016. Furthermore, the rates of glacier recession were 6.4 ± 0.4 km^2 yr^{-1} for 1990-2016, 10.9 ± 0.8 km^2 yr^{-1} for 1990-2000, 3.2 ± 0.2 km^2 yr^{-1} for 2000-2010, and 4.4 ± 0.3 km^2 yr^{-1} for 2010-2016.

Our sample of 206 glaciers showed that both absolute and relative changes in debris-free glacier area indicated that larger glaciers (>0.86 km^2) had the greatest change in area (Figure 2.2a). From 1990-2000, glaciers expressed the greatest change in area for all class sizes (Figure 2.2b), During this time, small glaciers (<0.125 km^2) expressed the greatest loss in relative area, although mapping results indicate greater temporal variability within this class size, as positive relative area values can be observed during other time periods. The highest absolute rates of recession during 1990-2016 and 1990-2000 can be partially attributed to the disintegration of large glaciers into smaller glaciers.

2.5.2.2 Changes in Glacier Topomorphology

Changes in glacier topomorphologic characteristics indicate significant glacier recession (Table 2.4). From 1990-2016, the mean elevation of debris-free glaciers increased by 33 m, with the largest increase of 20 m during 2010-2016. The minimum glacier elevation increased by 123 m from 1990-2016, with the largest increase of 94 m during 2000-2010 and only 5 m during 2010-2016. The mean elevation range decreased by 109 m during 1990-2016, with the largest decrease of 59 m during 1990-2000 and only 15 m during 2010-2016. The changes in minimum elevation and mean elevation range indicate that debris-free glaciers experienced the highest rates of recession from 1990-2000. Glacier hypsometries indicate that the debris-free glacier surface area below 3500 m decreased by 20.2% and by 15.5% above 3500 m (Figure 2.3).

From 1990-2016, the mean glacier slope more or less stagnated—it changed only from 20.4° to 20.3°. However, for smaller glaciers (<0.86 km^2) the mean slope decreased

by 1.4º from 23.0° to 21.6°, while for larger glaciers (>0.86 km^2) it decreased by 2.2º from 17.6° to 15.4°.

In 2016, debris-free glaciers with an eastern aspect (36.7%) constituted the largest surface area, followed by northeast (33.2%) and southeast (16.5%) aspects. Debris-free glaciers with a northeast, northwest, or northern aspect—aspects that in the northern hemisphere favor glacier health—had a share of 26% in 1990, 41% in 2000, 36% in 2010, and 39% in 2016 of the total glacier area. However, when looking at the total number of glaciers, these three aspects constituted 52% in 1990, 59% in 2000, 62% in 2010, and 62% in 2016, suggesting that small glaciers are mainly situated in northern aspects (Figure 2.4).

The rate of glacier change was negatively correlated with glacier area, mean elevation, and elevation range. Positive correlations were found between mean aspect, mean slope, and minimum elevation. Regressions performed on the rates of glacier change for 1990-2016 for all parameters were significant at the 99% confidence interval ($p < 0.01$). To identify fluctuations in controls of glacier recession, regressions were performed for rates of glacier change during 1990-2000, 2000-2010 and 2010-2016. Significance and correlations weakened for all three sub-periods relative to entire period of 1990-2016. Yet, glacier area and elevation range remained significant at the 99% confidence interval ($p < 0.01$) for all four periods. Mean elevation and mean aspect were significant at the 95% confidence ($p < 0.05$) interval. Minimum elevation was significant for all periods at the 90% confidence interval ($p < 0.1$). For the time periods of 2000-2010 and 2010-2016, mean slope became an insignificant control of the rate of glacier change at the 90% confidence interval ($p < 0.1$).

2.5.2.3 Qualitative Analysis of Glacier Change

Although this study did not attempt to apply a DEM-differencing approach to quantify glacier thinning (Tobias Bolch, Buchroithner, and Pieczonka 2008), the downwasting of debris-free glaciers is evident through qualitative visual inspection. Throughout all subregions of the Altai Mountains, many larger glaciers have disintegrated into smaller glaciers and most notably, this study presents the first evidence of the separation of the Altai's two largest glaciers, Potanin and Alexandra in the Northwest Interior (Figure 2.5). Downwasting is also documented through the development of

proglacial lakes and increased exposure of nunataks as a result of glacier recession (Frank Paul, Kääb, and Haeberli 2007).

2.5.3 Current Climatic Trends

Trend coefficients indicated an increase in mean annual air temperature (MAAT) of 0.007 °C yr^{-1} from 1962-2015, with an amplified increase of 0.19 °C yr^{-1} from 1989-2015. (Figure 2.6, Table 2.5). Seasonally and temporally aggregated air temperature trends indicated fluctuating positive and negative trends. From 1989-2015, the period of interest for our glacier monitoring, spring and summer seasons observed negative trends only during 2000-2010 (Figure 2.7). Further, the summer months observed the highest annual increase in air temperature at 0.12 °C yr^{-1} during 1989-2000, followed by 2010-2015 at 0.07 °C yr^{-1}.

From 1962-2015, regional precipitation trends had higher variability relative to temperature trends (Figure 2.8, Table 2.6). Yet, there was an observable increase in annual precipitation of 0.28 mm yr^{-1} from 1962-2015, and an amplified trend of 0.81 mm yr^{-1} from 1989-2015. However, within these overall increases in mean annual precipitation trends, there were distinct seasonal and temporal characteristics (Figure 2.9). The summer months during all time periods observed negative trends with highest trends occurring during 2010-2015 followed by 1989-2000. During the winter, spring and fall seasons, positive trends were observed for the most part during all time periods.

2.6 Discussion

2.6.1 Comparison Between Different Inventories

A comparison of our inventory results with those from Kamp & Pan (2015) proves challenging. As explained earlier, Kamp & Pan (2015) could not map all glaciers for 1990 owing to significant cloud cover in some satellite scenes and, hence, estimated and then added the missing glacier area to the mapped one. They put the decrease in glacier area in the Mongolian Altai at 28% between 1990 and 2010. By extending the study period to 1990-2016, we found a decrease in area of 35% for all 627 glaciers, and of 43% for only the 206 glaciers for which mapping results are available for all four years of 1990, 2000,

2010, and 2016. However, both cases document a continuation of the glacier recession after 2010.

The strong rates of glacier recession in the Mongolian Altai are above those documented in glacier inventories for regions with more maritime climates. For example, several authors reported a decrease in glacier area of 19% from 1985-2006/09 in the French Alps (Gardent et al., 2014), 25% from 1985-2011 in Northern Patagonia (Paul & Mölg, 2014), and 11% from 1985-2005 in western Canada (Bolch et al,. 2010). More locally relevant, observations in the Chuya Ridge and Russian Altai indicated a glacier area reduction of 19.7% from 1952-2004 (Shahgedanova et al. 2010; Khromova et al. 2010). Other glacier inventories within the region are in strong agreement with our results for the Mongolian Altai. For example, Stokes et al. (2013) documented a decrease in glacier area of around 40% from 1995-2011 in the Kodar Mountains of east-central Siberia.

Additionally, our results show that glaciers in the Altai Mountains decreased by 29% from 2000-2016, which is similar to the reduction of 24% from 2000-2014 for the Kamchatka Penninusla (Lynch et al. 2016). In the east Sayan, Baikalsky and Kodar Mountains of southeast Siberia, Osipov and Osipova (2014) found a reduction in glacier area of 27% from 2001/02–2006/11.

Notably, of the few glacier inventories within extreme continental climates (Surazakov et al., 2007; Stokes et al., 2013; Osipov & Osipova, 2014) and milder continental climates (Lynch et al. 2016), changes in glacier area are in the best agreement with the results for the Altai Mountains. The comparison of global and regional glacier inventories suggests that probably in recent decades continental alpine glaciers have observed a greater reduction in areal extent in comparison to maritime alpine glaciers. However, a more exhaustive review of the literature will be required to draw strong conclusions.

2.6.2 Topomorphological Characteristics and Glacier Recession

Despite the correlation and significance determined by regression analysis between glacier rates of change and topomorphological characteristics, it is difficult to determine the degree of influence of topomorphological glacier characteristics on their recession. A glacier's elevation is not entirely independent of the glacier area largely because the

elevation is an intrinsic characteristic of a glacier and results in high correlations between changes in mean and elevation ranges and the rates of glacier recession. In other words, it is difficult to determine the influence of topomorphological characteristics on glacier recession because mean elevation and elevation ranges are largely determined by a glacier's area. Hence, any changes in glacier area will be proportionally reflected in changes of mean elevation and elevation ranges. However, a glacier's minimum elevation is not a derivative of its length or a proxy of its size, providing credence to minimum elevation as being one of the more independent and appropriate topomorphological glacier parameters. We identified accelerated rates of glacier recession in glaciers that possess a minimum elevation above 3500 m a.s.l ($p < 0.001$) relative to rates of recession below 3500 m a.s.l ($p < 0.001$). The accelerated increase in glacier minimum elevation at higher elevations may be an indicator of glaciers trending towards slopes that are less shaded and are more exposed to solar radiation. Osipov & Osipova (2014) found results contrary to the results on minimum glacier elevation presented here, and other regional studies found no statistical significance between area loss and minimum elevation (Stokes et al., 2013; Lynch et al., 2016).

Tsutomu & Gombo (2007) used the term 'flat-top' to describe many of the glaciers throughout the Altai Mountains. This terminology is used to qualitatively define the topomorphological context of Altai glaciers, in that many of the glaciated mountain peaks are quite homogenous with shallower slopes. The homogeneity reduces the topographic complexity and increases the exposure of glaciers to solar radiation at higher elevations. We can interpret the decrease in mean slopes for glaciers throughout the Altai Mountains as a consequence of glaciers receding from lower elevations to the more exposed 'flat-top' regions of these mountain tops. This possibility is in line with the accelerated recession at higher elevations determined by changes in minimum elevation as the glaciers become more exposed to solar radiation (Tennant et al., 2012; Osipov & Osipova, 2014).

The northern aspect was the only aspect that consistently observed an increase in number of glaciers and consequently an increase in area for all years. As glaciers with initial aspects of northwest, northeast, or east begin to recede, they possess the propensity to recede in a fashion that evolves their aspect towards the north (DeBeer & Sharp, 2007), thus increasing the number of glaciers with a northerly aspect. Considering the minor

increase in area relative to the increase in number for glaciers with a north aspect, we conclude that these glaciers are smaller and protected by steeper slopes. Yet, even though small glaciers are transitioning into northern aspects, small glaciers still expressed higher relative rates of recession, and as a consequence we must consider aspect to possess a subdued role in the modulation of glacier recession (Granshaw & Fountain, 2006).

2.6.3 Regional Climatic Trends

Regional climatic trends throughout the mountain environments of western Mongolia and southern Siberia indicate consistent warming trends. From two climate stations in southeastern Siberia, Osipov & Osipova (2014) found a general trend of summer temperature increase at a rate of 1.7 ºC and 2.6 ºC, respectively, for 1970-2010. Within the adjacent Kodar Mountains, the mean summer temperature was 13.9 ºC for 1960-1995; however, in more recent decades, the mean summer temperatures increased by 1.1 ºC to 15 ºC for 1995-2010 (Stokes et al. 2013). In the more local Russian Altai, Shahgedanova et al. (2010) observed an increase in summer temperatures by 1.26 ºC from 1950-2004, and by 1.9 ºC from 1985-2004. Interestingly, from 1951-2000, mean summer temperatures in the Aktru Basin increased by 1.03 ºC below 2500 m a.s.l. and by 0.83 ºC above 2500 m a.s.l., which is attributed to increased summer precipitation at higher elevations (Surazakov et al. 2007). For the Altai Mountains, we observed an increase in summer temperatures of 1 ºC from 1962-2015. Indeed, our results of climatic trends also demonstrate accelerated rates of summer temperature increase in recent decades and are in agreement with the rates of glacier recession in the Altai Mountains.

Given that the climate stations are at lower elevations than the glaciers, it is difficult to assess the interaction between precipitation trends and glacier recession. Precipitation during the accumulation (October–March) season has been historically limited by the Siberian High. However, the Siberian High has been undergoing considerable weakening, allowing greater amounts of precipitation during the accumulation season (Shinneman et al., 2010). Our results indicate positive trends in winter precipitation (1962-2015, 1989-2015), though these trends are at low magnitude despite the weakening of the Siberian High. It could be possible that its weakening is expressed by increased spring precipitation, which could be a result of the Siberian High Pressure being replaced by the Asiatic Low at

an earlier time during the year. It is difficult to define how these changes in precipitation are influencing glacier recession in the Altai Mountains over time, particularly because it is unclear if the precipitation is falling as snow or rain. We can hypothesize that decreasing summertime precipitation can be a representative proxy for increased number of cloud-free days, which in turn enhances the amount of incoming solar radiation. However the dominant surface energy balance of Altai glaciers is unknown (Francou et al. 2003). While the increasing precipitation during the spring and fall seasons can be either rain or snow, with enhanced rates of increased temperature during these seasons, it is also possible that the glaciers in the Altai Mountains are receiving more rain in lieu of snow, which can accelerate the ablation processes (Osipov & Osipova, 2014).

2.7 Summary

We here continued our monitoring of glaciers in the Mongolian Altai and extended the period of the older inventory that covered the period from 1990-2010 (Kamp & Pan 2015) to now 2016 by using Landsat 8 OLI and Sentinel 2A-MSI. Our new glacier outlines for 2016—like the ones for 1990, 2000, and 2010 from the first inventorying study—can be accessed from the GLIMS database website free of charge (Kargel et al. 2005). The new inventory consists of 627 debris-free glaciers covering an area of 334.0 ± 42.3 km^2 as of 2016. Our analysis of glacier change on a subset of 206 glaciers showed a decrease in debris-free glacier area of 43% at a rate of 6.4 ± 0.4 km^2 yr^{-1} from 1990-2016. The highest rates of recession occurred during 1990-2000 at 10.9 ± 0.8 km^2 yr^{-1}. While some studies from other mountain ranges in the region present recession rates that are similar to the relatively strong recession of glaciers in the Mongolian Altai, others found much slower recessions. However, it seems that glaciers in the extreme continental Mongolian Altai are receding at higher rates than in many other mountain ranges worldwide. Mean summer temperatures are likely the primary driver of this accelerated glacier recession in the Altai Mountains, as there has been a measured increase of 1 ºC from 1962-2015 and an enhanced increase since 1990. The greatest increase in summer temperature correlates well to accelerated periods of glacier recession, particularly for 1990-2000 and 2010-2016. However, the topomorphological characteristics of debris-free glaciers also express certain controls on glacier recession.

2.8 References

Baast, P., 1998. Modern glaciers of Mongolia. Ulaanbaatar: Institute of Meteorology and Hydrology, Unpublished Report, 162 (In Russian).

Batima, P., Natsagdorj, L., Gombluudev, P., and Erdenetsetseg, B., 2005. Observed Climate Change in Mongolia. Nairobi: Assessments of Impacts and Adaptations to Climate Change (AIACC) Working Papers, No. 13, 26. http://www.aiaccproject.org/working_papers/working_papers.html.

Batjargal, Z., 1997. Desertification in Mongolia. In Agricultural Research Institute (ed.), Rangeland Desertification. Reykjavík: Agricultural Research Institute, RALA Report, 200: 107–113.

Bhambri, Rakesh, and Tobias Bolch. 2009. "Glacier Mapping : A Review with Special Reference to the Indian Himalayas." *Progress in Physical Geography* 33 (5): 672–704. https://doi.org/10.1177/0309133309348112.

Bishop, Michael P, Jeffrey A Olsenholler, John F Shroder, Roger G Barry, H Raup, Andrew B G Bush, Luke Copland, et al. 2004. "Global Land Ice Measurements from Space (GLIMS): Remote Sensing and GIS Investigations of the Earth ' s Cryosphere Global Land Ice Measurements from Space (GLIMS): Remote Sensing and GIS Investigations of the Earth ' s Cryosphere." *Geocarto International* 19 (2): 57–84.

Bolch, T., A Kulkarni, A Kääb, C Huggel, F Paul, J G Cogley, H Frey, et al. 2012. "The State and Fate of Himalayan Glaciers." *Science* 336 (6079): 310–14. https://doi.org/10.1126/science.1215828.

Bolch, Tobias. 2007. "Climate Change and Glacier Retreat in Northern Tien Shan (Kazakhstan / Kyrgyzstan) Using Remote Sensing Data." *Global and Planetary Change* 56: 1–12. https://doi.org/10.1016/j.gloplacha.2006.07.009.

Bolch, Tobias, Manfred Buchroithner, and Tino Pieczonka. 2008. "Planimetric and Volumetric Glacier Changes in the Khumbu Himal , Nepal , since 1962 Using Corona , Landsat TM and ASTER Data." *Journal of Glaciology* 54 (187): 592–600.

Bolch, Tobias, Brian Menounos, and Roger Wheate. 2010. "Landsat-Based Inventory of Glaciers in Western Canada , 1985 – 2005." *Remote Sensing of Environment* 114: 127–37. https://doi.org/10.1016/j.rse.2009.08.015.

Brown, Lee E., David M. Hannah, and Alexander M. Milner. 2007. “Vulnerability of Alpine Stream Biodiversity to Shrinking Glaciers and Snowpacks.” *Global Change Biology* 13 (5): 958–66. https://doi.org/10.1111/j.1365-2486.2007.01341.x.

Chand, Pritam, and Milap Chand Sharma. 2015. “Glacier Changes in the Ravi Basin, North-Western Himalaya (India) during the Last Four Decades (1971-2010/13).” *Global and Planetary Change* 135. Elsevier B.V.: 133–47. https://doi.org/10.1016/j.gloplacha.2015.10.013.

DeBeer, Christopher M C.M. M, and Martin J Sharp. 2007. “Recent Changes in Glacier Area and Volume within the Southern Canadian Cordillera.” *Annals of Glaciology* 46 (1): 215–21. https://doi.org/10.3189/172756407782871710.

Francou, Bernard, Mathias Vuille, Patrick Wagnon, Javier Mendoza, and Jean-Emmanuel Sicart. 2003. “Tropical Climate Change Recorded by a Glacier in the Central Andes during the Last Decades of the Twentieth Century: Chacaltaya, Bolivia, 16°S.” *Journal of Geophysical Research* 108 (D5): 4154. https://doi.org/10.1029/2002JD002959.

Frey, Holger, and Frank Paul. 2012. “On the Suitability of the SRTM DEM and ASTER GDEM for the Compilation of Topographic Parameters in Glacier Inventories.” *International Journal of Applied Earth Observations and Geoinformation* 18. Elsevier B.V.: 480–90. https://doi.org/10.1016/j.jag.2011.09.020.

Frey, Holger, Frank Paul, and Tazio Strozzi. 2012. “Compilation of a Glacier Inventory for the Western Himalayas from Satellite Data: Methods, Challenges, and Results.” *Remote Sensing of Environment* 124. Elsevier Inc.: 832–43. https://doi.org/10.1016/j.rse.2012.06.020.

Ganiushkin, Dmitry, Kirill Chistyakov, and Elena Kunaeva. 2015. “Fluctuation of Glaciers in the Southeast Russian Altai and Northwest Mongolia Mountains since the Little Ice Age Maximum.” *Environmental Earth Sciences* 74 (3): 1883–1904. https://doi.org/10.1007/s12665-015-4301-2.

Gardent, Marie, Antoine Rabatel, Jean-pierre Dedieu, and Philip Deline. 2014. “Multitemporal Glacier Inventory of the French Alps from the Late 1960s to the Late 2000s.” *Global and Planetary Change* 120. Elsevier B.V.: 24–37. https://doi.org/10.1016/j.gloplacha.2014.05.004.

Granshaw, Frank D, and Andrew G Fountain. 2006. “Glacier Change (1958 – 1998) in the North Cascades National Park Complex, Washington, USA.” *Journal of Glaciology* 52 (177): 251–56.

Grunert, Jörg, Frank Lehmkuhl, and Michael Walther. 2000. “Paleoclimatic Evolution of the Uvs Nuur Basin and Adjacent Areas (Western Mongolia).” *Quaternary International* 65–66: 171–92. https://doi.org/10.1016/S1040-6182(99)00043-9.

Herren, Pierre Alain, Anja Eichler, Horst Machguth, Tatyana Papina, Leonhard Tobler, Alexander Zapf, and Margit Schwikowski. 2013. “The Onset of Neoglaciation 6000 Years Ago in Western Mongolia Revealed by an Ice Core from the Tsambagarav Mountain Range.” *Quaternary Science Reviews* 69. Elsevier Ltd: 59–68. https://doi.org/10.1016/j.quascirev.2013.02.025.

Kääb, Andreas, Solveig Winsvold, Bas Altena, Christopher Nuth, Thomas Nagler, and Jan Wuite. 2016. “Glacier Remote Sensing Using Sentinel-2. Part I: Radiometric and Geometric Performance, and Application to Ice Velocity.” *Remote Sensing* 8 (7): 598. https://doi.org/10.3390/rs8070598.

Kadota, Tsutomu, Davaa Gombo, Purevdagva Kalsan, and Davaadorj Namgur. 2011. “Glaciological Research in the Mongolian Altai, 2003-2009.” *Bulletin of Glaciological Research* 29: 41–50.

Kamp, Ulrich, Kevin G. Mcmanigal, Avirmed Dashtseren, and Michael Walther. 2013. “Documenting Glacial Changes between 1910, 1970, 1992 and 2010 in the Turgen Mountains, Mongolian Altai, Using Repeat Photographs, Topographic Maps, and Satellite Imagery.” *Geographical Journal* 179 (3): 248–63. https://doi.org/10.1111/j.1475-4959.2012.00486.x.

Kamp, Ulrich, and Caleb G. Pan. 2015. “Inventory of Glaciers in Mongolia, Derived from Landsat Imagery from 1989 to 2011.” *Geografiska Annaler, Series A: Physical Geography* 97 (4): 653–69. https://doi.org/10.1111/geoa.12105.

Kargel, Jeffrey S., Michael J. Abrams, Michael P. Bishop, Andrew Bush, Gordon Hamilton, Hester Jiskoot, Andreas Kääb, et al. 2005. “Multispectral Imaging Contributions to Global Land Ice Measurements from Space.” *Remote Sensing of Environment* 99 (1–2): 187–219. https://doi.org/10.1016/j.rse.2005.07.004.

Khromova, Tatiana, Gennady Nosenko, Stanislav Kutuzov, Anton Muraviev, and

Ludmila Chernova. 2010. “Glacier Area Changes in Northern Eurasia.” *Environmental Research Letters* 9 (2014): 1–11. https://doi.org/10.1088/1748-9326/9/1/015003.

Krumwiede, Brandon S, Ulrich Kamp, Gregory J Leonard, S Kargel, Avirmed Dashtseren, and Michael Walther. 2014. “Recent Glacier Changes in the Mongolian Altai Mountains: Case Studies from Munkh Khairkhan and Tavan Bogd” 2.

Lutz, A. F., W. W. Immerzeel, A. B. Shrestha, and M. F. P. Bierkens. 2014. “Consistent Increase in High Asia’s Runoff Due to Increasing Glacier Melt and Precipitation.” *Nature Climate Change* 4 (7): 587–92. https://doi.org/10.1038/nclimate2237.

Lynch, Colleen M., Iestyn D. Barr, Donal Mullan, and Alastair Ruffell. 2016. “Rapid Glacial Retreat on the Kamchatka Peninsula during the Early 21st Century.” *Cryosphere* 10 (4): 1809–21. https://doi.org/10.5194/tc-10-1809-2016.

Muhlfeld, Clint C., J. Joseph Giersch, F. Richard Hauer, Gregory T. Pederson, Gordon Luikart, Douglas P. Peterson, Christopher C. Downs, and Daniel B. Fagre. 2011. “Climate Change Links Fate of Glaciers and an Endemic Alpine Invertebrate.” *Climatic Change* 106 (2): 337–45. https://doi.org/10.1007/s10584-011-0057-1.

Nuth, C., J. Kohler, M. König, A. Von Deschwanden, J. O. Hagen, A. Kääb, G. Moholdt, and R. Pettersson. 2013. “Decadal Changes from a Multi-Temporal Glacier Inventory of Svalbard.” *Cryosphere* 7 (5): 1603–21. https://doi.org/10.5194/tc-7-1603-2013.

Oerlemans, J. 2005. “Extracting a Climate Signla from 169 Glacier Records.” *Science* 308 (5722): 675–77. https://doi.org/10.1126/science.1107046.

Osipov, E Yu, and O P Osipova. 2014. “Mountain Glaciers of Southeast Siberia : Current State and Changes since the Little Ice Age.” *Annals of Glaciology* 55 (66): 167–76. https://doi.org/10.3189/2014AoG66A135.

Osmonov, Azamat, Tobias Bolch, Chen Xi, Alishir Kurban, and Wanqing Guo. 2013. “Glacier Characteristics and Changes in the Sary-Jaz River Basin (Central Tien Shan, Kyrgyzstan) – 1990–2010.” *Remote Sensing Letters* 4 (8): 725–34. https://doi.org/10.1080/2150704X.2013.789146.

Paul, F, N E Barrand, S Baumann, E Berthier, T Bolch, K Casey, G Nosenko, et al. 2013. “On the Accuracy of Glacier Outlines Derived from Remote-Sensing Data.” *Annals*

of Glaciology 54 (63): 171–82. https://doi.org/10.3189/2013AoG63A296.

Paul, Frank, Andreas Kääb, and Wilfried Haeberli. 2007. "Recent Glacier Changes in the Alps Observed by Satellite : Consequences for Future Monitoring Strategies." *Global and Planetary Change* 56: 111–22. https://doi.org/10.1016/j.gloplacha.2006.07.007.

Paul, Frank, Solveig Winsvold, Andreas Kääb, Thomas Nagler, and Gabriele Schwaizer. 2016. "Glacier Remote Sensing Using Sentinel-2. Part II: Mapping Glacier Extents and Surface Facies, and Comparison to Landsat 8." *Remote Sensing* 8 (7): 575. https://doi.org/10.3390/rs8070575.

Pope, Allen, W Gareth Rees, Adrian J Fox, and Andrew Fleming. 2014. "Open Access Data in Polar and Cryospheric Remote Sensing," 6183–6220. https://doi.org/10.3390/rs6076183.

Racoviteanu, A. E., Y. Arnaud, M. W. Williams, and W. F. Manley. 2015. "Spatial Patterns in Glacier Characteristics and Area Changes from 1962 to 2006 in the Kanchenjunga-Sikkim Area, Eastern Himalaya." *Cryosphere* 9 (2): 505–23. https://doi.org/10.5194/tc-9-505-2015.

Racoviteanu, Adina E., Frank Paul, Bruce Raup, Siri Jodha Singh Khalsa, and Richard Armstrong. 2009. "Challenges and Recommendations in Mapping of Glacier Parameters from Space: Results of the 2008 Global Land Ice Measurements from Space (GLIMS) Workshop, Boulder, Colorado, USA." *Annals of Glaciology* 50 (53): 53–69. https://doi.org/10.3189/172756410790595804.

Raup, Bruce, Andreas Kääb, Jeffrey S. Kargel, Michael P. Bishop, Gordon Hamilton, Ella Lee, Frank Paul, et al. 2007. "Remote Sensing and GIS Technology in the Global Land Ice Measurements from Space (GLIMS) Project." *Computers and Geosciences* 33 (1): 104–25. https://doi.org/10.1016/j.cageo.2006.05.015.

Roy, D. P., M. A. Wulder, T. R. Loveland, Woodcock C.E., R. G. Allen, M. C. Anderson, D. Helder, et al. 2014. "Landsat-8: Science and Product Vision for Terrestrial Global Change Research." *Remote Sensing of Environment* 145. Elsevier B.V.: 154–72. https://doi.org/10.1016/j.rse.2014.02.001.

Shahgedanova, Maria, Gennady Nosenko, Tatyana Khromova, and Anton Muraveyev. 2010. "Glacier Shrinkage and Climatic Change in the Russian Altai from the Mid -

20th Century : An Assessment Using Remote Sensing and PRECIS Regional Climate Model." *Journal of Geophysical Research* 115: 1–12. https://doi.org/10.1029/2009JD012976.

Shinneman, a. L.C., C. E. Umbanhowar, M. B. Edlund, and N. Soninkhishig. 2010. "Late-Holocene Moisture Balance Inferred from Diatom and Lake Sediment Records in Western Mongolia." *The Holocene* 20 (1): 123–38. https://doi.org/10.1177/0959683609348861.

Stokes, Chris R., Maria Shahgedanova, Ian S. Evans, and Victor V. Popovnin. 2013. "Accelerated Loss of Alpine Glaciers in the Kodar Mountains, South-Eastern Siberia." *Global and Planetary Change* 101. Elsevier B.V.: 82–96. https://doi.org/10.1016/j.gloplacha.2012.12.010.

Surazakov, a B, V B Aizen, E M Aizen, and S a Nikitin. 2007. "Glacier Changes in the Siberian Altai Mountains, Ob River Basin, (1952–2006) Estimated with High Resolution Imagery." *Environmental Research Letters* 2 (4): 045017. https://doi.org/10.1088/1748-9326/2/4/045017.

Syromyatina, M. V., Y. N. Kurochkin, D. P. Bliakharskii, and K. V. Chistyakov. 2015. "Current Dynamics of Glaciers in the Tavan Bogd Mountains (Northwest Mongolia)." *Environmental Earth Sciences* 74 (3). Springer Berlin Heidelberg: 1905–14. https://doi.org/10.1007/s12665-015-4606-1.

Tennant, C., B. Menounos, R. Wheate, and J. J. Clague. 2012. "Area Change of Glaciers in the Canadian Rocky Mountains, 1919 to 2006." *Cryosphere* 6 (6): 1541–52. https://doi.org/10.5194/tc-6-1541-2012.

Tielidze, Levan. 2016. "Glaciers Change over the Last Century, Caucasus Mountains, Georgia, Observed by the Old Topographical Maps, Landsat and ASTER Satellite Imagery." *Cryosphere* 10 (4): 713–25. https://doi.org/10.5194/tcd-9-3777-2015.

Tsutomu, Kadota, and Davaa Gombo. 2007. "Recent Glacier Variations in Mongolia." *Annals of Glaciology* 46: 185–88.

Winsvold, Solveig, Andreas Kääb, and Christopher Nuth. 2016. "Regional Glacier Mapping Using Optical Satellite Data Time Series." *IEEE Journal of Selected Topics in Applied Earth Observations and Remote Sensing* 9 (8): 3698–3711. https://doi.org/10.1109/JSTARS.2016.2527063.

Wulder, Michael A, Jeffrey G Masek, Warren B Cohen, Thomas R Loveland, and Curtis E Woodcock. 2012. “Remote Sensing of Environment Opening the Archive : How Free Data Has Enabled the Science and Monitoring Promise of Landsat.” *Remote Sensing of Environment* 122. Elsevier B.V.: 2–10. https://doi.org/10.1016/j.rse.2012.01.010.

Zemp, Michael, Holger Frey, Isabelle Gärtner-Roer, Samuel U. Nussbaumer, Martin Hoelzle, Frank Paul, Wilfried Haeberli, et al. 2015. “Historically Unprecedented Global Glacier Decline in the Early 21st Century.” *Journal of Glaciology* 61 (228): 745–62. https://doi.org/10.3189/2015JoG15J017.

Zhang, Yong, Hiroyuki Enomoto, Tetsuo Ohata, Hideyuki Kitabata, Tsutomu Kadota, and Yukiko Hirabayashi. 2016. “Projections of Glacier Change in the Altai Mountains under Twenty-First Century Climate Scenarios.” *Climate Dynamics*. Springer Berlin Heidelberg. https://doi.org/10.1007/s00382-016-3006-x.

Tables

Table 2.1 Information for the scenes used for the updated glacier inventory, including the classification threshold used for each image (Described in section 3.1).

Satellite	Date	Path/Row or Tile #	Sensor	Threshold
Landsat 8	9022014	141/26	OLI	1.21
Landsat 8	8242016	140/27	OLI	2.24
Landsat 8	8022015	143/26	OLI	1.24
Landsat 8	8272015	142/26	OLI	1.50
Sentinel 2A	8112016	T46TCS	MSI	3.05
Sentinel 2A	9062016	T45UXP	MSI	2.21
Sentinel 2A	9062016	T45UXRs	MSI	3.52
Sentinel 2A	9062016	T45UWQ	MSI	3.39
Sentinel 2A	9132016	T46UCU	MSI	4.70
Sentinel 2A	8312016	T46TES	MSI	3.40
Sentinel 2A	9132016	T45TYN	MSI	2.06
Sentinel 2A	9132016	T45UYP	MSI	3.38

Table 2.2 Climate stations utilized for climatic trend derivations within the Altai region ("Coverage" is the temporal data availability for a specific period).

Station	Latitude [dd]	Longitude [dd]	Elevation [m a.s.l.]	Period	Coverage [%]
Mongolia					
Baitag	46.12	91.47	1186	1963-2015	65
Khovd	48.02	91.57	1405	1962-2015	96
Omno Gobi	49.02	91.72	1590	1973-2015	62
Ulaangom	49.80	92.08	936	1962-2015	96
Ulgi	48.93	89.93	1715	1962-2015	57
Russia					
Kosch Agach	50.00	88.68	1759	1962-2015	94

Table 2.3 Mapping results from the 1990-2010 glacier inventory after Kamp & Pan (2015) and for the new 2016 glacier inventory (area in km^2; bracketed numbers indicate the number of glaciers). See Section 3.3 of the text.

	Year/Period	Total	Subsample (206)
Area [km^2]	1990	443.1 ± 54.9 [690] 515*	391.38 ± 41.7
	2000	428.6 ± 59 [716]	281.88 ± 31.8
	2010	371.1 ± 54.4 [671]	250.1 ± 36.7
	2016	334 ± 44.4 [627]	223.9 ± 29.8
Absolute Change [km^2]	1990-2016	181.0 ± 8.4	167.48 ± 11.36
	1990-2000	86.4 ± 3.3	109.5 ± 7.4
	2000-2010	57.5 ± 2.2	31.78 ± 2.2
	2010-2016	66.5 ± 2.7	26.2 ± 1.8
Rate of Change [km^2 yr^{-1}]	1990-2016	7.0 ± 0.3	6.4 ± 0.4
	1990-2000	8.6 ± 0.3	10.9 ± 0.8
	2000-2010	5.8 ± 0.2	3.2 ± 0.2
	2010-2016	11.1 ± 0.4	4.4 ± 0.3

** This is the corrected assumed total glacier area that makes up for missing satellite imagery. See the text for explanations.*

Table 2.4 Temporal changes of parameters of glaciers in the Mongolian Altai using the 206 subsampled glaciers.

Glacier Parameter	1990	2000	2010	2016
Mean Elevation [m a.s.l.]	3437	3442	3450	3470
Minimum Elevation [m a.s.l.]	2586	2610	2704	2709
Elevation Range [m]	412	353	318	303
Mean Slope [°]	20	20	20	20
Mean Aspect [°]	148	147	144	143

Table 2.5 Trend coefficients (°C yr^{-1}) of temperature derived as seasonal aggregate means from six climate stations within the Mongolian Altai.

Period	Winter	Spring	Summer	Fall	Annual
1962-2015	0.041	0.028	0.019	0.041	0.032
1962-1989	0.052	-0.007	0.000	0.065	0.019
1989-2015	-0.108	0.045	0.035	-0.046	-0.007
1989-2000	0.028	0.137	0.118	-0.152	0.038
2000-2010	-0.183	-0.061	-0.015	0.232	-0.009
2010-2015	0.183	0.196	0.069	-0.078	0.422

Table 2.6 Trend coefficients (mm yr^{-1}) of precipitation derived as seasonal aggregate means from within six climate stations with the Mongolian Altai.

Period	Winter	Spring	Summer	Fall	Annual
1962-2015	0.010	0.133	-0.350	0.239	0.063
1962-1989	-0.177	0.263	-0.499	0.048	-0.365
1989-2015	0.284	0.335	-2.085	0.381	-0.931
1989-2000	0.236	0.074	-3.110	1.220	-1.581
2000-2010	1.388	-0.787	-0.174	0.018	0.445
2010-2015	-0.310	6.346	-5.575	5.285	9.283

Figures

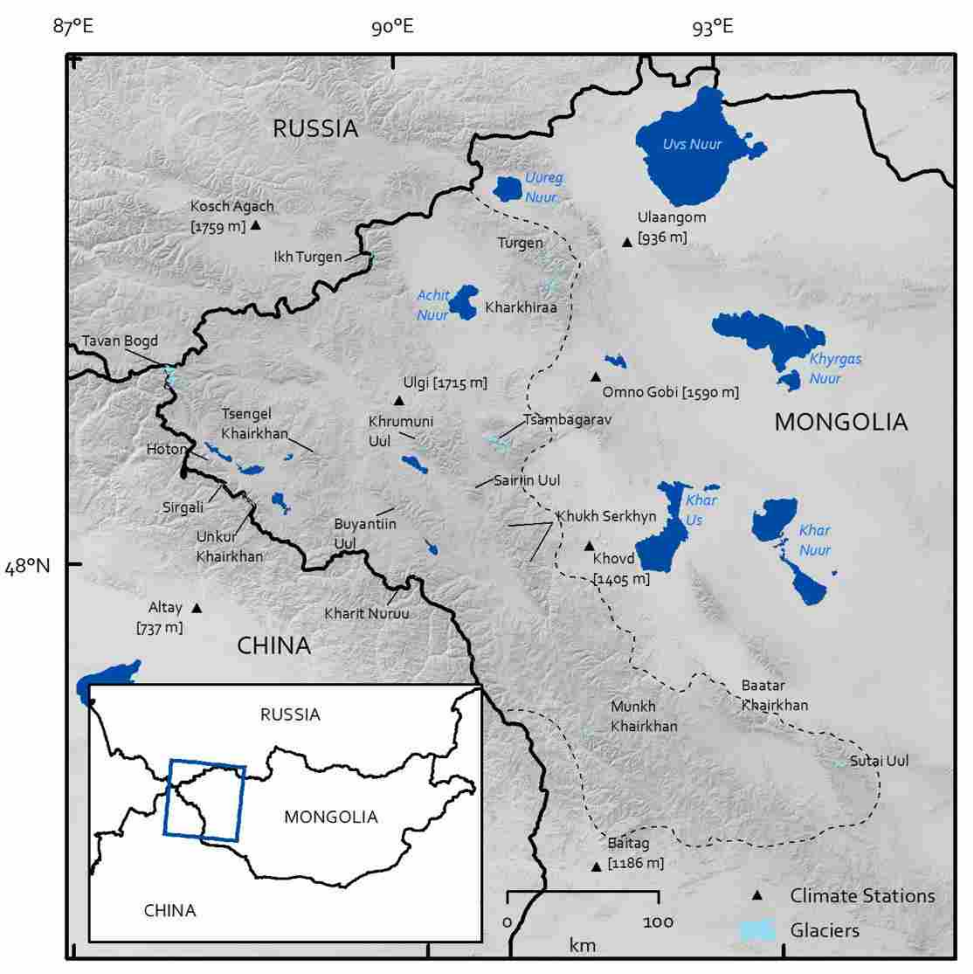

Figure 2.1 Overview map of the Altai Mountains of Mongolia (defined by the dashed line). Glaciated mountain ranges are identified within the greater Altai complex.

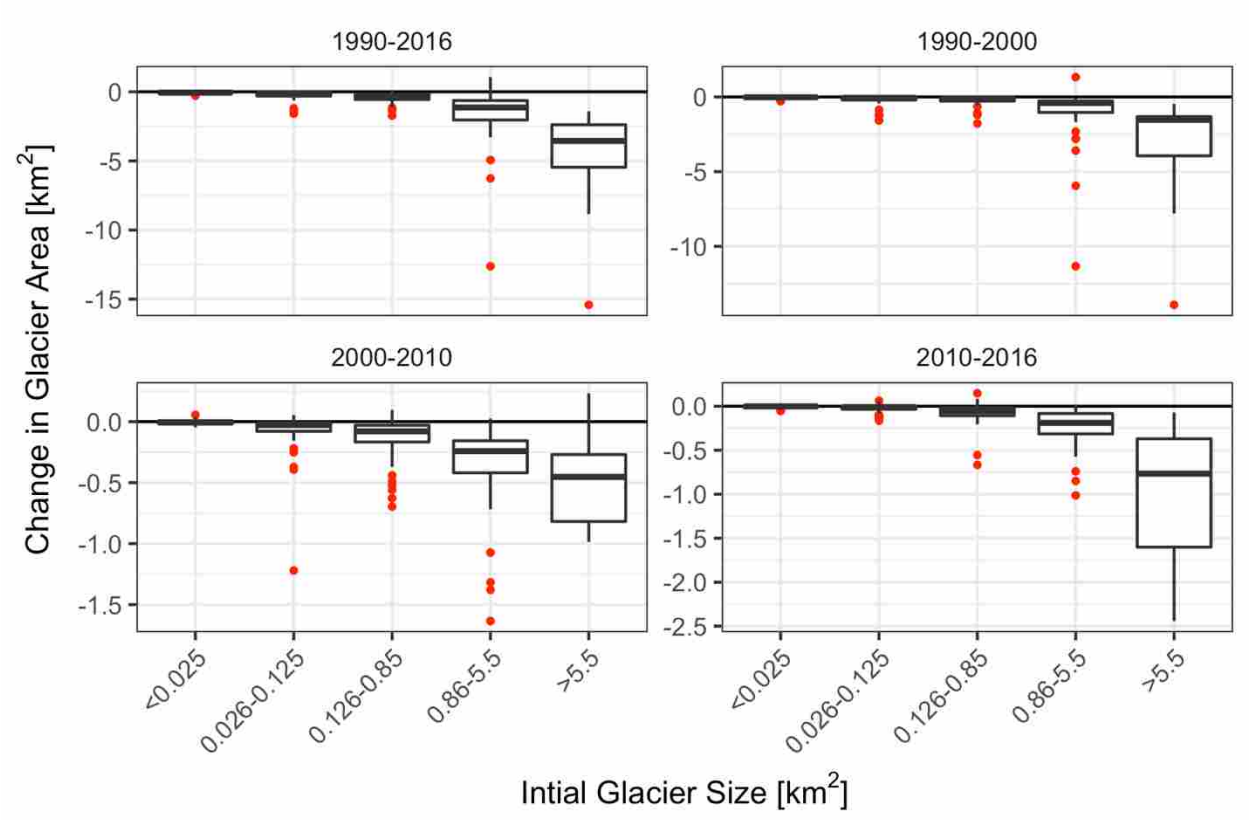

Figure 2.2a Boxplots of absolute change in glacier area by class size in the Mongolian Altai. Red dots indicate outliers.

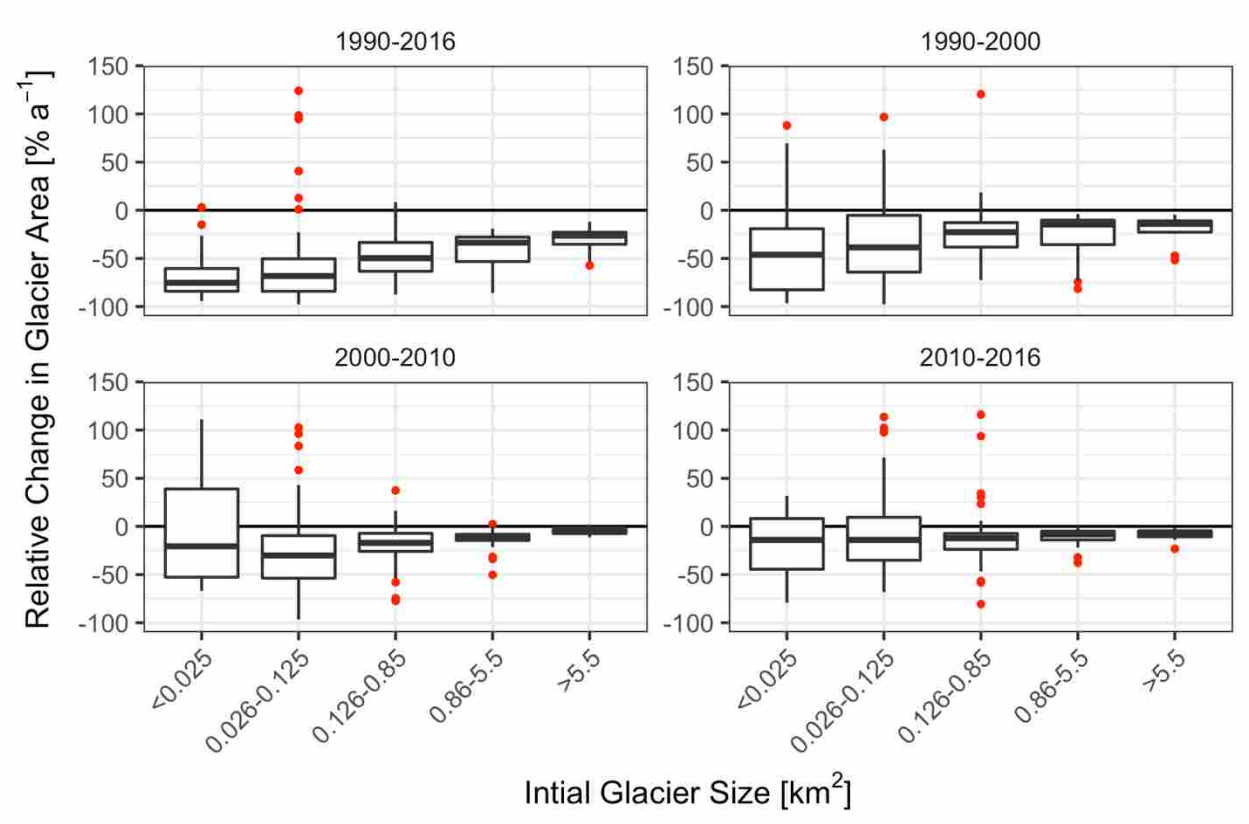

Figure 2.2b Boxplots of relative change in glacier area by class size in the Mongolian Altai. Red dots indicate outliers.

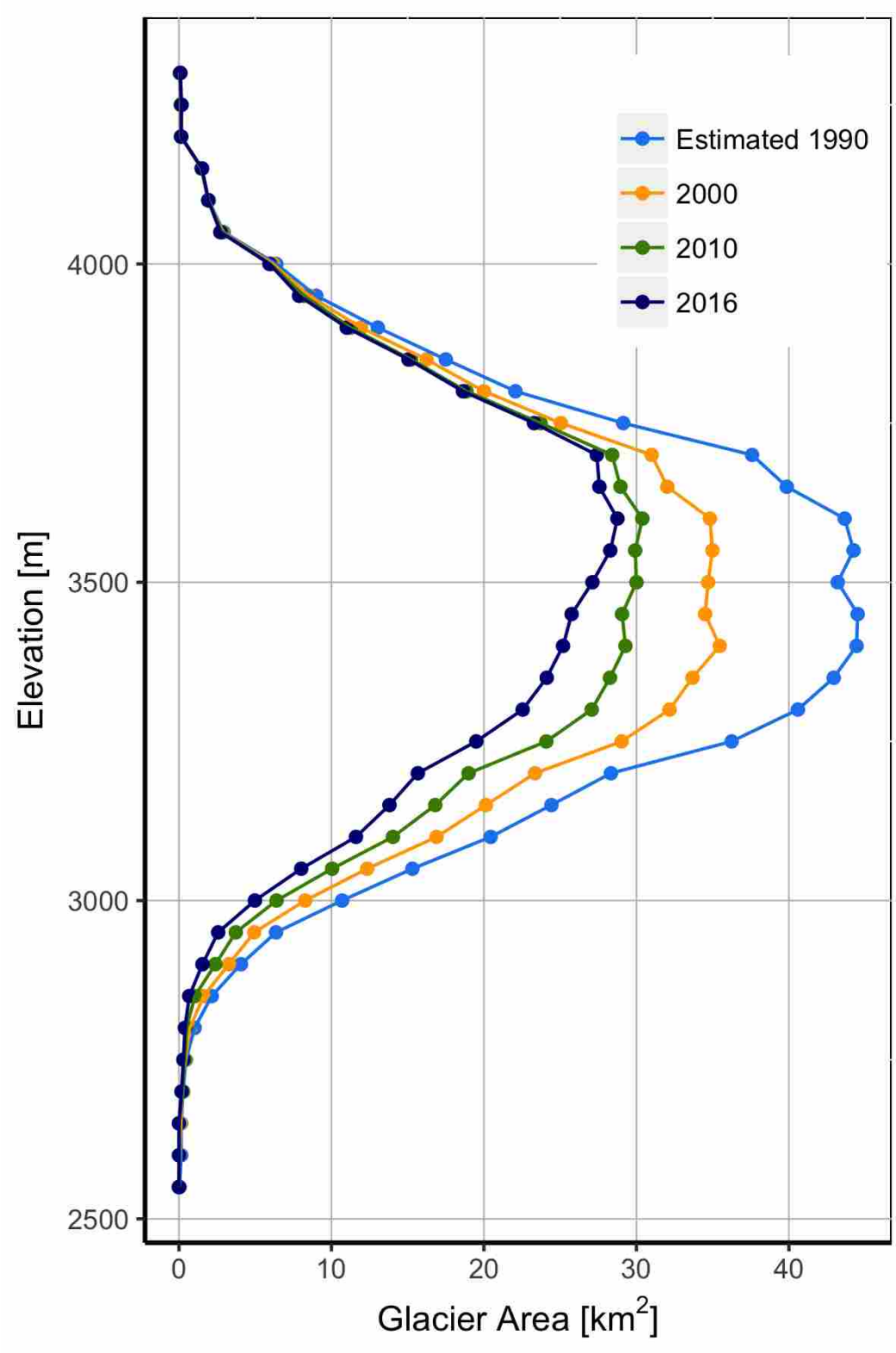

Figure 2.3 Hypsometries of glaciers in the Mongolian Altai, including debris-covered glaciers.

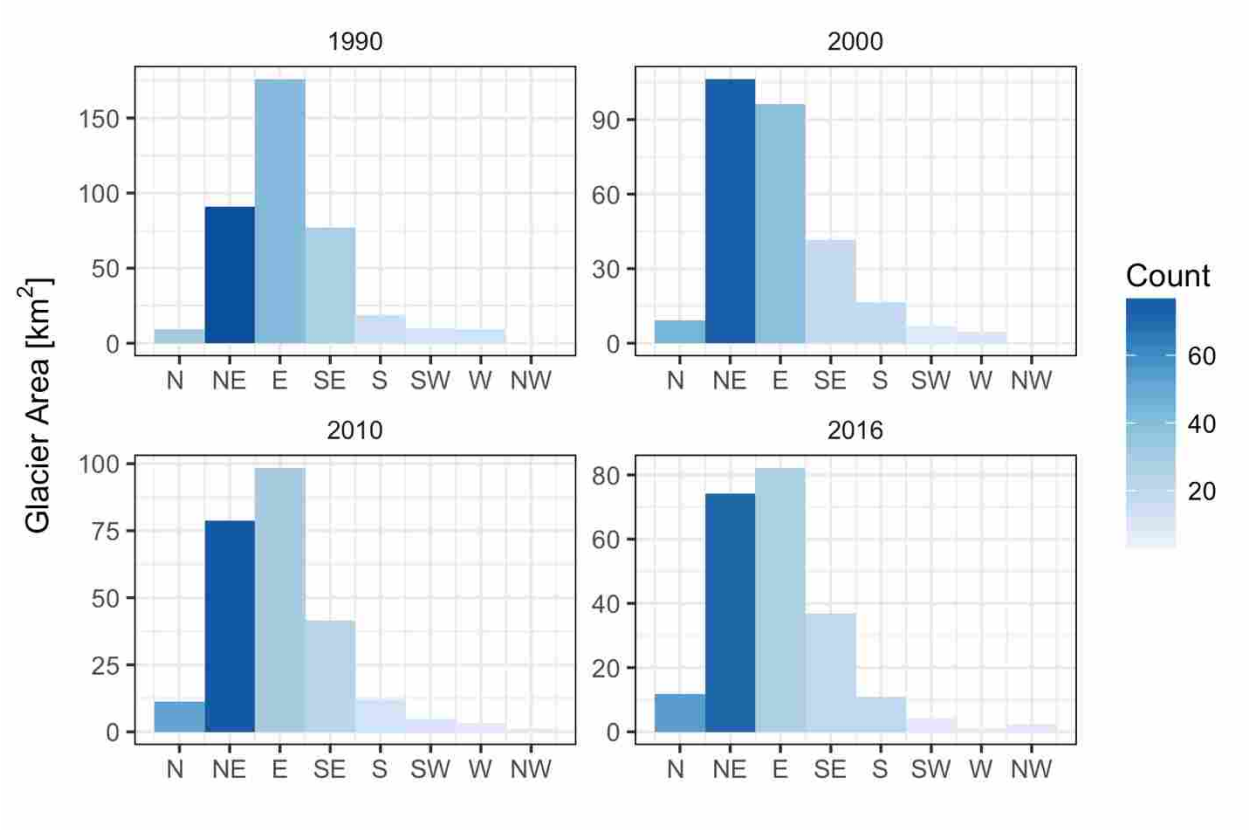

Figure 2.4 Distribution of area and number of glaciers by aspect in the Mongolian Altai.

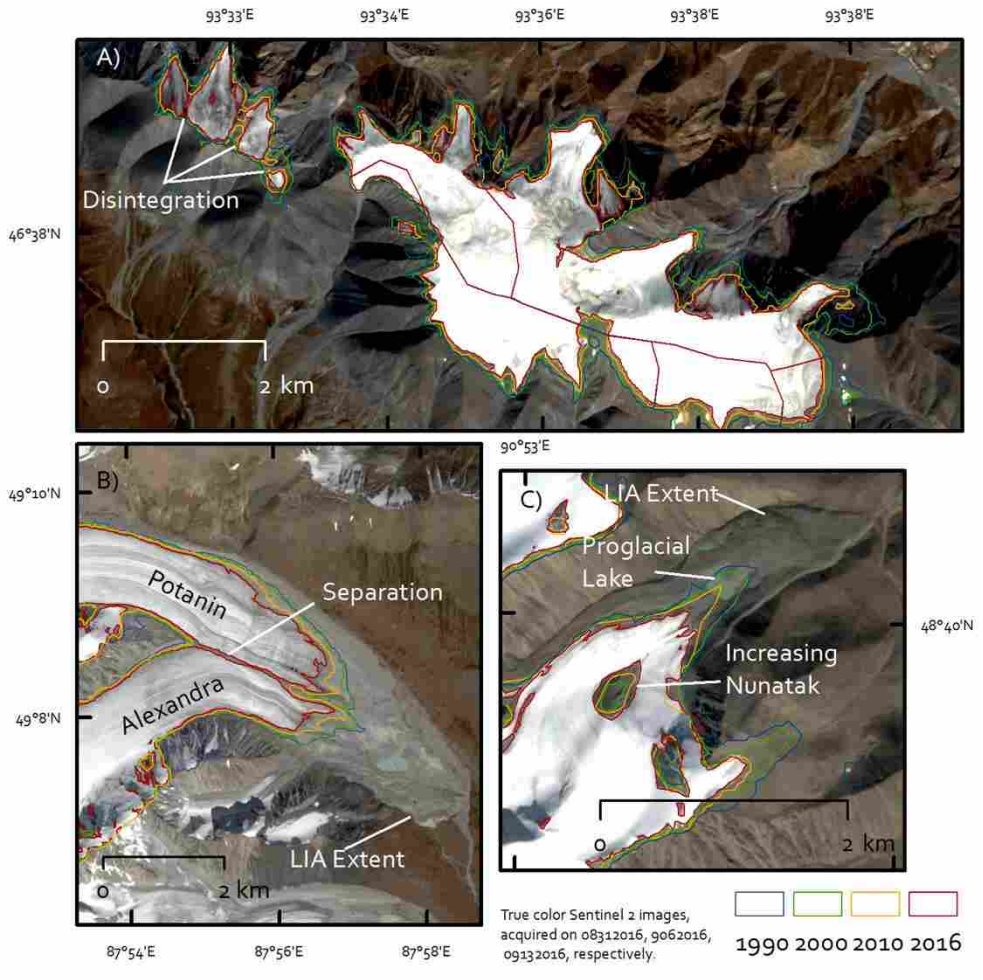

Figure 2.5 Examples of glacier change in the Mongolian Altai. A) Sutai Uul in the Southern Altai exhibits the disintegration of a larger glacier into smaller glaciers, a common trend throughout the region. B) The tongues of Mongolia's two largest glaciers, Potanin and Alexandra, began separating from each other for the first time in 2016. The distance of Alexandra to the end of the Little Ice Age (LIA) extent was about 2.6 km. From 1990-2016, the terminus of (originally combined) Potanin/Alexandra glacier retreated by 597 m. C) Tsambagarav Uul in the Central Altai demonstrates the development of a proglacial lake between 1990 and 2000, and a "growing" nunatak in the center of the lower portion of the glacier. The distance between the LIA extent and the 2016 termini was 1.6 km. Between 1990 and 2016, the terminus retreated by 636 m.

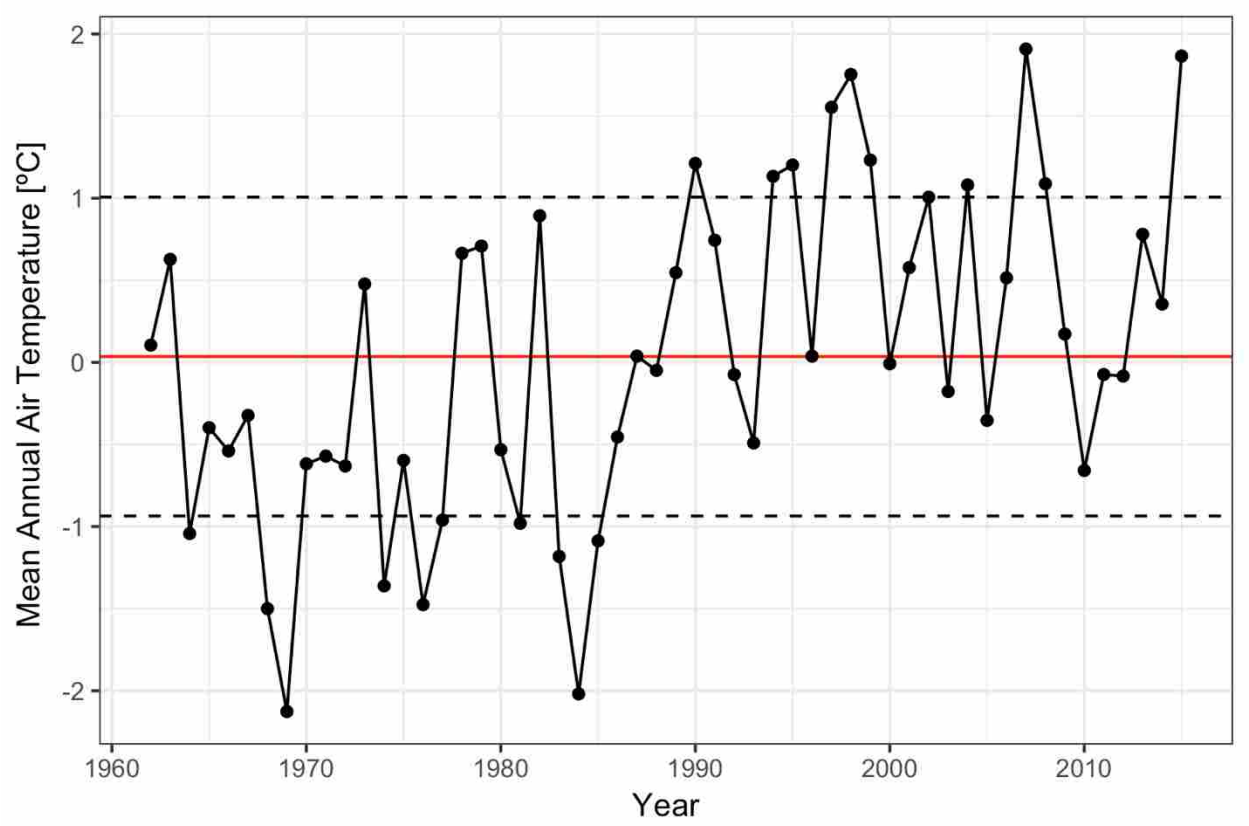

Figure 2.6 Mean annual air temperature from 1962-2015 in the Mongolian Altai. Red line indicates the mean MAAT. Dashed black lines indicate one standard deviation.

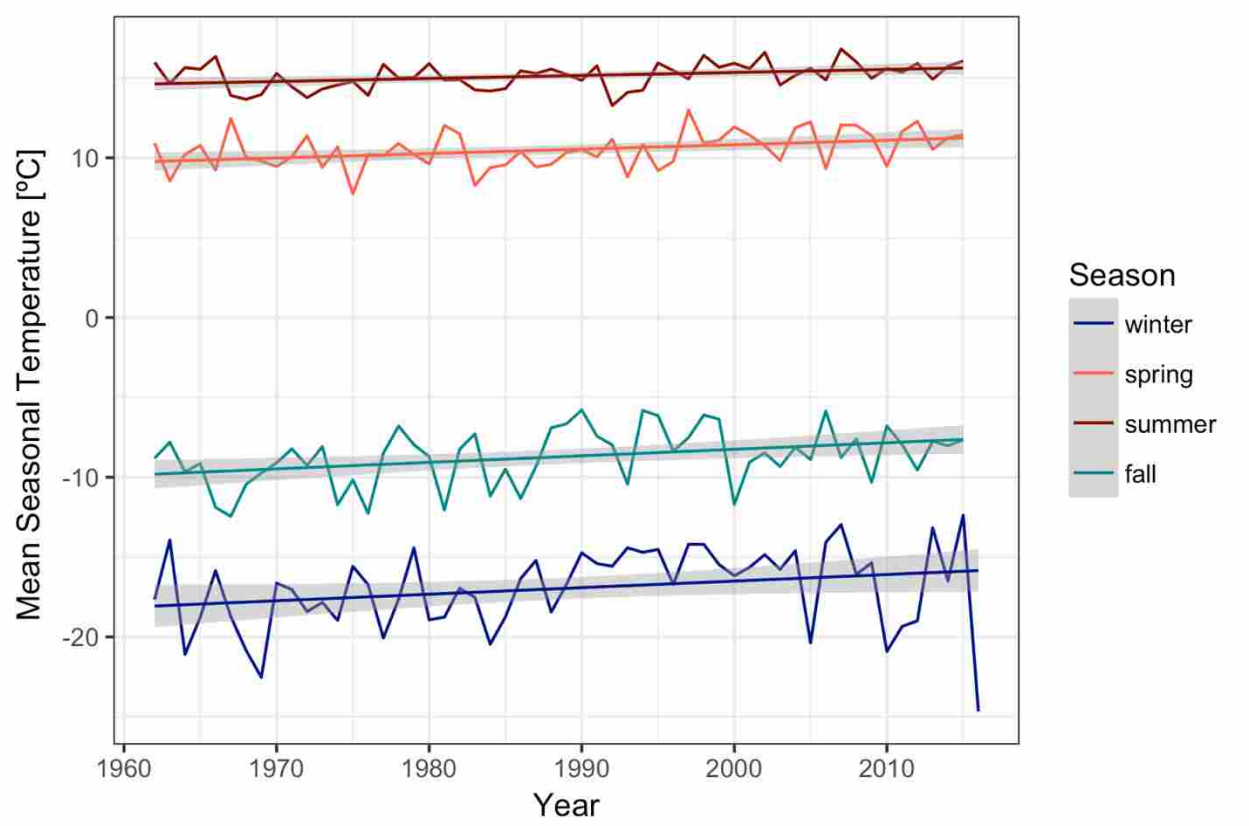

Figure 2.7 Seasonal temperature trends (including the standard deviation) between 1962 and 2015, derived from six climate stations within the Altai Mountains. Increasing temperature trends can be observed for all seasons.

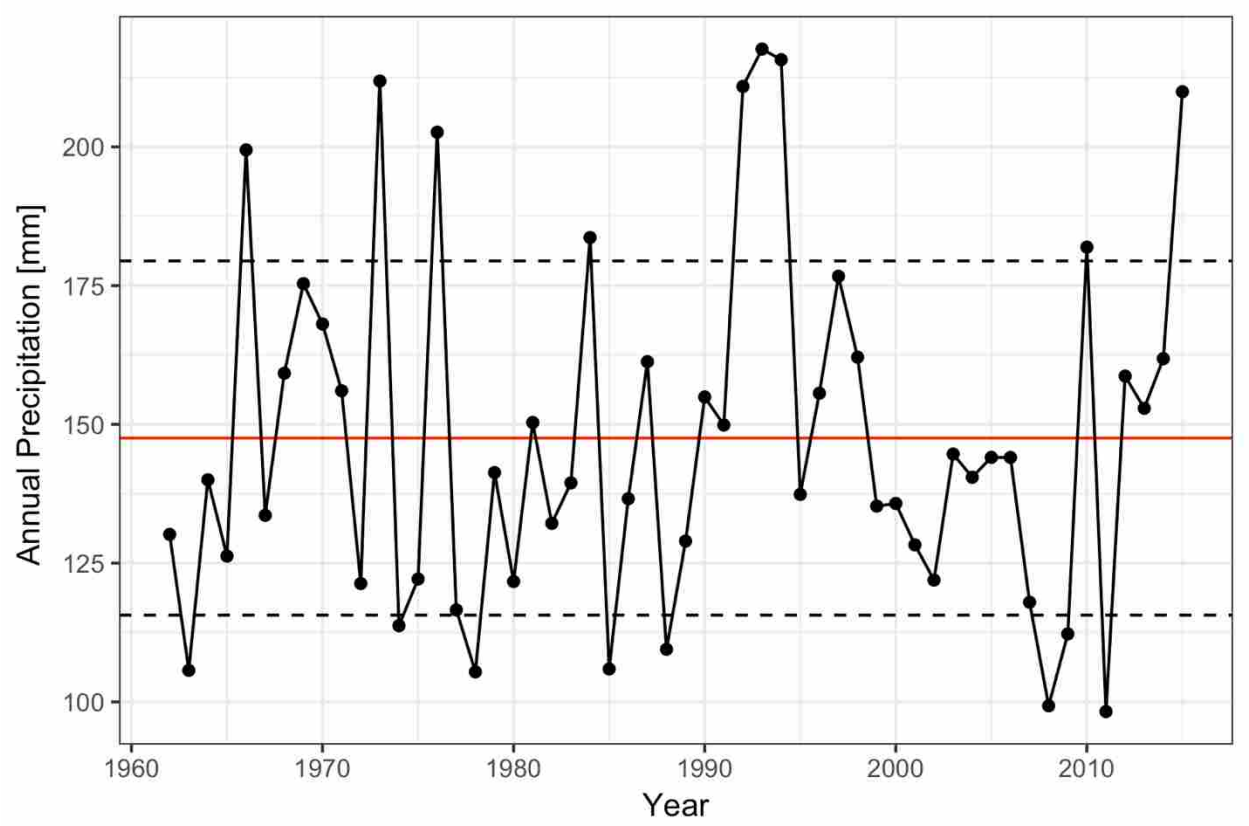

Figure 2.8 Annual precipitation from 1962-2015. Red line indicates the mean annual precipitation. Dashed black lines indicate one standard deviation.

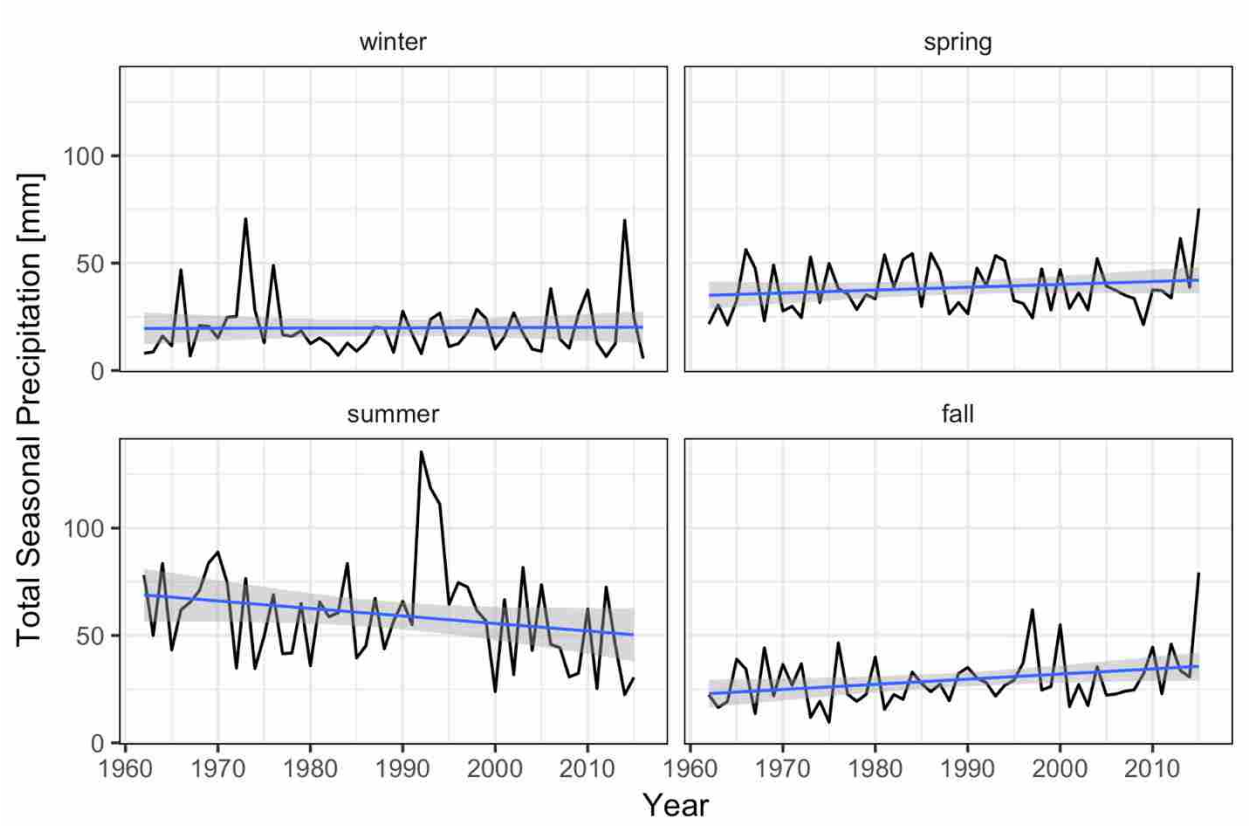

Figure 2.9 Seasonal precipitation trends (including the standard deviation) between 1962 and 2015, derived from six climate stations within the Altai Mountains. Decreasing summer precipitation can be observed while increasing precipitation trends are occurring in the fall and spring.

CHAPTER 3

Understanding the contribution and importance of glaciers to regional hydrology in Mongolia's Altai Mountains

Corresponding publication:

Pan, C. G., Kamp, U., Munkhjargal, M., Halvorson, S. J., Avirmed, D., and Walther, M. (submitted) Understanding the contribution and importance of glaciers to regional hydrology in Mongolia's Altai Mountains. *Mountain Research and Development.*

3.1 Abstract

In the (semi) arid climate of Mongolia, glaciers are critical contributors to water resources, particularly during the dry summer months. But as the glaciers in Mongolia's Altai Mountains continue to recede under unprecedented climatic change, our knowledge is still limited with respect to the overall contribution of glacier melt to the regional hydrology. This study investigates the impact of glacier recession on the regional hydrology of the Upper Khovd River Basin (UKRB) in northwestern Mongolia. The analysis coupled recent observations acquired through the glaciological method with satellite-derived glacier records to estimate the relative contribution of glaciers to the regional hydrology using a simple ice ablation model. The model was operated using a mass balance gradient (MBG) of 0.32 m water equivalent (w.e.) 100 m^{-1} for the years 2000, 2010, and 2016. Warm and cold conditions were also simulated by applying a sensitivity analysis of ±0.1 m w.e. 100 m^{-1}. Results showed that the glaciers contributed 13.7% to the UKRB's water resources in 2000, and that this contribution decreased to 11.5% in 2016. Hypsometries indicated that the glaciers decreased in area at all elevations, indicating that only small accumulation zones exist. Hence, our simulations of warmer conditions are likely more representative of the glacier contribution to total runoff, estimated at 18% in 2000 and 15% in 2016. The pattern of decreasing glacier melt to the regional hydrology indicates that the UKRB glaciers have passed the tipping point of an increased contribution that first follows enhanced melting. In light of the projected ongoing glacier recession, glaciers will contribute continuously less to the total water budget and, hence, to water availability.

3.2 Introduction

The mountains of Mongolia and Central Asia are uniquely positioned in an extreme continental climate that governs a semi-arid to arid landscape. Arid mountainous landscapes are limited by the availability of water, naturally reflected in the dry-tolerant grass and scrublands that dominate the region (Li et al. 2015). However, as Central Asia's populations increase, water demand will increase in synchronous, placing greater importance on regional water security issues (Karthe et al. 2017). Water security and related vulnerabilities are exasperated through several mechanisms in Central Asia, for example: agricultural consumption as a result of transitioning dry-tolerant vegetation for crops that are only possible by irrigation (Mosello 2008); the development of hydropower plants (HPPs) as a solution to increasing energy demand but also as regulators of downstream water flows (Gaudard et al. 2014); and a continued amplified warming (Chen et al. 2009) coupled with decreasing precipitation (Batima 2005). For much of Central Asia, the high mountains of the Pamirs, Tian Shan, and Altai are perceived as the source of water for much of the downstream populations (Sorg et al. 2012).

The glaciers and snowpack in Central Asia's mountains are known as the regional 'water towers' or 'wet islands' – an oasis providing water to the surrounding arid landscape and downstream services (Viviroli et al. 2007). Yet, as accelerated glacier recession continues in the twenty-first century with amplified warming (Zemp et al. 2015), understanding the role of glacier melt to the regional hydrology has become urgent and has received a great deal of attention from scientists, water planners, and development organizations. Much of the glacio-hydrologic research has focused on the Amu Darya and Syr Darya as these two basins extend to seven Central Asian countries. Particular interest has been given to their glaciated headwaters including sub-basins of the Tanimas in Tajikistan and of the Naryn in Kyrgyzstan (Wilfried Hagg et al. 2013; W Hagg et al. 2011). This melt-water is critical for sustaining water levels in the semi-arid to arid climates with little summer precipitation (Sorg et al. 2012). However, at the eastern fringes of Central Asia, in Mongolia, little scientific attention has been focused on analyzing the relationship of glaciers to regional hydrology.

Since the collapse of the Soviet Union in 1991, the trajectory of Mongolia's water availability has been connected to the country's top economic sectors. Mining as the largest economic driver has significantly increased since Mongolia's introduction to the free-market economy and is one of the country's most water-intensive industries (Bury et al. 2013; Karthe et al. 2017). Further, with accelerated attempts to reduce agricultural imports from Russia and China, Mongolia has rapidly developed agricultural production since 2008, consequently increasing the extent of irrigated land (Priess et al. 2011). In 2011, 93% of Mongolia's energy was derived from fossil fuels, 6% was imported from Russia, and only 1% was produced from hydropower (UNDP/ICSHP 2013). To transition away from fossil-heavy energy and become less dependent on energy imports, Mongolia dictated in its 2005 *National Renewable Energy Program* to increase its renewable energy supply to 20-25% by 2020 (Ministry of Energy w.y.). Hence, Mongolia is at the social-ecological crossroads in meeting water-intensive demands in a water-restricted country. But relative to regions of Central Asia affiliated with the Amu Darya and Syr Darya, the glaciers that make up Mongolia's 'water towers' are significantly smaller and underrepresented in the scientific literature.

Since 2010, international attention has focused on water-related issues across Mongolia, including the German-Mongolian sponsored research project Integrated Water Resources Management in Central Asia: Model Region Mongolia (IWRM MoMo) (Karthe et al. 2014) and the international Global Land Ice Measurements from Space (GLIMS) initiative that offers open access to glacier datasets (Kamp and Pan 2015). These relatively recent efforts support Mongolia's *Law on Water* from 2004 which created a framework for the establishment of broad stakeholder representation in the form of River Basin Councils (RBCs) charged with the implementation of an IWRM across 29 designated river basins, identified by the Ministry for Environment and Tourism (MET) (Horlemann and Dombrowsky 2012; Karthe et al. 2015)). In 2009, the MET in its *National Programme on Water* specified details on sustainable use, protection and conservation of water resources. Priority areas of recent research organized by these initiatives and legislation focus on rangeland ecology, water security, and the adoption of spatial units (river basins) to evaluate the human and biophysical influences on regional water resources.

This article seeks to build upon and extend environmental change research efforts in Central Asia in several inter-connected ways. First, our intent is to contribute to an understanding of water security issues in western Mongolia by bringing attention to the importance of glacier melt to regional hydrology; we couple recent *in situ* glaciological methods (Konya et al. 2013, Syromyatina et al. 2015) with remote sensing derived glacier records within an ice ablation model (Alford et al. 1992, Racoviteanu et al. 2013). In addition, as Mongolia's glaciers recede (Pan et al. 2017), we also seek to contextualize the importance of glacier melt to regional water security as Mongolia's climate and social-ecological systems rapidly change.

3.3 Study Area: Hydrologic Change in the Altai Mountains

In Mongolia, our knowledge of glacier contributions to regional hydrology is still limited owing to the overall poor quality of the sparse regional hydrographic network and data as well as limited observations collected using glaciological methods. Yet, streamflow in many glaciated catchments has been observed to increase in recent years, relative to non-glaciated basins (Davaa 2010). This is in line with the theoretical underpinnings that glacier recession will initially increase the stream discharge as a result of enhanced ice melting (Bury et al. 2013). Hence, for now, we know that at a minimum, glaciers are an important and significant contributor to regional hydrology.

Regardless of the status of glaciers in Mongolia, part of the strategy to secure water resources in the face of rapid economic and urban development has been the construction of several HPPs across Mongolia. Currently, Mongolia has 13 such HPPs, and eight additional ones are in the planning stage at some of the country's largest rivers. In the Mongolian Altai, three smaller HPPs are situated in its central parts, while the new 12 MW Durgun HPP and some diesel generators produce energy for its northern parts, where consumption in the Western Energy System more than doubled from 2008 to 2014 (UNIDO/ICSHP 2013, Ministry of Energy 2015). Of this total energy consumption, 22% was supplied by Durgun HPP, 76.5% by imports from Russia, and 1.5% by imports from China; the costs of the imported energy was six times the costs of local energy production. The Durgun HPP was erected between 2004 and 2008 and is expected to

meet more than 90% of the electricity demand of the three remote western provinces of Bayan Ulgii, Khovd and Uvs (UNFCCC 2005).

The Durgun HPP is located 120 km to the northeast of Khovd, the capital of Khovd Aimag, at the outflow of Khar Us Lake on the Chono Kharaikh River (henceforth referred to as the Durgun Basin). Yet, the primary inflow to Khar Us Lake is the Khovd River, which brings snow and glacier melt from its headwaters in the Altai Mountains. Our study focuses on the Upper Khovd River Basin (UKRB), which is defined as the watershed that contributes to the Khovd River at Ulgii and provides one of the most complete hydrologic datasets in the region. (Figure 3.1). The basin covers a total area of approximately 23,000 km^2 and includes the Tavan Bogd massif, where Mongolia's largest glaciers, Potanin and Alexandra, exist. In 2000, the UKRB contained 345 glaciers with a total area of 170.8 km^2 representing 42% of the entire glacier area in the Altai. In addition to glaciers and snow, the UKRB also has a mosaic of continuous and discontinuous permafrost at varying active layer depths (Dashtseren et al. 2014).

To our knowledge, only one study has quantified the contribution of glaciers to regional hydrology (Davaa *et al.* 2007). The earliest glaciological research in Mongolia used a volume-area scaling approach to determine that the total cumulative volume of glaciers across the country was 62.8 km^3 (Dashdeleg *et al.* 1983). Using an estimated total surface water value of 599 km^3 yr^{-1} and the total volume of glaciers from Dashdeleg *et al.* (1983) as an absolute value of water equivalent, it was determined that the glaciers in Mongolia store an accumulated 10% of the total annual water resources (Davaa *et al.* 2007). Given the relatively small area of glaciers in western Mongolia – the only recently glaciated region in the country – an annual contribution of 10% to the country's total water resources is likely an overestimation.

The Altai has a continental climate with long, cold, and dry winters, and mild and relatively short summers (Rudaya *et al.* 2009). The climate is largely controlled by the westerlies, bringing moisture from the Atlantic and Mediterranean (Blomdin *et al.* 2016). As moisture is brought in from the west, the windward side of the Altai receives most of the annual rainfall at around 1000 mm, whereas the leeward side receives only around 130-400 mm. Generally, the precipitation totals decrease from west to east across the Altai

(Rudaya *et al.* 2009, Lehmkuhl *et al.* 2016). Although the annual precipitation is low, the intensity can be high, potentially experiencing 40-60 mm in a single day. With the fate of these rain events resulting in 90% evaporation, of the remaining 10%, 64% becomes surface runoff and 36% infiltrates the soils (Batima *et al.* 2005). The mean winter temperatures can be as low as -20 °C, and mean summer temperatures can range from 15 to 20 °C (Rudaya et al. 2009; Ganiushkin, Chistyakov, and Kunaeva 2015; Lehmkuhl et al. 2016).

3.4 Data and Methods

In recent years, cryo-hydro-meteorological modeling has gained great prominence but results often vary leading to uncertainties and confusion among users (Alford *et al.* 2014). Therefore, we employ a relatively simple ice ablation model first described by Alford (1992) and later applied in several high mountain regions including the Pamir, Tien Shan, and Nepalese Himalayas (Alford *et al.* 2010, Racoviteanu *et al.* 2013, Alford *et al.* 2015, Kamp *et al.* 2016). The ice ablation model is a heuristic model developed specifically for high mountains, where limited information exists, and requires three input datasets: 1) glacier hypsometries; 2) daily hydrographic measurements; and 3) a mass balance gradient (MBG). Glacier hypsometries were generated from glacier outlines downloaded from the Global Land Ice Measurements from Space (GLIMS) initiative website for the years 2000, 2010, and 2016 (Table 3.1) (Kamp and Pan 2015, Pan *et al.* 2017). To determine the altitudinal distribution of the glaciers, a 30 m SRTM digital elevation model (DEM) was downloaded from CGIAR CSI (www.cgiar-csi.org). Hydrographic data were acquired from the Mongolian Ministry of Nature and Environment (MNE) and span from 2000 to 2012, with missing observations from 2003 to 2006 (Figure 3.2). Mean daily discharge observations ($m^3\ s^{-1}$) were employed to create total mean daily discharge ($m^3\ day^{-1}$).

The MBG is here defined as the water equivalent of ice melt per one hundred meters of vertical elevation change within a given ablation zone (Racoviteanu *et al.* 2013). More specifically, at the equilibrium line altitude (ELA), the MBG equals zero; for every 100 m below the ELA, the MBG linearly and cumulatively increases by a defined value (meter water equivalent; m w.e.). For this study, the MBG was drawn from the literature. A number of recent studies have published MBGs across Central Asia (Wang *et al.* 2012,

Kronenberg *et al.* 2016), but only a few exist for the Altai Mountains (Konya *et al.* 2013, Syromyatina *et al.* 2015). Konya *et al.* (2013) calculated a MBG of 0.55 m w.e. 100 m^{-1} at Potanin glacier during the 2008 ablation season, and 0.41 m w.e. 100 m^{-1} at Maliy Aktru, a glacier north of Potanin in the Russian Altai. Syromyatina *et al.* (2015) presented a MBG of 0.01 m w.e. 100 m^{-1} during the ablation season of 2014 for Kozlov Glacier, a south-facing glacier, just north of Khoton Nuur in Tavan Bogd. We used the mean of these three MBGs, i.e. 0.32 m w.e. 100 m^{-1}. A sensitivity analysis of ± 0.1 m w.e. 100 m^{-1} was applied to accommodate for the spatial heterogeneity of the MBG and to simulate below and above normal seasonal temperatures.

This study is concerned with the glacier melt component of the annual streamflow, hence, the hydrologic continuity equation describing the relationship between glaciers and streamflow volume is:

$$Q_t = R + M_s + M_i - E_t \pm \Delta_s \quad (1)$$

Where Q_t is total runoff, R is input as rain, M_s is snowmelt runoff, M_i is glacier melt runoff (ablation), E_t is evaporation, and Δ_s is the change in storage as snow, glacier ice, or groundwater. In the glacier ablation zone, evaporation is assumed to be minimal, and the change in groundwater storage for the hydrologic year is assumed to be zero (Rasmussen and Tangborn 1976). As a first approximation, the hydrologic continuity equation reduces to a determination of the relative importance of snow melt and glacier ablation in the hydrologic regime of the UKRB:

$$Q_t = M_s + M_i \quad (2)$$

The ice ablation model takes the following form:

$$Q = \sum_{=1}^{n} M_i * A_i \quad (3)$$

Where Q is the glacier melt volume in cubic meters, b_n is the specific ice melt for a given elevation range, and A_i is the glacier area within the given elevation range (Racoviteanu *et al.* 2013). The employed model deviated from previous studies by using s glacier-specific ELAs rather than a basin-wide ELA. By applying glacier-specific ELAs, Equation 3 was

applied to each glacier in the UKRB, and we then summed to acquire the total annual specific glacier melt.

3.5 Results

Hydrographic data provide a qualitative assessment in the relative contribution of glaciers to streamflow. Within heavily glaciated basins in arid regions, hydrographs will express a second peak during the ablation season, attributed to glacier melt runoff. In the UKRB, the seasonal hydrologic flow peaks in late June and early July indicating the onset of the ablation season as snow cover has melted (Figure 3.3). Since only less than 1% of the UKRB is glaciated, a distinct second peak cannot be easily observed in the hydrograph. However, after the main peak, the total daily discharge decreases sharply before stabilizing in the latter half of July and early August, as glacier meltwater begins to contribute to regional hydrology during the dry periods of summer. The duration between the sharp decrease in total daily discharge and the stabilized period can be described as the lag time between the initiation of the ablation season and the moment the early season glacier meltwater reaches Ulgii.

Our results determined that the glacier runoff was 0.083 km^3 in 2000, 0.08 km^3 in 2010, and 0.07 km^3 in 2016. Sensitivity analysis results showed that during periods of cooler temperatures, glacier runoff for these same years was as low as 0.057 km^3, 0.055 km^3, and 0.048 km^3. However, during periods of warmer temperatures, melt runoff from glaciers can be potentially significant and amounted to 0.11 km^3, 0.11 km^3, and 0.09 km^3 (Table 3.2). While such numbers may seem rather negligible when compared to other heavily glaciated basins, they must be interpreted in the context of the small mean annual discharge at the Ulgii station at only 1.64 $km^3\ yr^{-1}$: in the UKRB, the glaciers contributed 13.7% in 2000 and 13.1% in 2010 to the total discharge, and in the following years until 2016, this contribution decreased to 11.5%. For simulated conditions of cooler than average temperatures, glaciers contributed between 9.4% and 7.9% in all three years, while it was between 15.0% and 18.0% during simulated conditions of warmer than average temperatures (Table 3.3). In semi-arid to arid climates, glacier melt runoff is most critical during the dry summer periods (Viviroli *et al.* 2007). During the ablation period, the mean annual discharge at the Ulgii station was 0.32 km^3 and results in a significant

contribution from glaciers of 26% in 2000, 25% in 2010, and 22% in 2016. In addition, using the simulated warm conditions during 2016, the glacier melt runoff contributed 29% to the total runoff in the UKRB.

Temporal changes in glacier runoff indicated a reduction in glacier area of 19.3 km^2 from 2000 to 2010, and in both years the glaciers contributed almost the same amount to the total basin discharge. However, from 2010 to 2016, there was an observed decrease in glacier area of 20 km^2, but the glacier contribution decreased by 2%. Glacier hypsometries showed that changes in glacier area between 2000 and 2010 compared to between 2010 and 2016 were distributed differently with respect to elevation. From 2000 to 2010, change in glacier area was confined to lower elevations, whilst a significant decrease in glacier area at higher elevations occurred between 2010 and 2016 (Figure 3.4).

3.6 Discussion

3.6.1 Glaciers and Hydrology

The hypsometric changes in ice loss between 2000 and 2016 signify that the ELA is actually higher than the mean elevation and, hence, is an underrepresentation of the ablation zone, which demonstrates the model's inability to capture periods of accelerated melting (Buytaert *et al.* 2017). Regardless, the hydrographic data in conjunction with the ice ablation model illustrate the critical contribution of glacier melt runoff to the regional hydrology of the UKRB, both annually and during the ablation season.

As the glaciers of the Altai Mountains recede in reaction to increasing summer temperature trends (Pan *et al.* 2017), their melt runoff will continue to be a critical component to the water availability in the UKRB. The observed decrease in glacier area near the glacier's maximum elevation indicates that only disproportionally small accumulation zones remain. Consequently, the large ablation zones equate to the maximum glacier melt runoff contribution annually; hence, the ice ablation model results should be perceived as a minimum and warmer simulations using a MBG of 0.42 m w.e. 100 m^{-1} are feasible. Without a substantial accumulation zone, the longevity of the glaciers is unknown; however, the large ablation zones point out that the glaciers are currently contributing their

maximum potential. Unfortunately, in the years to come, the glacier contribution will increasingly decrease—we already glimpsed at a slight decrease from 2010 to 2016.

Results derived from the ice ablation modeling indicate that the contribution of glaciers in the Mongolian Altai to the total water availability in the entire Mongolia must be less than the 10% asreported by Davaa *et al.* (2007). Their results were derived from a volume-area scaling approach that included glaciers from the formerly (insignificantly) glaciated mountains of Otgon Tenger, Khentii, and Khanghai, the contribution of glaciers to regional hydrology decreases with increasing distance from glaciated basins (Racoviteanu *et al.* 2013).

The determination of the contribution of glaciers to regional hydrology in the UKRB is a key step forward in creating adaptations and building resilience within an environment and culture that is vulnerable to slight environmental fluxes. Furthermore, these environmental fluxes often manifest in water availability and demand. Yet, glacier melt runoff as a contributor to hydroelectricity, with respect to the Durgun HPP, might be negligible as surface water in the Durgun Basin will be diluted by other sources. Nevertheless, climatic and land use changes (Karthe *et al.* 2015) will likely have more influence on water availability in the Durgun Basin, than glacier retreat alone.

3.6.2 Glaciers and Water Resources

The portrait of water availability and demand is a complex mosaic of environmental conditions, governance, and socio-economic conditions (Buytaert *et al.* 2017). Nevertheless, water scarcity will probably increase across Mongolia in the near future: from the 1980s to 2010, 63 lakes (> 1 km^2) disappeared and about 683 rivers dried up (Tao *et al.* 2015, Szumińska 2016). Surface water withdrawals by mining and livestock irrigation have been found to be the dominant drivers of decreasing lake levels (Tao *et al.* 2015), while projected climatic changes that manifest through decreasing precipitation and increasing air temperature have been identified as a secondary driver (Szumińska 2016). How glacier recession fits into this picture of disappearing lakes is unknown. Water consumption in Mongolia is principally distributed to mining (26.7%), domestic use (20.3%), livestock (20.2%), and irrigation (14.9%) (Batsukh *et al.* 2008). As Mongolia's water demand from livestock precipitously increased after 1990, the mining industry is

expected to become the greatest consumer of water in the coming years (Hofmann *et al.* 2015, Karthe *et al.* 2015).

In 2004, a United Nations water and sanitation report stated that only 30% of Mongolia's rural population had access to an 'improved' water source, whilst the remaining population relied on lakes, rivers, and springs (Shinneman *et al.* 2009). Within the Durgun Basin and UKRB, the quality of these natural resources has seen significant degradation, particularly through increased salinity and eutrophication (Shinneman *et al.* 2010) and is likely a consequence of reduced glacier melt in sync with increased livestock grazing in riparian zones (Vorobyeva *et al.* 2015). In addition to livestock, mining implications also contribute to the deterioration of surface water quality with increased sulfates and pH values from small scale artisanal mining (Mcintyre *et al.* 2016). The socio-economic development in Mongolia has created a positive feedback loop, such that the demand for water has increased and the consequence of livestock production and mining further degrade the water quality in the already water-restricted country, thereby marginalizing rural populations' access to water.

3.7 Conclusion

As Mongolia continues to develop water-dependent economic sectors, we must begin to reconsider and posit the likelihood that the water availability in the UKRB will begin to decrease as the Altai's glaciers continue to recede. In this case, water-based decisions in western Mongolia must be exceptionally well-informed to maintain the country's commitment to sustainable use, household access, protection, and conservation of water resources. We suggest that sustainable economic development is best informed by consistent and long-term environmental monitoring. In this paper, we estimated the contribution of glacier melt within a data-scarce region by selecting a glacier-hydrologic model that required accessible and limited data inputs. Importantly, our model is restricted by its inability to project the future contribution of glacier melt due to limited data, providing credence to transitioning important watersheds within the Altai Mountains from data scarce to data rich to provide the strongest scientific foundations in developing water-based decisions in western Mongolia.

Regardless of our suggestions, there must first be a consensus amongst stakeholders, non-governmental organizations and government sectors as Mongolia's temperature continues to increase at twice the global rate. It is unlikely that any glacier's lost accumulation zones will be recovered. Therefore, understanding the consequences of a reduced glacier melt contribution to the livelihoods of western Mongolia's population remains critical. Future water availability in western Mongolia is particularly uncertain because it is dictated by a complex interaction between climate and an evolving land use. HPP development can be a possible solution, but the longevity of the region's glaciers must be acknowledged. It is certain, however, that effective water management and strategies must be developed to increase Mongolia's resilience to water vulnerabilities and security in the Altai Mountains.

3.8 References

Alford D. 1992. *Hydrological Aspects of the Himalayan Region*. Occasional Paper, 18: 68, International Center for Integrated Mountain Development Kathmandu, Nepal

Alford D, Archer D, Bookhagen B, Grabs W, Halvorson S, Hewitt K, Immerzeel W, Kamp U, Krumwiede B. 2014. *Monitoring of Glaciers, Climate, and Runoff in the Hindu Kush–Himalaya Mountains*. The World Bank, Report 67668-SAS, Washington, DC.

Alford D, Kamp U, Pan C. 2015. *Assessment of the Role of Glaciers in Stream Flow from the Pamir and Tien Shan Mountains*. The World Bank, Report ACS12128, Washington, DC.

Batima P, Natsagdorj L, Gombluudev P, Erdenetsetseg B. 2005. *Observed Climate Change in Mongolia*. Assessments of Impacts and Adaptations to Climate Change (AIACC) Project, Working Papers, 13, Nairobi.

Batsukh N, Dorjsuren D, Batsaikhan G. 2008. *The Water Resources, Use and Conservation in Mongolia*. First National Report, National Water Committee: Ulaanbaatar, Mongolia.

Blomdin, R., A. P. Stroeven, J. M. Harbor, N. A. Lifton, J. Heyman, N. Gribenski, D. A. Petrakov, et al. 2016. "Evaluating the Timing of Former Glacier Expansions in the Tian Shan: A Key Step towards Robust Spatial Correlations." *Quaternary Science Reviews* 153: 78–96. https://doi.org/10.1016/j.quascirev.2016.07.029.

Bury, Jeffrey, Bryan G. Mark, Mark Carey, Kenneth R. Young, Jeffrey M. McKenzie, Michel Baraer, Adam French, and Molly H. Polk. 2013. "New Geographies of Water and Climate Change in Peru: Coupled Natural and Social Transformations in the Santa River Watershed." *Annals of the Association of American Geographers* 103 (2): 363–74. https://doi.org/10.1080/00045608.2013.754665.

Buytaert, Wouter, Simon Moulds, Luis Acosta, Bert De Bievre, Carlos Olmos, Marcos Villacis, Tovar Carolina, and Verbis Koen MJ. 2017. "Glacier Melt Content of Water Use in the Tropical Andes." *Environmental Research Letters* 12: 0–21.

Chen, Fahu, Jinsong Wang, Liya Jin, Qiang Zhang, Jing Li, and Jianhui Chen. 2009.

"Rapid Warming in Mid-Latitude Central Asia for the Past 100 Years." *Frontiers of Earth Science in China* 3 (1): 42–50. https://doi.org/10.1007/s11707-009-0013-9.

Dashtseren, Avirmed, Mamoru Ishikawa, Yoshihiro Iijima, and Yamkin Jambaljav. 2014. "Temperature Regimes of the Active Layer and Seasonally Frozen Ground under a Forest-Steppe Mosaic, Mongolia." *Permafrost and Periglacial Processes* 25 (4): 295–306. https://doi.org/10.1002/ppp.1824.

Ganiushkin, Dmitry, Kirill Chistyakov, and Elena Kunaeva. 2015. "Fluctuation of Glaciers in the Southeast Russian Altai and Northwest Mongolia Mountains since the Little Ice Age Maximum." *Environmental Earth Sciences* 74 (3): 1883–1904. https://doi.org/10.1007/s12665-015-4301-2.

Gaudard, Ludovic, Franco Romerio, Francesco Dalla Valle, Roberta Gorret, Stefano Maran, Giovanni Ravazzani, Markus Stoffel, and Michela Volonterio. 2014. "Climate Change Impacts on Hydropower in the Swiss and Italian Alps." *Science of the Total Environment* 493. Elsevier B.V.: 1211–21. https://doi.org/10.1016/j.scitotenv.2013.10.012.

Hagg, W, M Hoelzle, S Wagner, and Z Klose. 2011. "Estimation of Future Glaciation and Runo Ff in the Tanimas Basin , Eastern Pamirs." https://doi.org/10.5194/hessd-8-1507-2011.

Hagg, Wilfried, Martin Hoelzle, Stephan Wagner, Elisabeth Mayr, and Zbynek Klose. 2013. "Glacier and Runoff Changes in the Rukhk Catchment , Upper Amu-Darya Basin until 2050." *Global and Planetary Change* 110. Elsevier B.V.: 62–73. https://doi.org/10.1016/j.gloplacha.2013.05.005.

Horlemann, Lena, and Ines Dombrowsky. 2012. "Institutionalising IWRM in Developing and Transition Countries: The Case of Mongolia." *Environmental Earth Sciences* 65 (5): 1547–59. https://doi.org/10.1007/s12665-011-1213-7.

Kamp, Ulrich, Brandon Krumwiede, Kevin Mcmanigal, Caleb Pan, Michael Walther, and Avirmed Dashtseren. 2013. "The Glaciers of Mongolia." *INSTAAR Occasional Paper*, no. 61.

Kamp, Ulrich, and Caleb G. Pan. 2015. “Inventory of Glaciers in Mongolia, Derived from Landsat Imagery from 1989 to 2011.” *Geografiska Annaler, Series A: Physical Geography* 97 (4): 653–69. https://doi.org/10.1111/geoa.12105.

Karthe, Daniel, Iskandar Abdullaev, Bazartseren Boldgiv, Dietrich Borchardt, Sergey Chalov, Jerker Jarsjö, Lanhai Li, and Jeffrey A. Nittrouer. 2017. “Water in Central Asia: An Integrated Assessment for Science-Based Management.” *Environmental Earth Sciences* 76 (20). https://doi.org/10.1007/s12665-017-6994-x.

Karthe, Daniel, Sonja Heldt, Annabelle Houdret, and Dietrich Borchardt. 2014. “IWRM in a Country under Rapid Transition: Lessons Learnt from the Kharaa River Basin, Mongolia.” *Environmental Earth Sciences* 73 (2): 681–95. https://doi.org/10.1007/s12665-014-3435-y.

Karthe, Daniel, Jürgen Hofmann, Ralf Ibisch, Sonja Heldt, Katja Westphal, Lucas Menzel, Saulyegul Avlyush, and Marcus Malsy. 2015. “Science-Based IWRM Implementation in a Data-Scarce Central Asian Region: Experiences from a Research and Development Project in the Kharaa River Basin, Mongolia.” *Water (Switzerland)* 7 (7): 3486–3514. https://doi.org/10.3390/w7073486.

Konya, Keiko, Tsutomu Kadota, Fumio Nakazawa, Gombo Davaa, Purevdagva Kalsan, Hironori Yabuki, and Tetsuo Ohata. 2013. “Surface Mass Balance of the Potanin Glacier in Mongolian Altai Mountains and Comparison with Russian Altai Glaciers in 2005, 2008 and 2009.” *Bulletin of Glaciological Research* 31: 9–18.

Kronenberg, Marlene, Martina Barandun, Martin Hoelzle, Matthias Huss, Daniel Farinotti, Erlan Azisov, Ryskul Usubaliev, Abror Gafurov, Dmitry Petrakov, and Andreas Kääb. 2016. “Mass-Balance Reconstruction for Glacier No. 354, Tien Shan, from 2003 to 2014.” *Annals of Glaciology* 57 (71): 92–102. https://doi.org/10.3189/2016AoG71A032.

Krumwiede, Brandon S, Ulrich Kamp, Gregory J Leonard, S Kargel, Avirmed Dashtseren, and Michael Walther. 2014. “Recent Glacier Changes in the Mongolian Altai Mountains: Case Studies from Munkh Khairkhan and Tavan Bogd” 2.

Lehmkuhl, Frank, Michael Klinge, Henrik Rother, and Daniela Hülle. 2016. “Distribution and Timing of Holocene and Late Pleistocene Glacier Fluctuations in Western Mongolia.” *Annals of Glaciology* 57 (1): 1–10. https://doi.org/10.3189/2016AoG71A030.

Li, Zhi, Yaning Chen, Weihong Li, Haijun Deng, and Gonghuan Fang. 2015. “Potential Impacts of Climate Change on Vegetation Dynamics in Central Asia.” *Journal of Geophysical Research : Atmospheres* 120 (12): 345–56. https://doi.org/10.1002/2015JD023618.

Mcintyre, Neil, Nevenka Bulovic, Isabel Cane, and Phill Mckenna. 2016. “A Multi-Disciplinary Approach to Understanding the Impacts of Mines on Traditional Uses of Water in Northern Mongolia.” *Science of the Total Environment* 557–558. The Authors: 404–14. https://doi.org/10.1016/j.scitotenv.2016.03.092.

Pan, Caleb G., Allen Pope, Ulrich Kamp, Avirmed Dashtseren, Michael Walther, and Margarita V. Syromyatina. 2017. “Glacier Recession in the Altai Mountains of Mongolia in 1990–2016.” *Geografiska Annaler: Series A, Physical Geography* 0 (0). Taylor & Francis: 1–19. https://doi.org/10.1080/04353676.2017.1407560.

Priess, Joerg A., Christian Schweitzer, Florian Wimmer, Ochirbat Batkhishig, and Matthias Mimler. 2011. “The Consequences of Land-Use Change and Water Demands in Central Mongolia.” *Land Use Policy* 28 (1). Elsevier Ltd: 4–10. https://doi.org/10.1016/j.landusepol.2010.03.002.

Racoviteanu, Adina E., Richard Armstrong, and Mark W. Williams. 2013. “Evaluation of an Ice Ablation Model to Estimate the Contribution of Melting Glacier Ice to Annual Discharge in the Nepal Himalaya.” *Water Resources Research* 49 (9): 5117–33. https://doi.org/10.1002/wrcr.20370.

Rasmussen, Lowell A., and Wendell V. Tangborn. 1976. “Hydrology of the North Cascades Region, Washington: 1. Runoff, Precipitation, and Storage Characteristics.” *Water Resources Research* 12 (2): 187–202. https://doi.org/10.1029/WR012i002p00187.

Rudaya, Natalia, Pavel Tarasov, Nadezhda Dorofeyuk, Nadia Solovieva, Ivan Kalugin, Andrei Andreev, Andrei Daryin, et al. 2009. “Holocene Environments and Climate in the Mongolian Altai Reconstructed from the Hoton-Nur Pollen and Diatom Records: A Step towards Better Understanding Climate Dynamics in Central Asia.” *Quaternary Science Reviews* 28 (5–6). Elsevier Ltd: 540–54. https://doi.org/10.1016/j.quascirev.2008.10.013.

Shinneman, a. L.C., C. E. Umbanhowar, M. B. Edlund, and N. Soninkhishig. 2010. “Late-Holocene Moisture Balance Inferred from Diatom and Lake Sediment Records in Western Mongolia.” *The Holocene* 20 (1): 123–38. https://doi.org/10.1177/0959683609348861.

Shinneman, Avery L C, James E. Almendinger, Charles E. Umbanhowar, Mark B. Edlund, and Soninkhishig Nergui. 2009. “Paleolimnologic Evidence for Recent Eutrophication in the Valley of the Great Lakes (Mongolia).” *Ecosystems* 12 (6): 944–60. https://doi.org/10.1007/s10021-009-9269-x.

Sorg, Annina, Tobias Bolch, Markus Stoffel, Olga Solomina, and Martin Beniston. 2012. “Climate Change Impacts on Glaciers and Runoff In.” *Nature Climate Change* Advance On: 1–7. https://doi.org/10.1038/NCLIMATE1592.

Syromyatina, M. V., Y. N. Kurochkin, D. P. Bliakharskii, and K. V. Chistyakov. 2015. “Current Dynamics of Glaciers in the Tavan Bogd Mountains (Northwest Mongolia).” *Environmental Earth Sciences* 74 (3). Springer Berlin Heidelberg: 1905–14. https://doi.org/10.1007/s12665-015-4606-1.

Szumińska, Danuta. 2016. “Changes in Surface Area of the Böön Tsagaan and Orog Lakes (Mongolia, Valley of the Lakes, 1974–2013) Compared to Climate and Permafrost Changes.” *Sedimentary Geology* 340: 62–73. https://doi.org/10.1016/j.sedgeo.2016.03.002.

Tao, Shengli, Jingyun Fang, Xia Zhao, Shuqing Zhao, Haihua Shen, Huifeng Hu, Zhiyao Tang, Zhiheng Wang, and Qinghua Guo. 2015. “Rapid Loss of Lakes on the Mongolian Plateau.” *Proceedings of the National Academy of Sciences of the United States of America* 112 (7): 2281–86. https://doi.org/10.1073/pnas.1411748112.

Viviroli, Daniel, Hans H. Dürr, Bruno Messerli, Michel Meybeck, and Rolf Weingartner. 2007. “Mountains of the World, Water Towers for Humanity: Typology, Mapping, and Global Significance.” *Water Resources Research* 43 (7): 1–13. https://doi.org/10.1029/2006WR005653.

Vorobyeva, S. S., V. A. Trunova, O. G. Stepanova, V. V. Zvereva, S. K. Petrovskii, M. S. Melgunov, T. O. Zheleznyakova, L. G. Chechetkina, and A. P. Fedotov. 2015. “Impact of Glacier Changes on Ecosystem of Proglacial Lakes in High Mountain Regions of East Siberia (Russia).” *Environmental Earth Sciences* 74 (3). Springer Berlin Heidelberg: 2055–63. https://doi.org/10.1007/s12665-015-4164-6.

Wang, WenBin, ZhongZin Li, GuoFei Zhang, and XuLiang Li. 2012. “The Processes and Characteristics of Mass Balance on the Urumqi Glacier No. 1 during 1958-2009.” *Sciences in Cold and Arid Regions* 4 (6): 505. https://doi.org/10.3724/SP.J.1226.2012.00505.

Zemp, Michael, Holger Frey, Isabelle Gärtner-Roer, Samuel U. Nussbaumer, Martin Hoelzle, Frank Paul, Wilfried Haeberli, et al. 2015. “Historically Unprecedented Global Glacier Decline in the Early 21st Century.” *Journal of Glaciology* 61 (228): 745–62. https://doi.org/10.3189/2015JoG15J017.

Tables

Table 3.1 The number and area of glaciers in the UKRB during 2000, 2010, and 2016. Glacier area and numbers are also aggregated for the Bayan-Ulgii Aimag and the entire Altai for reference.

	Upper Khovd River Basin		Bayan-Ulgii Aimag	Entire Altai
Year	Glacier Count	Glacier Area [km^2]	Glacier Area [km^2]	Glacier Area [km^2]
2000	345	170.8	307.3	428.6
2010	333	151.5	268.6	371.1
2016	311	131.5	237.3	334

Table 3.2 Ice ablation model results for the years 2000, 2010, and 2016; included are MBG sensitivity results of ± 0.1m w.e. 100 m^{-1}.

MBG [m w.e. 100 m^{-1}]	Clean Ice Runoff [km^3]		
	2000	2010	2016
0.32	0.083	0.080	0.070
0.22	0.057	0.055	0.048
0.42	0.109	0.105	0.092

Table 3.3 Percent of glacier contribution to regional hydrology in the UKRB for the years 2000, 2010, and 2016.

MBG [m w.e. 100 m^{-1}]	Clean Ice Contribution [%]		
	2000	2010	2016
0.32	13.68	13.12	11.45
0.22	9.41	9.02	7.87
0.42	17.96	17.22	15.02

Figures

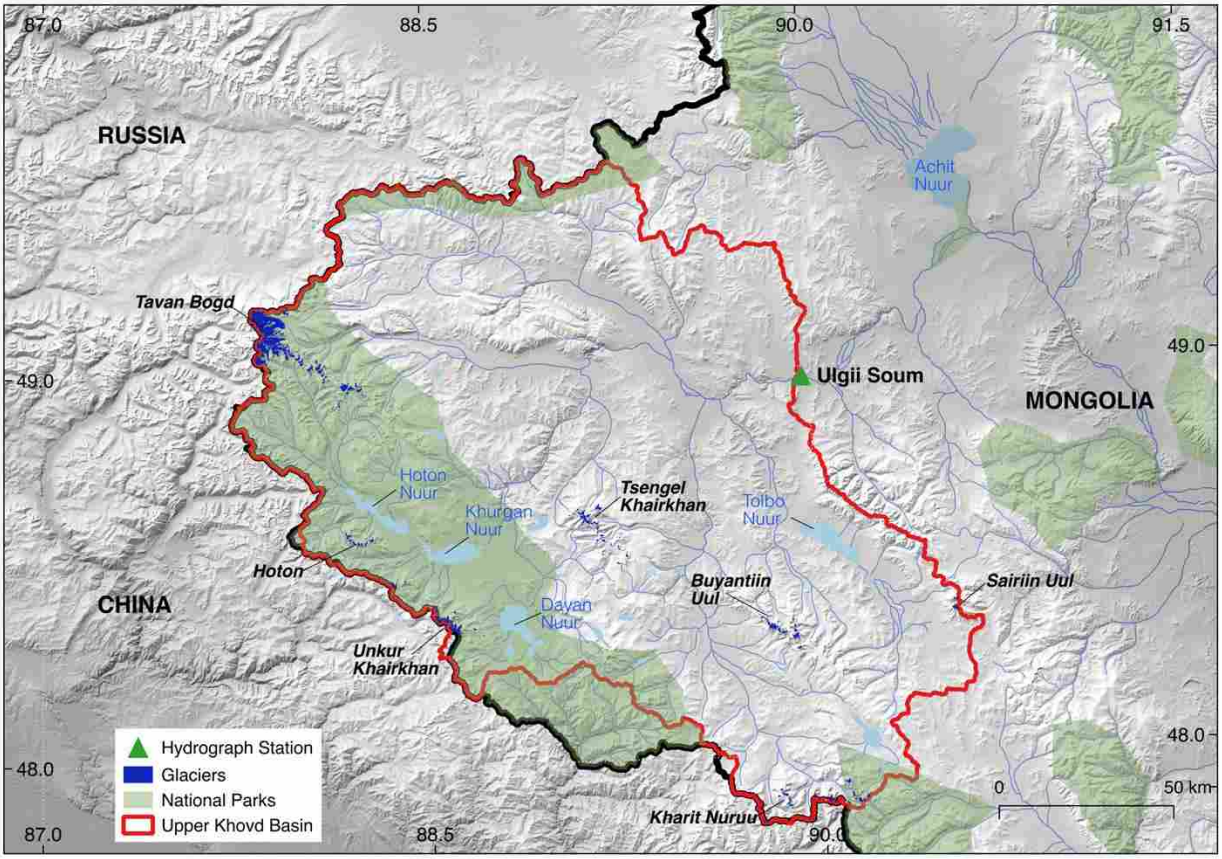

Figure 3.1 The defined study area is the Upper Khovd river basin the Altai Mountains of northwest Mongolia. The hydrograph station is located Ulgi, Mongolia and is the soum center of Bayan-Ulgii aimag.

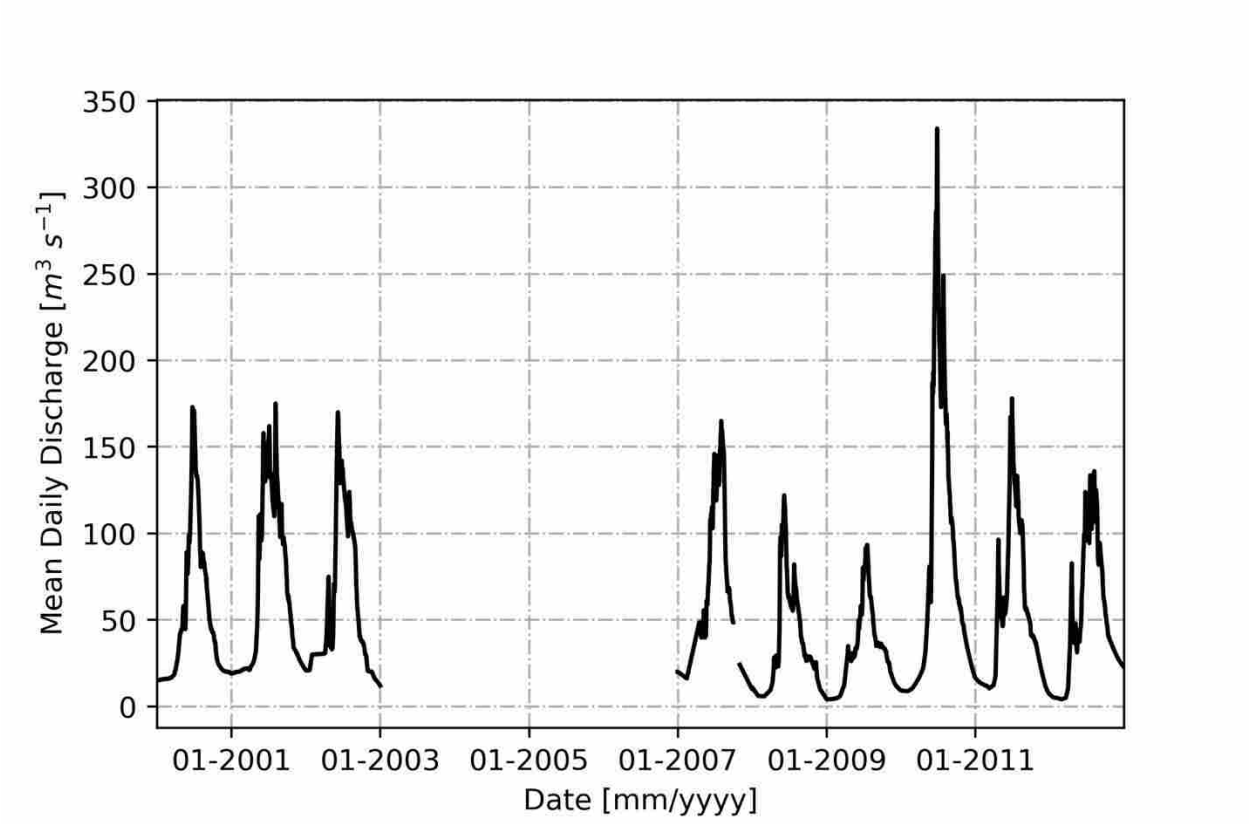

Figure 3.2 Mean daily discharge observed at Ulgii, Mongolia in the Upper Khovd River Basin (UKRB).

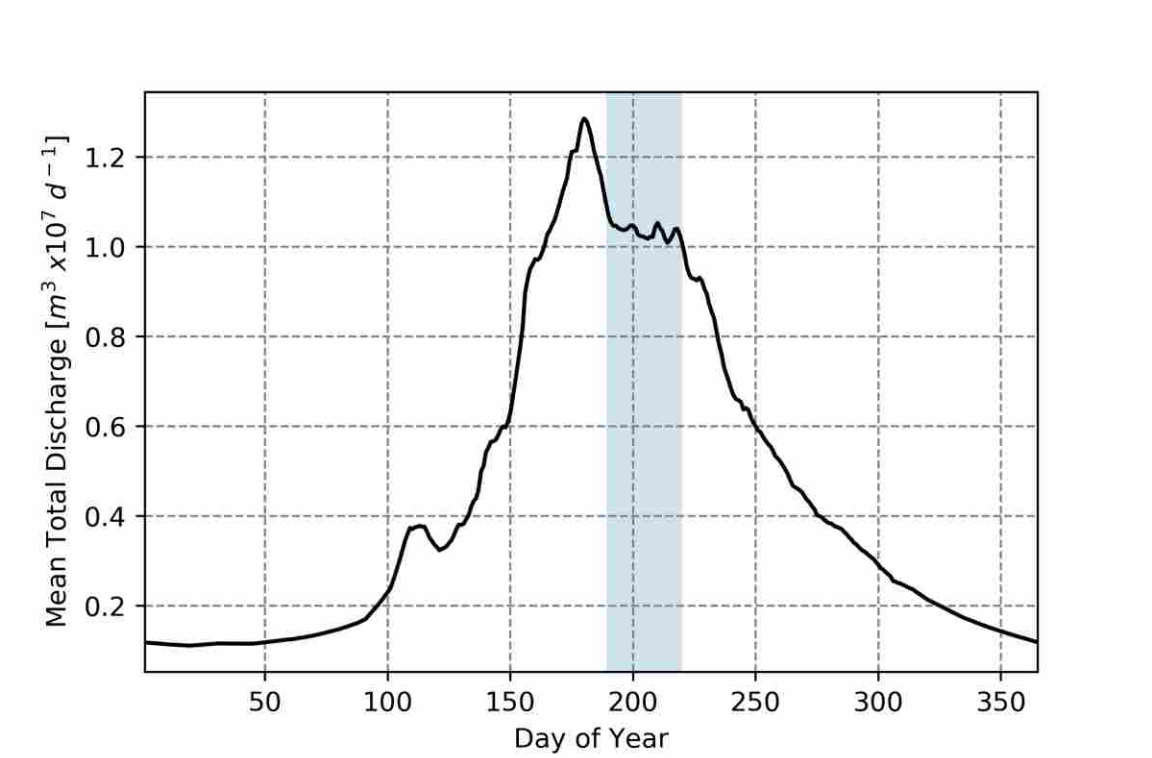

Figure 3.3 Mean total daily discharge observed at Ulgii, Mongolia. The shaded region highlights the period of significant the ablation period.

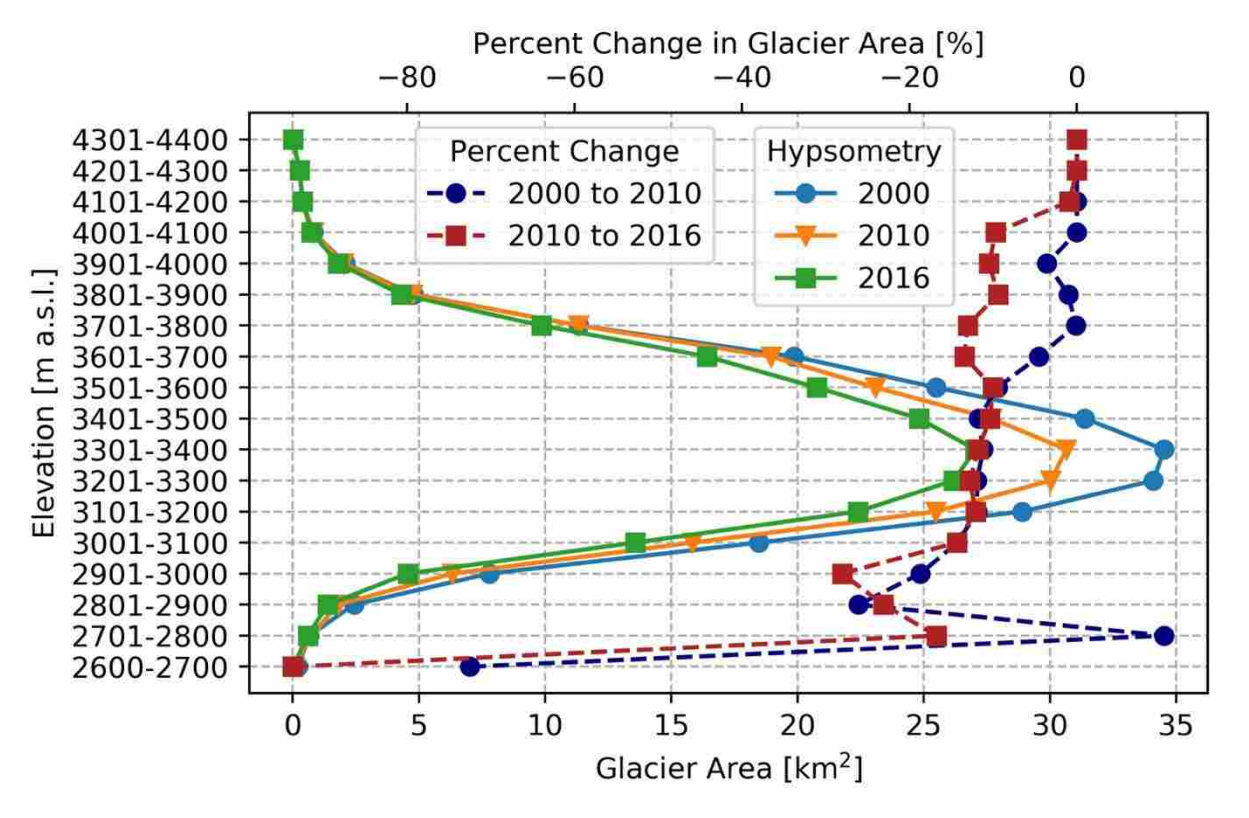

Figure 3.4 Glacier hypsometries within the Upper Khovd River Basin (UKRB) (solid lines) and associated percent change (dashed lines).

CHAPTER 4

Rain-on-snow events in Alaska, and their frequency and distribution from satellite observations

Corresponding publication:

Pan, C. G., Kirchner, P., Kimball, J., Kim, Y., Jinyang, D. (2018). Rain-on-snow events in Alaska, and their frequency and distribution from satellite observations. *Environmental Research Letters* **13** 075004 DOI: 10.1088/1748-9326/aac9d3.

4.1 Abstract

Wet snow and the icing events that frequently follow wintertime rain-on-snow (ROS) effect high latitude ecosystems at multiple spatial and temporal scales, including hydrology, carbon cycle, wildlife, and human development. However, the distribution of ROS events and their response to climatic changes are uncertain. In this study, we quantified ROS spatiotemporal variability across Alaska during the cold season (Nov-Mar) and clarified the influence of precipitation and temperature variations on these patterns. A satellite based daily ROS geospatial classification was derived for the region by combining remote sensing information from overlapping MODIS and AMSR sensor records. The ROS record extended over the recent satellite record (water years 2003-2011 and 2013-2016) and was derived at a daily time step and 6-km grid, benefiting from finer (500m) resolution MODIS snow cover observations and coarser (12.5 km) AMSR microwave brightness temperature based freeze-thaw retrievals. The classification showed favorable ROS detection accuracy (75-100%) against *in situ* climate observations across Alaska. Pixel-wise correlation analysis was used to clarify relationships between the ROS patterns and underlying physiography and climatic influences. Our findings indicate that cold season ROS events are most common during autumn and spring months along the maritime Bering Sea Coast (BSC) and boreal Interior (INT) regions, but are infrequent on the colder arctic North Slope (NS). The frequency and extent of ROS events coincided with warm temperature anomalies ($p < 0.1$), but showed a generally weaker relationship with precipitation. The weaker precipitation relationship was attributed to several factors, including large uncertainty in cold season precipitation measurements, and the important contribution of humidity and turbulent energy transfer in driving snowmelt and icing events independent of rainfall. Our results suggest that as

high latitude temperatures increase, wet snow and ROS events will also increase in frequency and extent, particularly in the southwestern and interior regions of Alaska.

4.2 Introduction

The atmospheric conditions typically associated with high latitude winter rainfall affect the physical properties of the snowpack, including energy content, water content, depth, density and grain size, frequently resulting in a wet snow surface (Singh *et al.* 1997). These effects are due to the associated transfers of latent and sensible heat, either directly or through turbulent exchanges that hasten snow melt (Marks *et al* 1998). Whenever snow surface layers reach 0°C, additional energy flux to the snow surface contributes to melt and rising water content; snowmelt will continue to occur whenever the cold content of the snowpack exceeds 0°C or until the snow has completely melted (Dingman 2014). Thus, wintertime rain events can be a major driver of wet surface snow conditions indicated from satellite observations (Frei *et al* 2012). However, rain is not required for wet snow to exist, nor do wet snow conditions always follow rainfall events. Different science communities have used the term "rain-on-snow" to collectively refer to wet surface snow conditions and the many physical processes that lead to their occurrence. We recognize that rain-on-snow is not necessarily synonymous with wet snow, but that the occurrence of rain on a winter snowpack frequently precedes the presence of wet snow conditions at high latitudes. We therefore retain the usage of the term rain-on-snow (ROS) in this investigation to collectively describe these processes.

Wet snow, and the icing events that frequently follow ROS, affect several ecosystem processes including hydrology, carbon cycling, wildlife movement and human transportation, at multiple spatial and temporal scales (Putkonen and Roe 2003, McCabe *et al* 2007). ROS events, and the positive heat flux to the snowpack often associated with them, are one of the dominant drivers of winter/springtime flooding in mountainous regions and at higher latitudes (Marks *et al* 1998, Guan *et al* 2016, Jeong and Shushama 2017). Enhanced liquid water content (LWC) to the snowpack whether by ROS or melt events can also reduce a snowpack's insulating effect on the soil (Lafrenière *et al* 2013, Kim *et al* 2015). Furthermore, accumulated water at the soil surface from ROS driven snowmelt can release latent heat into the soil horizon, and in turn result in accelerated

thawing of frozen ground (Putkonen and Roe 2003, Rennert *et al* 2009). These thawing processes ultimately hasten the release of soil carbon to the watershed and atmosphere in the form of dissolved organic matter or gasses (Hobbie *et al* 2000). Further, accumulated water between the soil surface and snowpack also has the potential to freeze, forming a significant ice barrier to browsing ungulates, which can contribute to large wintertime die-offs (Grenfell and Putkonen 2008; Riseth et al. 2011; Loe et al. 2016; Berger et al. 2018). As intensified warming of the high latitudes, known as 'Arctic Amplification', continues (Serreze and Francis 2006, Cohen *et al.* 2014), an increase in the frequency, distribution, and intensity of ROS events is predicted (Jeong and Shushama 2017), with potentially adverse impacts to Arctic ecosystems and the communities that depend on them.

The Arctic Boreal Vulnerability Experiment (ABoVE) is a broad-scale international and interdisciplinary field campaign initiated by NASA to understand environmental change in the Arctic and boreal region (ABR) of western North America and associated linkages to social-ecological systems (Kasischke *et al*. 2014). The ABoVE science objectives include quantifying changes in the condition and distribution of snow, and its impact on ecosystem structure and function. A key limitation for quantifying and understanding ROS in the region is a general lack of available observations, which are constrained by remoteness, severe climate and sparse regional weather station networks. Alternatively, satellite remote sensing methods have for detecting and mapping ROS in the ABR have been developed. Successful approaches include the use of active and passive microwave sensors from polar-orbiting satellites that provide frequent observations and enhanced sensitivity to landscape freeze-thaw dynamics (Kimball *et al.* 2004, Bartsch 2010b, Semmens *et al.* 2013, Wilson *et al.* 2013). However, these approaches have generally involved only limited areas and periods, or relatively coarse (~10-25 km resolution) retrievals.

The objectives of this study were to quantify spatiotemporal variability in ROS across Alaska during the winter season (Nov-Mar) and clarify the influence of precipitation and temperature anomalies on ROS frequency and distribution. The domain for this study is the state of Alaska, which has a long snow season and faces challenges to both natural resources management and socio-economic structure due to changing snow

conditions due to regional warming trends (Bokhorst *et al.* 2016, Kontar *et al.* 2018). Much of Alaska is in the ABoVE domain, where a better understanding of the distribution and underlying drivers of ROS will contribute to the ABoVE science objectives and provide critical information to Alaskan land managers.

To address the study objectives, we generated a daily ROS geospatial classification across Alaska by combining synergistic remote sensing information from overlapping MODIS (Moderate Resolution Imaging Spectroradiometer) and AMSR (Advanced Microwave Scanning Radiometer) sensors. Here, MODIS provides 8-day repeat coverage and relatively fine scale (500m resolution) information on snow cover extent, while AMSR provides daily microwave brightness temperature (T_b) retrievals sensitive to landscape freeze-thaw dynamics, but within a relatively coarse (~12.5 km) sensor footprint. The combined information from these sensors provides a means for ROS mapping with enhanced (~6-km resolution) gridding suitable for resolving regional ROS patterns and underlying physiographic and climate drivers.

The application of satellite remote sensing to detect ROS events has progressed in recent years through the development of new data sources and techniques, including both radar (Kimball *et al.* 2004, Bartsch 2010b, Bartsch *et al.* 2010a), and passive microwave (PM) sensors (Grenfell and Putkonen 2008, Wang *et al.* 2013, Wang *et al*. 2016). In Alaska, these sensors have been applied to detect ROS using different classification algorithms, including backscatter change detection (Kimball *et al.* 2001, Bartsch 2010b, Wilson *et al.* 2013), Diurnal Amplitude Variation (DAV) from PM T_b retrievals (Semmens *et al.* 2013), and a T_b differencing approach (Wang *et al.* 2016). More recently, spectral gradient ratios, including the Gradient Ratio (GR, Grenfell and Putkonen 2008) and Gradient Ratio Polarization (GRP, Dolant *et al*. 2016), were developed to exploit complimentary information from different microwave frequencies and polarizations for ROS detection. The PM based GRP approach was also observed to be effective in detecting ROS and associated winter melt events within the ABR (Dolant *et al*. 2016, Langlois *et al.* 2017). However to our knowledge, this study provides the only available ROS satellite record for Alaska that provides 6 km daily resolution from current operational satellites that overlaps with the timing of the ABoVE campaign.

In this study, we used the GRP approach with PM observations from the Advanced Microwave Scanning Radiometer sensors AMSR-E and AMSR2 (hereafter denoted as AMSR) for daily classification of ROS events across Alaska. The AMSR GRP based ROS classification was conducted over snow covered areas defined from MODIS. The study period for this investigation encompassed water years (WY) 2003-2016 and the available AMSR record, which overlapped with the first phase of the ABoVE campaign (Kasischke *et al*. 2014). The daily ROS record encompassed the months of November through March (Nov-Mar) when snowmelt from solar irradiance is minimal and snow cover is widespread and relatively consistent throughout the region (Lindsay *et al*. 2015). The ROS classification was mapped to a 6-km resolution grid and used to quantify and understand ROS spatiotemporal variability and underlying drivers across Alaska.

4.3 Data and Methods

4.3.1 Spatial domain

The state of Alaska spans approximately 20° of latitude and 50° of longitude, encompassing the North Pacific and Arctic Boreal regions of the northern hemisphere. Within the region many gradients influence the climate including: latitude, distance from large water bodies, the relative thermal mass and circulation of coastal waters, terrain and elevation. Alaska a peninsula with over 10,000 km of coastline, is bounded by the Pacific Ocean to the south and the shallower seasonally ice covered Bearing, Chukchi and Beaufort seas to the west and north, respectively. The eastern border of Alaska runs through boreal forest characterized by a cold interior continental climate. Thirteen different climate divisions have been described for the state of Alaska (Bieniek et al. 2012). For the spatial analysis of ROS distributions, we aggregated the thirteen climate divisions into four larger regions delineated by National Hydrography Hydrologic Unit Code (HUC 8) watersheds (USGS, 2017) (Figure 4.1). The aggregated Alaska HUC 8 divisions examined for this study include the Alaska Gulf Coast (AGC), Interior (INT), Bering Sea Coast (BSC) and North Slope (NS). These areas reflect the major Alaska climatic regions, of the relatively moderate Pacific maritime, cold-dry boreal interior, and polar arctic northwest coast and North Slope regions. The high latitude ecosystems found

in these climate divisions play an important role in Earth's energy, water and carbon cycles and are some of the most vulnerable to recent climate warming (Chapin *et al.* 2014, O'Neel *et al* 2015).

4.3.2 Satellite data used for ROS classification

The AMSR-E sensor was launched in 2002 on-board the NASA Aqua satellite and operated until 2011 (Kawanishi *et al* 2003). The AMSR2 follow-on mission was successfully launched in 2012 on-board the JAXA GCOM-W satellite and continues normal operations (Imaoka *et al* 2010; Du *et al* 2014). We used combined calibrated T_b records from AMSR-E for WY 2003-2011 and AMSR2 for WY 2013-2016. The AMSR record was derived using an empirical calibration of similar frequency T_b retrievals from overlapping FY3B MWRI (Microwave Radiation Imager) observations (Du et al. 2014). The AMSR record has twice-daily, vertical (V) and horizontal (H) polarization T_b retrievals acquired from ascending and descending polar orbital equatorial crossings at 1:30 pm and 1:30 am, which is suitable for detecting ROS (Dolant *et al* 2016, Du *et al* 2016). Lower frequency T_b retrievals (18.7 GHz and 36.5 GHz, henceforth rounded to 19 and 37) from the AMSR record were used for ROS detection in this study, as they are sensitive to snow cover properties and landscape freeze-thaw dynamics (Kim et al. 2017) but insensitive to potential signal degradation from polar darkness, low solar illumination, cloud cover and atmospheric aerosol contamination effects (Rees 2010, Tedesco 2015). The native AMSR T_b footprints are relatively coarse at 19 GHz (27 km x 16 km for AMSR-E and 22 km x 14 km for AMSR2) and 37 GHz (14 km x 8 km and 12 km x 7 km) due to naturally low PM earth emissions (Kawanishi *et al* 2003, Imaoka *et al* 2010, Frei *et al* 2012). In this study, we used spatially resampled ascending orbit T_b retrievals from the calibrated AMSR record in conjunction with MOD10A2 8-day maximum snow cover extent (SCE) derived from the Moderate Resolution Imaging Spectroradiometer (MODIS) (D. K. Hall et al. 2002; D. Hall and Riggs 2007).

4.3.3 Spatially resampled AMSR

The AMSR orbital swath T_b data were spatially re-sampled to a 6-km resolution polar EASE-Grid (version 2) geographic projection using an inverse distance squared

weighting method (Brodzik et al. 2012; Du et al. 2017). To ensure cross-sensor consistency, the gridded AMSR2 T_b data were empirically calibrated against the same AMSR-E frequencies using a Double-Differencing method and similar overlapping observations from the FY3B MWRI sensor record (Du et al. 2014). The new 6-km grid provided an intermediate resolution between the finer scale (500 m) MODIS SCE and coarser (~12.5 km) resolution AMSR T_b observations, while enabling enhanced assessment of terrain and land cover spatial heterogeneity.

4.3.4 Theoretical approach to the ROS classification

We operationally defined ROS days as the satellite PM detection of abrupt changes in surface snow wetness and isothermal states induced by physical processes, such as sensible, latent and turbulent heat exchange that are often associated with winter rainfall. The physical basis of the PM ROS algorithm is the differential response in microwave emissions at 19 (V, H*)* GHz and 37 (V, H) GHz frequencies to changes in snow cover density and liquid water content (LWC) within the snowpack surface. As relatively dry snow initially transitions to wet snow with increasing LWC, T_b increases due to absorption by wet snow (Tedesco 2015). Yet, the interaction between T_b and snow wetness varies over different regions of the microwave spectrum. T_b at 19 (V and H) GHz will change with LWC to a lesser degree than at 37 (V and H) GHz (Rees et al. 2010; Vuyovich et al. 2017). Grenfell and Putkonen (2008) found distinct patterns in dielectric properties at 19 and 37 GHz in response to ROS events, leading to their application of a spectral Gradient Ratio (GR) that portrays larger differences between V and H polarized (*pol*) T_b retrievals at these frequencies following ROS events (Eq. 1).

$$GR\left(pol_{(37,19)}\right) = \frac{[T_b(pol,37) - T_b(pol,19)]}{[T_b(pol,37) + T_b(pol,19]} \quad (1)$$

Dolant *et al*. (2016) found that during ROS events, the GR derived from H *pol* T_b (GR-h) returned negative values, while the GR derived from V *pol* T_b (GR-v) returned positive values. This inverse relationship led to the development of the gradient ratio polarization (GRP) between GR-v and GR-h, allowing for the ability to set designated thresholds to classify ROS events. Dolant *et al* (2016) and Langlois *et al* (2017) applied

the GRP (Eq. 2) to single-pixel T_b timeseries from SMMR, SSM/I, and AMSR-E to detect ROS in areas of Quebec and the Canadian Arctic Archipelago, respectively.

$$GRP = \frac{GR-\mathrm{v}}{GR-h} \quad (2)$$

4.3.5 ROS workflow

In the current study, we applied a similar GRP approach developed from previous studies at point locations (Grenfell and Putkonen 2008, Dolant *et al* 2016, Langlois *et al* 2017) for mapping daily ROS patterns across Alaska. The Alaska regional classification was derived using daily ascending V and H *pol* T_b retrievals at 19 and 37 GHz from the 6-km resolution polar EASE-grid AMSR record. The created workflow is summarized in Figure S4.1 and described below.

We masked water contaminated pixels induced by the conical scanning AMSR sensor records (Derksen et al. 2012; Du et al. 2016) using a 24-km (~4 pixel) shoreline and water-body buffer created from the 2011, 30 m resolution National Land Cover Database (NLCD) (Homer *et al.* 2015). We then used the MODIS SCE record to identify snow covered areas after screening out low quality pixels, including missing or degraded snow cover observations, identified by the MOD10A2 product quality flags. The AMSR 37 GHz V *pol* T_b record was analyzed separately to identify potential snow covered pixels outside of the water body buffer where $T_b < 265$ K (Vuyovich et al. 2017). Pixels identified as snow covered by both the MODIS SCE and AMSR T_b records were then used to derive daily GR and subsequent GRP values for each classified snow pixels over the multi-year (2003-2011, 2013-2016) study period defined by the AMSR record. We applied two different GRP thresholds to classify ROS events for different elevation zones, where GRP < 1 was used to identify ROS events below 900 m, while GRP < -5 was used for elevations above 900 m; a more detailed description of the GRP threshold selection is in the supplementary section (S1). A spatial connectivity threshold of > 10 pixels was then used as a designated size threshold to isolate and analyze more regionally extensive ROS events (Wilson *et al.* 2013).

4.3.6 Two-Tiered validation

4.3.6.1 Tier 1 – Empirical in-situ ROS observations

The Tier-1 validation coupled empirical ROS observations by an observer at the National Weather Service (NWS) field office in Fairbanks, Alaska (Table 4.1), with in situ weather station measurements acquired from Fairbanks International Airport (MesoWest ID-PAFA, 134 m a.s.l.). To determine the agreement between the in-situ observations and the satellite PM derived ROS classification, daily mean GRP values were created from 6-km pixels located within a 50-km radius around the Fairbanks station location. Next, the occurrence of the daily mean GRP values < 1 were examined in conjunction with: 1) ROS events empirically observed by the NWS observer; 2) precipitation and fog observations (Wang et al. 2016) at the station; and 3) measured precipitation the day before or the day where GRP was < 1.

4.3.6.2 Tier 2 - Climate observation network

The Tier 2 validation involved an expanded spatial domain employing climate observations across Alaska acquired through the MesoWest & SynopticLabs API (https://synopticlabs.org/api/). The API provided data from several regional weather station networks including National Weather Service (NWS), remote automated weather stations (RAWS), and snow telemetry network (SNOTEL) stations. The climate data were assembled from 235 individual stations to acquire daily surface meteorological parameters including minimum and maximum air temperature (T_{min}, T_{max}), average (24-hour) air temperature (T_{avg}), 24 hour (hr) accumulated precipitation (prcp), dew point temperature (T_{dew}), and relative humidity (RH). For the study period, 53 of the 235 stations had all of the requested climate variables. The developed Tier 2 workflow is shown in Figure S4.3 and described below.

ROS days classified from the satellite record were validated using in situ weather observations from collocated climate stations to identify if rain occurred either the day of or the day before ($_{i-1}$) a classified ROS event (Obs_{rain}), or if the observed station precipitation was null (Obs_{null}). Given the limitations of wintertime precipitation measurements (Merenti-Valimaki 2001, Martinaitis *et al* 2015, Grossi *et al* 2017), Obs_{null} included conditions where either no precipitation was measured or there was no effective precipitation measurement. Three temperature driven variables were therefore created

and used as a proxy for the rainfall observations (Obs_{rain}), which can have large measurement uncertainty during freeze-thaw transitions (Martinaitis et al. 2015). The temperature based Obs_{rain} metrics included wet bulb temperature (T_w), the ratio between daily T_{dew} and T_{avg} (T_{dew}/T_{avg},), and the ratio between daily T_{max} and T_{min} (T_{max}/T_{min}), which were used as indicators for atmospheric moisture and energy flux to surface snow. A more detail description of the temperature-based precipitation metrics can be found in the supplementary section (S2). We then constrained Obs_{null} by the mean and standard deviations derived from temperature based Obs_{rain} metrics. ROS days which met all the constraining conditions set by Obs_{rain} were classified as commission whereas all Obs_{null} observations that did not meet the defined conditions were classified as omission.

4.3.7 Statistical methods and climate anomalies

Due to the relatively short study period and a data gap between the AMSR-E and AMSR2 records for 2012, we did not attempt to perform a temporal trend analysis of the ROS results. However, we did calculate the mean, standard deviation and coefficient of variation (C_v) of monthly total ROS days. The C_v was used to characterize the relative dispersion of ROS days (Sugg et al. 2017), with higher values equating to high variability and low predictability, with the inverse being true as the C_v approaches zero (Frei *et al* 2012).

Pixel-wise correlations were performed to determine the sign and strength of relationships between monthly total ROS days and respective climate anomalies. Climate anomalies were derived using 1-km resolution gridded daily surface weather station observations from the North America Daymet record (Thornton, Running, and White 1997). Daymet was one of the few products available for Alaska with a spatial (1 km^2) and temporal resolution similar to the AMSR derived ROS record. Daymet daily T_{min}, T_{max}, and prcp for the period from 1980 to 2016 were acquired from the DOE ORNL data portal (www.daymet.ornl.gov/dataaccess.html). The 1-km Daymet data were resampled to the 6-km study grid and used to create a baseline monthly mean climatology and standard deviation for each pixel and climate parameter. Here, the baseline climatology was assembled from a 22-year Daymet historical record (1980 to 2002). Monthly mean annual values of each climate parameter were then derived for each year of record from

2003-2016 (excluding 2012) and used with the respective climatology for each pixel to create gridded normalized anomalies (Figure 4.2).

4.4 Results

4.4.1 Tier-1 validation

The Tier 1 validation indicated strong agreement between PM observed ROS and the occurrence of liquid precipitation from both direct measurements and empirical observations. Of the three types of precipitation validation measurements and observations, no single type showed consistent agreement with the PM observed ROS record (Table 4.2). Of the 11 ROS event observations made by the NWS observer over the 13-year record, 10 were detected as PM observed ROS days. The precipitation type observations (rain, fog) from the PAFA station provided more overall observations than the direct precipitation measurements, but were unable to identify all ROS events consistently (Figure 4.3 (a), Figure 4.3 (b)). Yet, for the years of interest, ROS omission errors indicated from all three types of validation observations ranged from 0 to 5 events, with associated accuracies ranging from 75-100 %.

The results summarized in Figure 4.3 (a,b) also show several days in early November when the GRP was < 1, suggesting early wintertime freeze/thaw transitions due to sensible and latent heat flux, as there was limited precipitation measured during this period. Also, significant snowfall is reported in late February (Figure 4.3 (a)) and early December (Figure 4.3 (b)). During these snowfall events, the GRP remained above the detection threshold, which suggested confidence in the identification of ROS rather than snowfall events when GRP was < 1 and measured precipitation was > 0.

4.4.2 Tier-2 validation

During the study period, 278 PM detected ROS events occurred at the 53 Alaska climate station locations. Of these 278 events, 54 coincided with in situ station precipitation measurements either the day of or before the PM detected ROS event (Obs_{rain}). The remaining 224 PM days with ROS coincided with *null* precipitation observations (Obs_{null}). After the constraining process, 41 Obs_{null} observations were classed as errors of omission, while the remaining 183 Obs_{null} observations were classed

as errors of commission. The combined commission errors with Obs_{rain} produced a final PM ROS classification accuracy of 86 % (Table 4.3). Further discussion on the limitations and caveats of validating the PM derived ROS events is presented in the supplement (S4)

.

4.4.3 Temporal and spatial patterns of ROS

For the entire study period, about 52% of Alaska was affected by at least one ROS day on average; however, the ROS distribution showed large temporal variability (Figure 4.4). For example, in WY 2005 about 38% of the domain experienced a ROS event compared to a maximum of 72% in WY 2014. With respect to frequency, during the study period about 27% of the domain experienced at least 5 ROS days in a given year; this percentage peaked at 51% in WY 2014 and dropped to 16% in WY 2006. Some years of record showed relatively frequent and widespread ROS occurrences (WY 2003, 2005, 2014), while other years had far fewer ROS events (e.g. WY 2004, 2006, 2011). A visual comparison between our annual results and Wilson *et al*. (2013) showed good agreement, particularly for WY 2003 and 2005. However, results must be seen as a relative comparison as Wilson *et al.* (2013) included October and April in their annual summations. Both studies indicated a higher occurrence of freeze-rethaw or ROS days in the southwestern portion of Alaska. Bartsch (2010b) also detected melt events across Alaska using daily 13.4 GHz (Ku-band) radar backscatter retrievals from QuickSCAT during the same period and as Wilson *et al.* (2013) and found similar results. But more interesting, PM derived melt events (Semmens *et al.* 2013, Wang *et al.* 2016) and active microwave melt events (Bartsch 2010b, Wilson *et al.* 2013) demonstrated similar results to this study, an increasing trend in events moving from the central interior region and into southwest Alaska.

The PM observed ROS days showed the greatest occurrence in the southwest and central portions of Alaska, including the BSC, AGC, and INT regions, but the frequency and intensity of these events showed large year-to-year variability. The temporal variation by WY and month in PM detected ROS days for each Alaska sub-region is shown in Figure 4.5; these results indicate that the BSC and north central portions of the AGC consistently possessed the highest mean number of annual ROS days [pixel $^{-1}$].

Except for WY 2003 and WY 2014, the INT and NS regions experienced ROS almost exclusively in the month of November.

An inter-annual comparison between Wilson's *et al.* (2013) freeze-rethaw record derived from QuickSCAT and our calculated ROS events showed strong agreement from November to March (2003-2008). Both studies indicated that the largest spatial coverage of such events occurred in November, while the NS experienced no events during March for both studies. Wilson *et al.* (2013) reported that the NS did not observe any form of melt events until April. The results from Wang's *et al.* (2016) analysis of melt events from 25-km PM retrievals also supported the temporal and geographical pattern in the NS. Summary statistics in Table 4.4 show that the C_v during November and December in the NS is quite high at 0.91 and 1, respectively. These values indicate that even during November and December, ROS days are still an uncommon event across the NS.

4.4.4 Correspondence between ROS events, temperature, and precipitation

Linear regressions between temperature departure data, provided by the Alaska Climate Data Center (Figure S4.4), and the PM derived mean seasonal ROS events indicated that temperature had the greatest explanatory power for predicting ROS events within the BSC ($p < 0.001$) followed by the INT ($p < 0.01$) and AGC ($p < 0.01$) regions (Figure 4.6). In the NS, the temperature departure was insensitive to ROS occurrence ($p < 0.9$), likely due to colder climate conditions and a lower overall number of ROS events detected in the region. However, ROS events are sensitive to not just temperature, but rather the interactions between temperature, humidity and precipitation. Correlation analysis between PM derived ROS and Daymet derived climate anomalies aided in exploring these interactions.

The correlations between monthly (Nov-Mar) climate anomalies and days with ROS were statistically significant ($p \leq 0.1$) in many locations (Figure 4.7). Overall, days with ROS coincided with above-normal precipitation and temperature with notable temporal and spatial variability in both the sign and strength of the relationships. The relationships between days with ROS and temperature, and precipitation showed greater spatial heterogeneity in November than in December as both positive and negative relationships are observed. However, from January through March, ROS days and

climate anomaly correlations became positive, with the strongest of these positive correlations occurring in February. Correlation patterns were similar for both daily minimum and maximum air temperatures and ROS events over all months represented.

Aggregated correlations for ROS days and associated climate anomalies by Alaska climate regions showed consistently positive correlations from January through March for all regions except the NS (Figure 4.8). In November and December, the mean temperature correlations remained positive, but had a large spread in the correlation distribution including both positive and negative relationships. The mean precipitation correlations from Nov-Dec were negative in the BSC and INT regions, but like temperature, also showed a large range of variability. The negative correlations may be a consequence of the uncertainty introduced by the Daymet model (Daly et al. 2008; Oyler et al. 2015), but could also be a consequence of using a maximum snow cover extent product (MOD10A2) during periods of intermittent snow. The NS region showed a predominantly positive relationship with temperature, but a more variable relationship with minimum temperature in March. Precipitation correlations in the NS were sporadic and weak due to the characteristic colder and drier Arctic climate of the region, which showed a paucity of PM derived ROS events during the Dec-Mar period when seasonal temperatures are generally well below freezing and the cold Arctic air mass holds little moisture. Also, shown in Figure 4.2 are below normal temperature anomalies across the NS during the study period, which also likely contributed to infrequent occurrence of ROS days across the region.

4.5 Discussion

4.5.1 Sources of error, limitations, and advances

The PM ROS events over Alaska showed variable correlations with the selected climate anomalies during November and December, particularly in regions with low elevation (< 200 m) pixels. Inconsistent correlations may also indicate the occurrence of misclassified pixels at lower elevations. The combination of the high variability in correlations and greater occurrence of PM derived ROS events indicates that these areas are influenced by wet snow and shallow, transient snowpack conditions frequently found in low-elevation landscapes (Rees et al. 2010). The high-density network of tundra lakes

at low elevations in the BSC region in addition to large proglacial lakes in southwest Alaska, may also contribute to the higher number of PM derived ROS observations in the region (Wilson *et al.* 2013, Wang *et al.* 2016). The generally greater occurrence of freeze/thaw events in early November and late March in these regions may contribute additional uncertainty such that the ROS algorithm may be detecting increased LWC introduced by snowmelt in the absence of rainfall or atmospheric condensation (C. Dolant et al. 2016).

Our validation results from Fairbanks, AK, showed that most ROS events occurred in early November. The timing of ROS events coincided with many fog observations, indicating that latent and turbulent heat flux driven snowmelt may have contributed to the ROS detection during periods with no measured precipitation (Semmens *et al.* 2013, Wang *et al.* 2016). These results are also consistent with a prior study indicating that fog and positive temperatures are a primary driver of melt events in the YBR, and that that the presence of fog is an effective indicator for warm air intrusions (Semmens *et al.* 2013).

The results from this study were similar to the ROS spatial and seasonal patterns reported from previous studies involving different satellite microwave sensors, classification algorithms and study periods (Bartsch 2010b, Semmens *et al.* 2013, Wilson *et al.* 2013, and Wang *et al.* 2016). These similar findings include generally greater occurrence of melt events in the southwestern portion of Alaska. The studies show that melt events are very infrequent from November to March, but increase dramatically further into spring. While the combined results from these studies indicated multiple effective methods for classifying and documenting ROS and associated melt events from different algorithms and sensors they do not utilize ongoing sensor missions and/or report ROS events at a 6-km resolution. In this study we address this by 1) creating a new ROS record over Alaska using synergistic MODIS and AMSR-E/2 observations that are overlapping with the NASA ABoVE campaign, while enabling continuity of the ROS record through continuing satellite operations; 2) our algorithm approach required only limited inputs emphasizing MODIS SCE and AMSR T_b retrievals, while the combined information from these sensors supported finer (6-km) resolution delineations of ROS patterns and environmental gradients; 4) our study also provided a regional application of

the GRP algorithm, which extended previous localized GRP applications involving in situ field sites (Grenfell and Putkonen 2008, Dolant *et al*. 2016, Langlois *et al.* 2017).

Future ROS record versions will continue to focus on refining the GRP threshold to more effectively account for variations in snow conditions and constraining uncertainties over different landcover types. Yet, regardless of the threshold challenges, this study demonstrated the utility and effectiveness in using the GRP to detect ROS and associated melt events across a large boreal-Arctic landscape. Potential applications of the GRP to detect other snow processes including snow onset, melt onset, and duration remain to be explored.

4.5.2 Consequences of climate change and ROS events in Alaska

Studies examining projected temperature and precipitation trends over Alaska in the latter part of the 21st -Century indicated future warmer winter and annual temperature conditions across the state (Stafford *et al* 2000, Serreze and Francis 2006, Bieniek *et al* 2014); and historically, over the past 60 years, Alaska has experienced almost double the rate of warming relative to other regions in the United States (Chapin *et al.* 2014). While our results from both temperature departures and climate anomalies indicated that ROS frequency is intensified in years with anomalously high temperatures, these temperature anomalies are often driven by large-scale atmospheric circulation patterns that have been found to be highly-correlated with ROS (Cohen *et al*. 2015). Such warm events in Alaska are associated with southwesterly flows and Pacific-North American (PNA) pressure systems that promote ROS and melt events from October to December (Rennert *et al*. 2009, Semmens *et al.* 2013). More recent studies indicated that stratospheric circulations (i.e. polar vortex) strongly influence Alaskan winter temperatures. Specifically, during periods of a weak polar vortex, cold polar air masses are replaced by warmer conditions known as 'warm Arctic cold continents' (Overland *et al.* 2010, Cohen *et al.* 2014, Kretschmer *et al.* 2018), which may promote ROS and associated melt events. The atmospheric blocking and enhanced winter temperatures are also purported to be a major driver of recent record warm Arctic temperatures and record low sea ice extents (Cohen 2016).

Projected warming trends across Alaska and the Arctic (Chapin *et al*. 2005) are expected to increase variability in regional snow cover conditions. Model simulations projected a 10-20% decrease in SCE across the Arctic by 2050 with the greatest losses over Alaska (Callaghan *et al.* 2011). These warming trends may also increase the frequency, duration and extent of surface thawing and refreezing, rainfall and mixed precipitation events, altering snowpack structure and decreasing snow covered area and duration (Chapin *et al*. 2005, Callaghan *et al* 2011, Cohen *et al* 2015, Kim *et al*. 2015). All these factors are expected to contribute to the polar amplification of global warming due to the important role of snow cover on surface albedo and the terrestrial energy budget (Serreze and Francis 2006, Derksen and Brown 2012). The changing snow cover conditions are also expected to impact regional hydrology and ecosystem processes due to the role of snow cover as an important water storage and thermal buffer influencing underlying soil active layer temperature and moisture constraints on ecosystem processes, and permafrost stability (Cohen *et al*. 2012, Yi *et al*. 2015). Some studies suggested that ROS events will become more common in a warming climate across the ABR (Semmens *et al.* 2013, Jeong and Shushama 2017), which is consistent with an analysis of the recent historical record reporting an annual increase of about 7 melt event days yr^{-1} from 1998-2013 over the pan-Arctic (Wang *et al.* 2016). However, the long-term influence of enhanced ROS and melt events within Alaska and the associated impacts of these changes on the regional hydrology, ecosystems and human populations remain uncertain.

4.6 Summary

This paper presented a new satellite derived ROS dataset derived from MODIS snow cover observations and a passive microwave spectral gradient ratio based classification (Dolant *et al.* 2016) derived using calibrated 6-km AMSR T_b records at 19 GHz and 37 GHz frequencies. The daily ROS classification was conducted over Alaska for the winter months (Nov-Mar) from WY 2003-2016 (excluding 2012). A two-tiered validation approach using regional weather station observations indicated favorable ROS classification accuracies ranging from 75-100%. The resulting multi-year satellite record revealed markedly higher ROS frequencies in the southwest and central portions of Alaska. The ROS days also occurred most frequently in November and December and

coincided with warm temperature anomalies. ROS events were consistently observed in the BSC and AGC during all months of the year, and often occurred during periods of above-normal temperatures in the INT and NS regions. These results were similar to previous remote sensing based ROS studies derived over different periods and using different classification algorithms; together, these results indicate strong sensitivity of satellite microwave remote sensing to freeze-thaw related ROS processes.

The northern boreal and Arctic regions are characterized by an extended period of seasonal snow cover, which strongly influence regional ecosystems, hydrologic processes, the surface energy budget and global climate. As the northern-latitudes continue to experience accelerated warming at roughly twice the mean global rate, ROS is expected to play a more significant role in both ecological and hydrologic processes. To understand future implications of enhanced ROS events, we presented a ROS algorithm that utilized satellite observations from current operational satellites (AMSR2, MODIS), enabling ROS retrievals over Alaska that are overlapping with recent extensive and planned field campaigns from the NASA ABoVE. Thus, the data record developed in this study, when synthesized with other biophysical observations, are anticipated to contribute to addressing several data gaps and ABoVE science objectives pertaining to climate related impacts on boreal and Arctic ecosystems, wildlife, permafrost hydrology and snow processes, and associated climate impacts on human-natural systems.

4.7 References

Alford, Donald. 1967. “Density Variations in Alpine Snow.” *Journal of Glaciology* 6 (46).

Beniston, Martin, and Markus Stoffel. 2016. “Rain-on-Snow Events, Floods and Climate Change in the Alps: Events May Increase with Warming up to 4C and Decrease Thereafter.” *Science of the Total Environment* 571 (May 1999). Elsevier B.V.: 228–36. https://doi.org/10.1016/j.scitotenv.2016.07.146.

Berger, J., C. Hartway, A. Gruzdev, and M. Johnson. 2018. “Climate Degradation and Extreme Icing Events Constrain Life in Cold-Adapted Mammals.” *Scientific Reports* 8 (1). Springer US: 1156. https://doi.org/10.1038/s41598-018-19416-9.

Bieniek, Peter A., Uma S. Bhatt, Richard L. Thoman, Heather Angeloff, James Partain, John Papineau, Frederick Fritsch, et al. 2012. “Climate Divisions for Alaska Based on Objective Methods.” *Journal of Applied Meteorology and Climatology* 51 (7): 1276–89. https://doi.org/10.1175/JAMC-D-11-0168.1.

Bieniek, Peter A., John E. Walsh, Richard L. Thoman, and Uma S. Bhatt. 2014. “Using Climate Divisions to Analyze Variations and Trends in Alaska Temperature and Precipitation.” *Journal of Climate* 27 (8): 2800–2818. https://doi.org/10.1175/JCLI-D-13-00342.1.

Brodzik, Mary J, Brendan Billingsley, Terry Haran, Bruce Raup, and Matthew H Savoie. 2012. “EASE-Grid 2.0: Incremental but Significant Improvements for Earth-Gridded Data Sets.” *ISPRS Int. J. Geo-Inf* 1: 32–45. https://doi.org/10.3390/ijgi1010032.

Callaghan, Terry V., Margareta Johansson, Ross D. Brown, Pavel Ya Groisman, Niklas Labba, Vladimir Radionov, Roger G. Barry, et al. 2011. “The Changing Face of Arctic Snow Cover: A Synthesis of Observed and Projected Changes.” *Ambio* 40: 17–31. https://doi.org/10.1007/s13280-011-0212-y.

Cohen, Judah, Hengchun Ye, and Justin Jones. 2015. “Trends and Variability in Rain-on-Snow Events.” *Geophysical Research Letters* 42: 1–8.

https://doi.org/10.1002/2015GL065320.Received.

Daly, Christopher, Michael Halbleib, Joseph I Smith, Wayne P Gibson, Matthew K Doggett, George H Taylor, and Phillip P Pasteris. 2008. “Physiographically Sensitive Mapping of Climatological Temperature and Precipitation across the Conterminous United States.” *International Journal of Climatology* 28: 2031–64. https://doi.org/10.1002/joc.

Derksen, C., and R. Brown. 2012. “Spring Snow Cover Extent Reductions in the 2008-2012 Period Exceeding Climate Model Projections.” *Geophysical Research Letters* 39 (19): 1–6. https://doi.org/10.1029/2012GL053387.

Derksen, C, P Toose, J Lemmetyinen, J Pulliainen, A Langlois, N Rutter, and M C Fuller. 2012. “Remote Sensing of Environment Evaluation of Passive Microwave Brightness Temperature Simulations and Snow Water Equivalent Retrievals through a Winter Season.” *Remote Sensing of Environment* 117. Elsevier B.V.: 236–48. https://doi.org/10.1016/j.rse.2011.09.021.

Dolant, C., A. Langlois, B. Montpetit, L. Brucker, A. Roy, and A. Royer. 2016. “Development of a Rain-on-Snow Detection Algorithm Using Passive Microwave Radiometry.” *Hydrological Processes* 30: 3184–96. https://doi.org/10.1002/hyp.10828.

Dolant, Caroline, A. Langlois, L. Brucker, A. Royer, A. Roy, and B. Montpetit. 2017. “Meteorological Inventory of Rain-on-Snow Events in the Canadian Arctic Archipelago and Satellite Detection Assessment Using Passive Microwave Data.” *Physical Geography* 3646. Taylor & Francis: 1–17. https://doi.org/10.1080/02723646.2017.1400339.

Du, Jinyang, J. S. Kimball, L. A. Jones, and J. D. Watts. 2016. “Implementation of Satellite Based Fractional Water Cover Indices in the Pan-Arctic Region Using AMSR-E and MODIS.” *Remote Sensing of Environment* 184. Elsevier Inc.: 469–81. https://doi.org/10.1016/j.rse.2016.07.029.

Du, Jinyang, John S. Kimball, Jiancheng Shi, Lucas A. Jones, Shengli Wu, Ruijing Sun,

and Hu Yang. 2014. “Inter-Calibration of Satellite Passive Microwave Land Observations from AMSR-E and AMSR2 Using Overlapping FY3B-MWRI Sensor Measurements.” *Remote Sensing* 6 (9): 8594–8616. https://doi.org/10.3390/rs6098594.

Du, Jinyang, John S Kimball, Claude Duguay, Youngwook Kim, and Jennifer D Watts. 2017. “Satellite Microwave Assessment of Northern Hemisphere Lake Ice Phenology from 2002 to 2015.” *Cryosphere* 11: 47–63. https://doi.org/10.5194/tc-11-47-2017.

Feld, Shara I., Nicoleta C. Cristea, and Jessica D. Lundquist. 2013. “Representing Atmospheric Moisture Content along Mountain Slopes: Examination Using Distributed Sensors in the Sierra Nevada, California.” *Water Resources Research* 49 (7): 4424–41. https://doi.org/10.1002/wrcr.20318.

Frei, Allan, Marco Tedesco, Shihyan Lee, James Foster, Dorothy K. Hall, Richard Kelly, and David A. Robinson. 2012a. “A Review of Global Satellite-Derived Snow Products.” *Advances in Space Research* 50 (8). COSPAR: 1007–29. https://doi.org/10.1016/j.asr.2011.12.021.

———. 2012b. “A Review of Global Satellite-Derived Snow Products.” *Advances in Space Research* 50 (8). COSPAR: 1007–29. https://doi.org/10.1016/j.asr.2011.12.021.

Grenfell, T. C., and J. Putkonen. 2008. “A Method for the Detection of the Severe Rain-on-Snow Event on Banks Island, October 2003, Using Passive Microwave Remote Sensing.” *Water Resources Research* 44 (3): 1–9. https://doi.org/10.1029/2007WR005929.

Grossi, Giovanna, Amerigo Lendvai, Giovanni Peretti, and Roberto Ranzi. 2017. “Snow Precipitation Measured by Gauges: Systematic Error Estimation and Data Series Correction in the Central Italian Alps.” *Water (Switzerland)* 9 (7): 1–14. https://doi.org/10.3390/w9070461.

Guan, Bin, Duane E Waliser, F Martin Ralph, Eric J Fetzer, and Paul J Neiman. 2016.

"Hydrometeorological Characteristics of Rain-on-Snow Events Associated with Atmospheric Rivers." *Geophysical Research Letters* 43: 2964–73. https://doi.org/10.1002/2016GL067978.Received.

Hall, Dorothy K, George A Riggs, Vincent V Salomonson, Nicolo E DiGirolamo, and Klaus J Bayr. 2002. "MODIS Snow-Cover Products." *Remote Sensing of Environment* 83 (1–2): 181–94. https://doi.org/http://dx.doi.org/10.1016/S0034-4257(02)00095-0.

Hall, Dorothy, and George Riggs. 2007. "Accuracy Assessment of the MODIS Snow Products." *Hydrological Processes* 21: 1534–47. https://doi.org/10.1002/hyp.6715.

Imaoka, K., M. Kachi, M. Kasahara, N. Ito, K. Nakagawa, and T. Oki. 2010. "Instrument Performance and Calibration of AMSR-E and AMSR2." *International Archives of the Photogrammetry, Remote Sensing and Spatial Information Sciences - ISPRS Archives* 38 (8): 13–18. http://www.scopus.com/inward/record.url?eid=2-s2.0-84907463202&partnerID=tZOtx3y1.

Jeong, Dae Il, and Laxmi Shushama. 2017. "Rain-on-Snow Events over North America Based on Two Canadian Regional Climate Models." *Climate Dynamics*. Springer Berlin Heidelberg. https://doi.org/10.1007/s00382-017-3609-x.

Kawanishi, Toneo, Toshihiro Sezai, Yasuyuki Ito, Keiji Imaoka, Toshiaki Takeshima, Yoshio Ishido, Akira Shibata, Masaharu Miura, Hiroyuki Inahata, and Roy W. Spencer. 2003. "The Advanced Microwave Scanning Radiometer for the Earth Observing System (AMSR-E), NASDA's Contribution to the EOS for Global Energy and Water Cycle Studies." *IEEE Transactions on Geoscience and Remote Sensing* 41 (2): 184–93. https://doi.org/10.1109/TGRS.2002.808331.

Kim, Youngwook, J S Kimball, D A Robinson, and C Derksen. 2015. "New Satellite Climate Data Records Indicate Strong Coupling between Recent Frozen Season Changes and Snow Cover over High Northern Latitudes." *Environmental Research Letters* 10 (084004). IOP Publishing: 1–10. https://doi.org/10.1088/1748-9326/10/8/084004.

Kim, Youngwook, John S Kimball, Joseph Glassy, and Jinyang Du. 2017. “An Extended Global Earth System Data Record on Daily Landscape Freeze – Thaw Status Determined from Satellite Passive Microwave Remote Sensing.” *Earch System Science Data* 9: 133–47. https://doi.org/10.5194/essd-9-133-2017.

Langlois, A., C. A. Johnson, B. Montpetit, A. Royer, E. A. Blukacz-Richards, E. Neave, C. Dolant, et al. 2017. “Detection of Rain-on-Snow (ROS) Events and Ice Layer Formation Using Passive Microwave Radiometry: A Context for Peary Caribou Habitat in the Canadian Arctic.” *Remote Sensing of Environment* 189. Elsevier B.V.: 84–95. https://doi.org/10.1016/j.rse.2016.11.006.

Loe, Leif Egil, Brage B. Hansen, Audun Stien, Steve D. Albon, Richard Bischof, Anja Carlsson, R. Justin Irvine, et al. 2016. “Behavioral Buffering of Extreme Weather Events in a High-Arctic Herbivore.” *Ecosphere* 7 (6): 1–13. https://doi.org/10.1002/ecs2.1374.

Marks, Danny, John Kimball, Dave Tingey, and Tim Link. 1998. “The Sensitivity of Snowmelt Processes to Climate Conditions and Forest Cover during Rain-on-Snow : A Case Study of the 1996 Pacific Northwest Flood.” *Hydrological Processes* 12: 1569–87.

Martinaitis, Steven M., Stephen B. Cocks, Youcun Qi, Brian T. Kaney, Jian Zhang, and Kenneth Howard. 2015. “Understanding Winter Precipitation Impacts on Automated Gauge Observations within a Real-Time System.” *Journal of Hydrometeorology* 16 (6): 2345–63. https://doi.org/10.1175/JHM-D-15-0020.1.

McCabe, Gregory, Martyn Clark, and Lauren Hay. 2007. “Rain-on-Snow Events in the Western United States.” *Bulletin of American Meteorological Society* March: 319–28. https://doi.org/10.1175/BAMS-88-3-319.

Merenti-Valimaki, Hanna-Leena. 2001. “Present Weather: Comparing Human Observations and One Type of Automated Sensor.” *Meteorological Applications* 8: 491–96. http://journals.ametsoc.org/doi/10.1175/JHM-D-15-0020.1.

O’Neel, Shad, Eran Hood, Allison L. Bidlack, Sean W. Fleming, Mayumi L. Arimitsu,

Anthony Arendt, Evan Burgess, et al. 2015. “Icefield-to-Ocean Linkages across the Northern Pacific Coastal Temperate Rainforest Ecosystem.” *BioScience* 65 (5): 499–512. https://doi.org/10.1093/biosci/biv027.

Oyler, Jared W, Ashley Ballantyne, Kelsey Jencso, and Steven W Running. 2015. “Creating a Topoclimatic Daily Air Temperature Dataset for the Conterminous United States Using Homogenized Station Data and Remotely Sensed Land Skin Temperature.” *International Journal of Climatology* 35: 2258–79. https://doi.org/10.1002/joc.4127.

Pistocchi, A. 2016. “Simple Estimation of Snow Density in an Alpine Region.” *Journal of Hydrology: Regional Studies* 6. Elsevier B.V.: 82–89. https://doi.org/10.1016/j.ejrh.2016.03.004.

Putkonen, J, and G Roe. 2003. “Rain-on-Snow Events Impact Soil Temperatures and Affect Ungulate Survival.” *Geophysical Research Letters* 30 (4): 1–4. https://doi.org/10.1029/2002GL016326.

Rees, Andrew, Juha Lemmetyinen, Chris Derksen, Jouni Pulliainen, and Michael English. 2010. “Remote Sensing of Environment Observed and Modelled Effects of Ice Lens Formation on Passive Microwave Brightness Temperatures over Snow Covered Tundra.” *Remote Sensing of Environment* 114 (1). Elsevier B.V.: 116–26. https://doi.org/10.1016/j.rse.2009.08.013.

Rennert, J. Kevin, Gerard Roe, Jaakko Putkonen, and M. Bitz, Cecilia. 2009. “Soil Thermal and Ecological Impacts of Rain on Snow Events in the Circumpolar Arctic.” *Journal of Climate* 22: 2302–15. https://doi.org/10.1175/2008JCLI2117.1.

Riseth, Jan Åge, Hans Tømmervik, Elina Helander-Renvall, Niklas Labba, Cecilia Johansson, Eirik Malnes, Jarle W. Bjerke, et al. 2011. “Sámi Traditional Ecological Knowledge as a Guide to Science: Snow, Ice and Reindeer Pasture Facing Climate Change.” *Polar Record* 47 (242): 202–17. https://doi.org/10.1017/S0032247410000434.

Serreze, Mark C, and Jennifer A Francis. 2006. “The Arctic Amplification Debate.”

Climatic Change 76: 241–64. https://doi.org/10.1007/s10584-005-9017-y.

Sims, H. Elizabeth, and Guosheng Liu. 2015. "A Parameterization of the Probability of Snow – Rain Transition." *Journal of Hydrometeorology* 16: 1466–77. https://doi.org/10.1175/JHM-D-14-0211.1.

Stafford, J. M., G. Wendler, and J. Curtis. 2000. "Temperature and Precipitation of Alaska: 50 Year Trend Analysis." *Theoretical and Applied Climatology* 67 (1–2): 33–44. https://doi.org/10.1007/s007040070014.

Sugg, Johnathan W., Christopher M. Fuhrmann, L. Baker Perry, Dorothy K. Hall, and Charles E. Konrad. 2017. "Sub-Regional Snow Cover Distribution across the Southern Appalachian Mountains." *Physical Geography* 38 (2). Taylor & Francis: 105–23. https://doi.org/10.1080/02723646.2016.1162020.

Thornton, P. E., S. W. Running, and M. A. White. 1997. "Generating Surfaces of Daily Meteorological Variables in Complex Terrain.Pdf." *Journal of Hydrology* 190: 214–51.

Tomsett, A. C., and R. Toumi. 2000. "Diurnal Temperature Range and Rainfall Probability over the United Kingdom." *Geophysical Research Letters* 27 (9): 1279–82. https://doi.org/10.1029/1999GL011335.

Vuyovich, Carrie M., Jennifer M. Jacobs, Christopher A. Hiemstra, and Elias J. Deeb. 2017. "Effect of Spatial Variability of Wet Snow on Modeled and Observed Microwave Emissions." *Remote Sensing of Environment* 198. Elsevier Inc.: 310–20. https://doi.org/10.1016/j.rse.2017.06.016.

Wang, Libo, Peter Toose, Ross Brown, and Chris Derksen. 2016. "Frequency and Distribution of Winter Melt Events from Passive Microwave Satellite Data in the Pan-Arctic, 1988-2013." *Cryosphere* 10 (6): 2589–2602. https://doi.org/10.5194/tc-10-2589-2016.

Tables

Table 4.1 2003 – 2016 observations of ROS events and precipitation totals from Fairbanks, AK (64.80°N, -147.88°W).

Date	Precipitation [mm]
March 23 -26 2016	8.89
November 26 2015	< 2.54
February 21 - 22 2015	5.8
December 31 2014	< 2.54
January 23 - 24 2014	1.02
December 5 2013	0.51
November 14 - 15 2013	18.54
January 14 2013	3.81
November 22 - 24 2010	24.13
November 2 - 8 2003	11.18
March 2 2003	0.25
February 8 - 10 2003	7.37

Table 4.2 Tier-1 validation of PM observed ROS omissions and accuracy.

WY	NWS Empirical[1]	PAFA Prcp type[2]	PAFA Measured prcp[3]	Total ROS Events	Accuracy %	+/- Error ROS Events
2003	3/3	9	6	15	100.00	0
2004	1/1	9	0	9	100.00	0
2011	1/1	17	14	22	95.45	1
2013	1/1	5	7	8	75.00	2
2014	1/1	35	38	46	89.13	5
2015	1/2	6	1	22	100.00	0
2016	2/2	15	15	16	93.75	1

[1]PM detected ROS days/empirical ROS observations made by NWS observer;

[2]Precipitation observed at PAFA, includes rain and fog; [3]Measured precipitation at PAFA the day of, or before, a detected ROS event.

Table 4.3 Tier-2 validation of PM observed ROS days.

	Nov-Mar
Obs_{rain}	54
Obs_{null}	224
Commission	183
Omission	41
Total ROS Events	278
Accuracy [%]	85.9
+/- Error [ROS Events]	39

Table 4.4 Monthly ROS statistics by climate region.

	North Slope (NS)			Bering Sea Coast (BSC)			AK Gulf Coast (AGC)			Interior (INT)		
	mean	sd	Cv	mean	sdCv	mean	sd	Cv	mean	sd	Cv	
November	0.91	0.71	0.91	4.04	2.07	0.49	1.93	0.92	0.42	1.56	1.19	0.66
December	0.15	0.15	1.00	2.67	1.30	0.58	1.63	0.66	0.51	0.65	0.49	0.82
January	0.04	0.04	NA	2.29	1.81	0.63	2.19	0.50	0.30	0.37	0.34	0.95
February	0.02	0.02	NA	2.12	1.79	0.78	2.11	0.61	0.35	0.29	0.28	0.96
March	0.01	0.01	NA	2.14	1.52	0.63	2.79	0.87	0.32	0.38	0.40	0.87

Figures

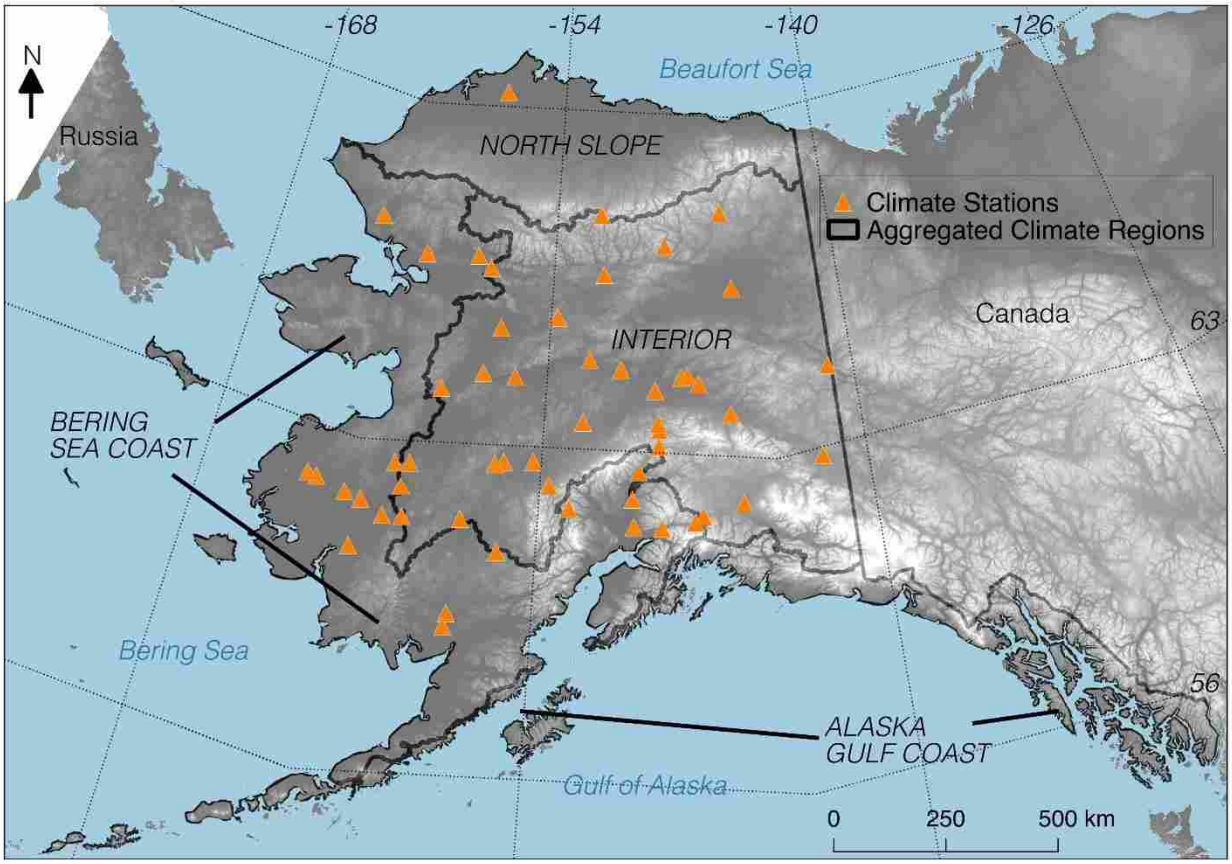

Figure 4.1 Alaska study domain shown with digital elevation model, climate stations used for tier 2 validation and climate regions used for the ROS correlation analysis.

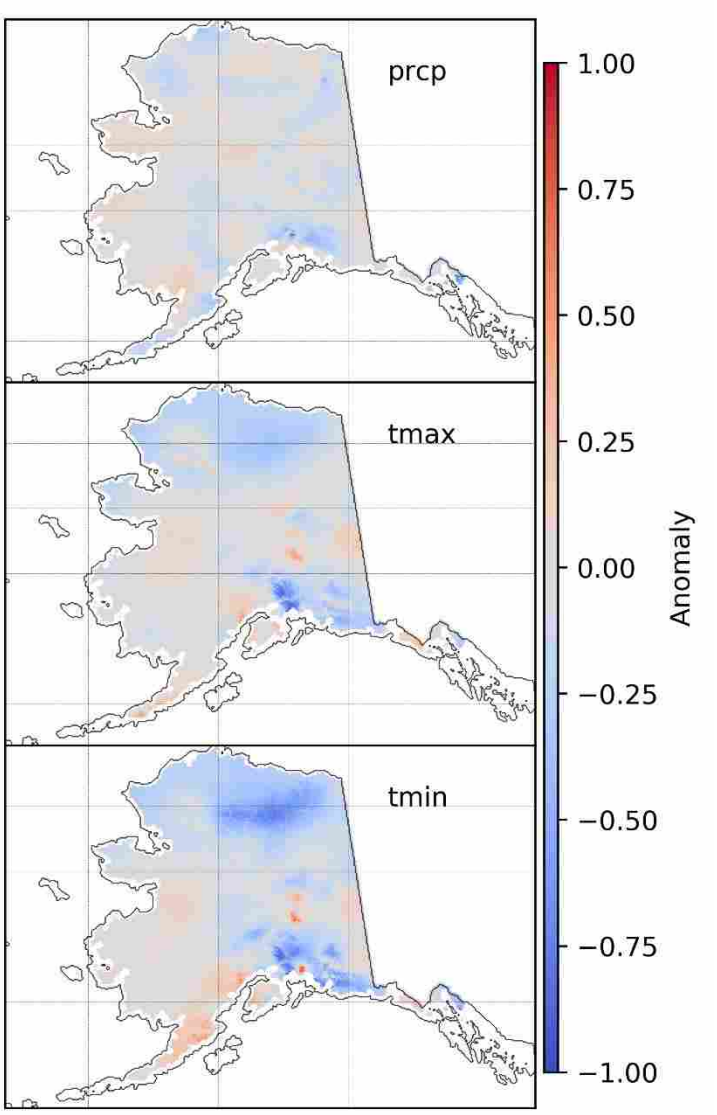

Figure 4.2 Daymet derived standardized anomalies for prcp (top), T_{min} (middle), and T_{max} (bottom) from 2003-2016 (excluding 2012) over the Alaska study domain; a 24 km coastal mask (white areas) is used to minimize open water body effects on the PM retrievals.

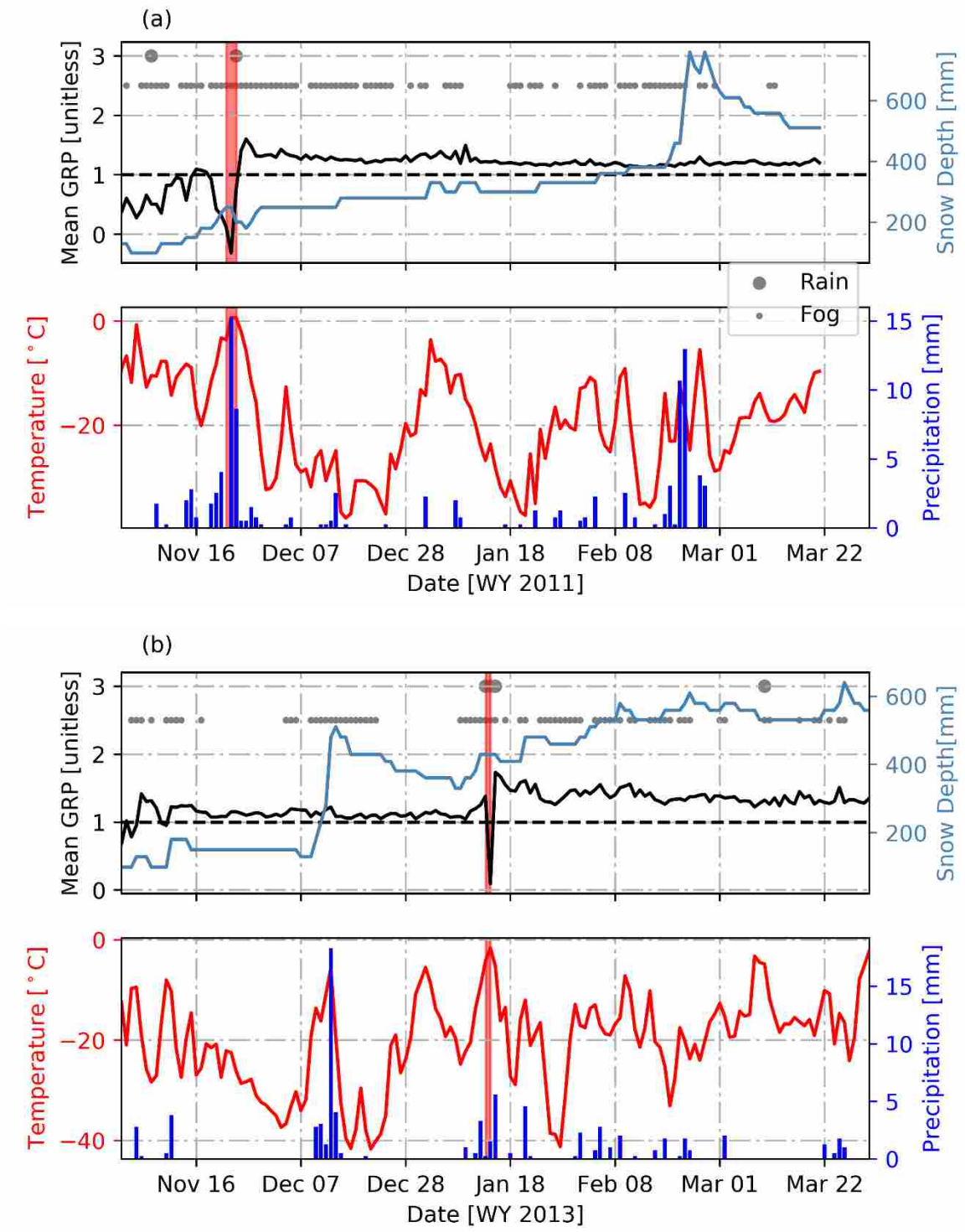

Figure 4.3 (a, b) PM derived daily mean GRP values and in situ precipitation, temperature, snow depth, rain and fog observations from Fairbanks, Alaska for 2011 and 2013 water years; red vertical bars indicate NWS observer ROS events and dashed black horizontal line indicates the GRP threshold.

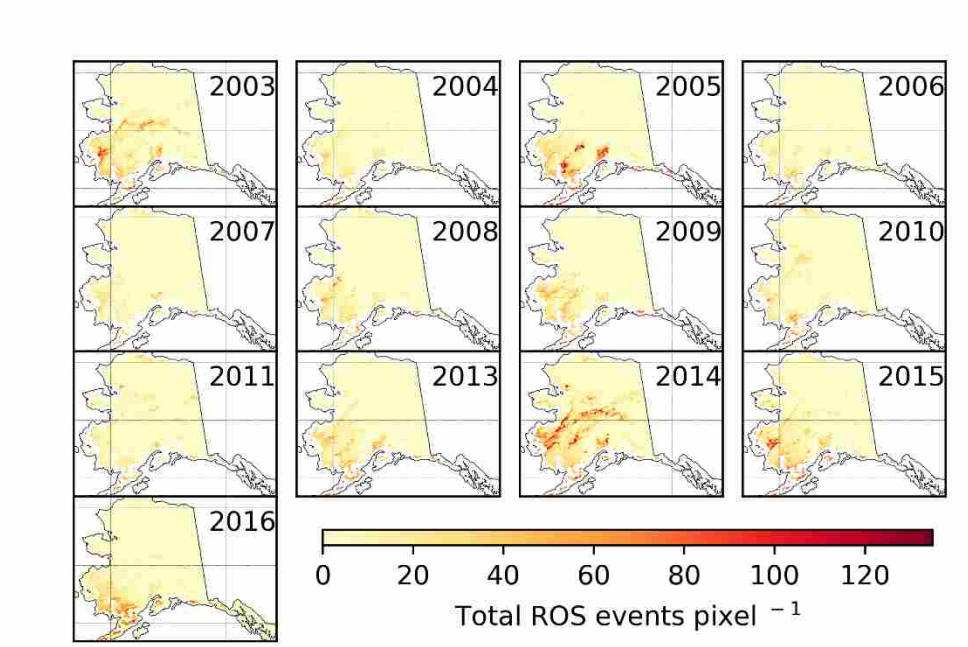

Figure 4.4 Time series of annual days with ROS summed for each pixel, with 24 km coastal mask used to minimize open water body effects on the PM retrievals.

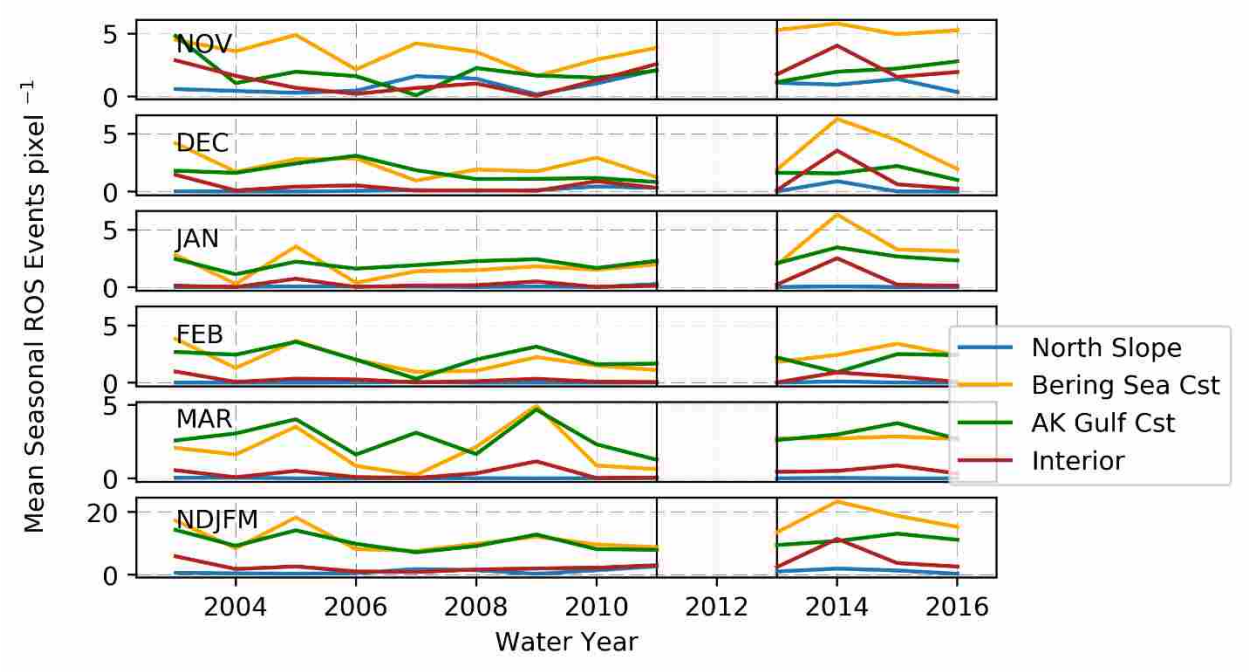

Figure 4.5 Timeseries of mean ROS days pixel^{-1} WY^{-1} for aggregated Alaskan climate regions from WY 2003 - 2016.

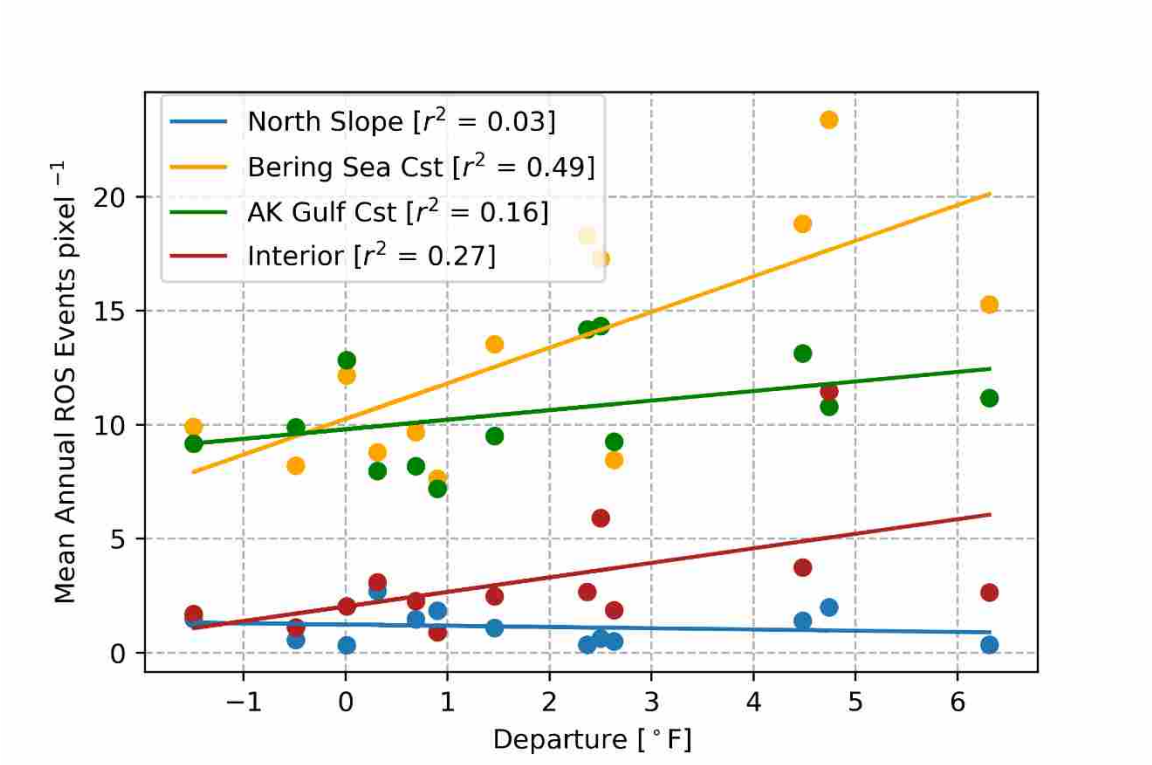

Figure 4.6 Relationship between mean annual (WY) days with ROS pixel^{-1} and surface air temperature departures (°F) aggregated within each Alaska climate region for each year of record from 2003-2016.

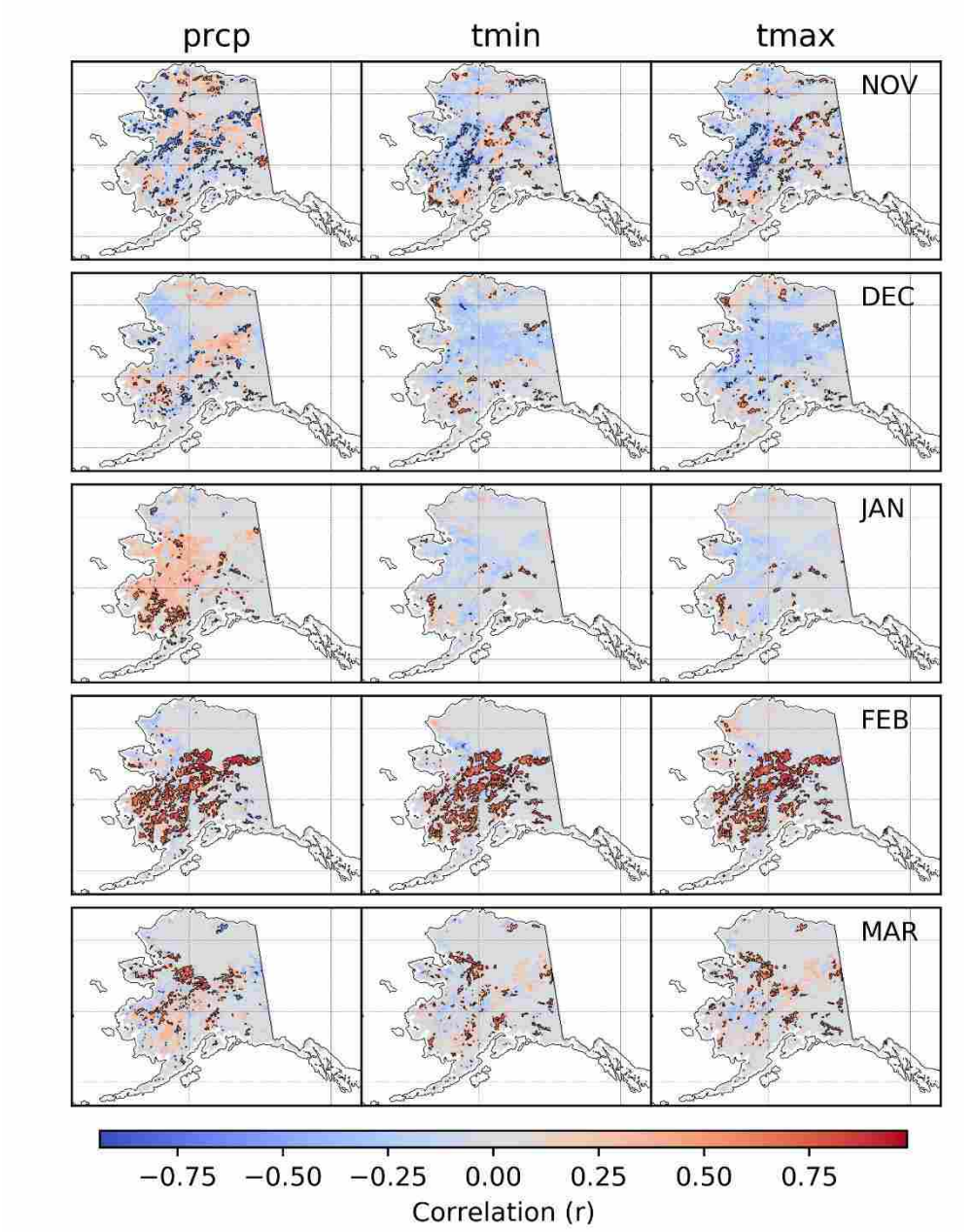

Figure 4.7 Daymet derived climate anomalies and ROS correlations from November to March in Alaska from 2003-2016 (2012 excluded), black contour lines indicate pixels with ≥ 90 % confidence level.

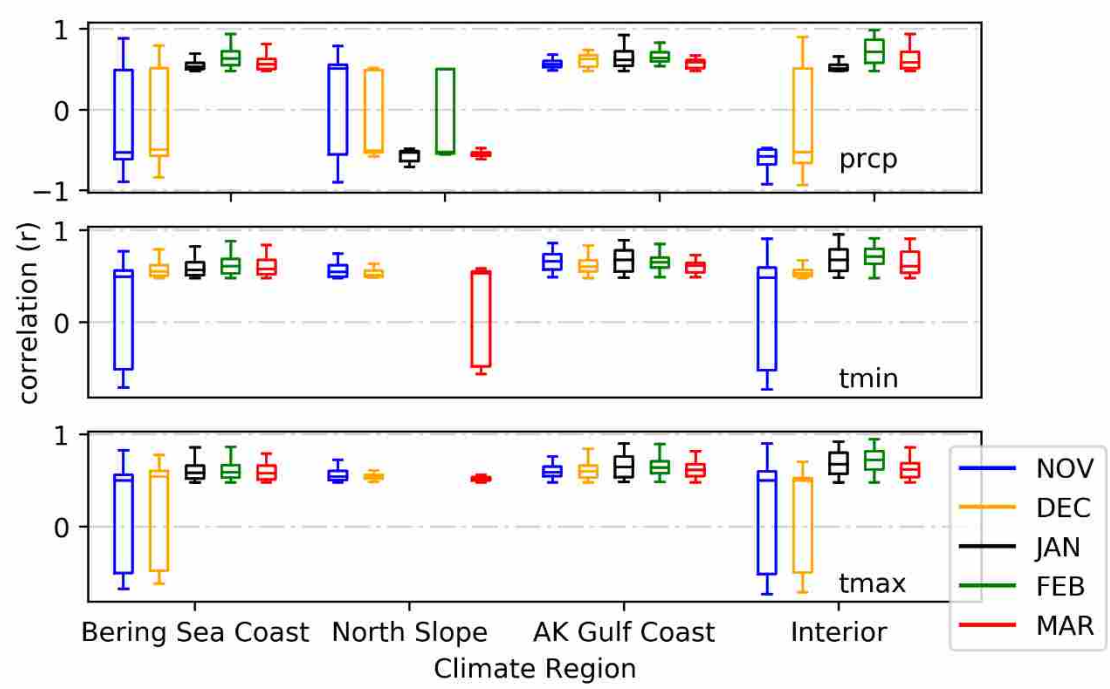

Figure 4.8 Boxplot summaries for climate anomaly and ROS day correlations for all pixels where $p \leq 0.1$, aggregated by Alaska climate region for each month (Nov – Mar) from 2003-2016 (excluding 2012).

Supplemental

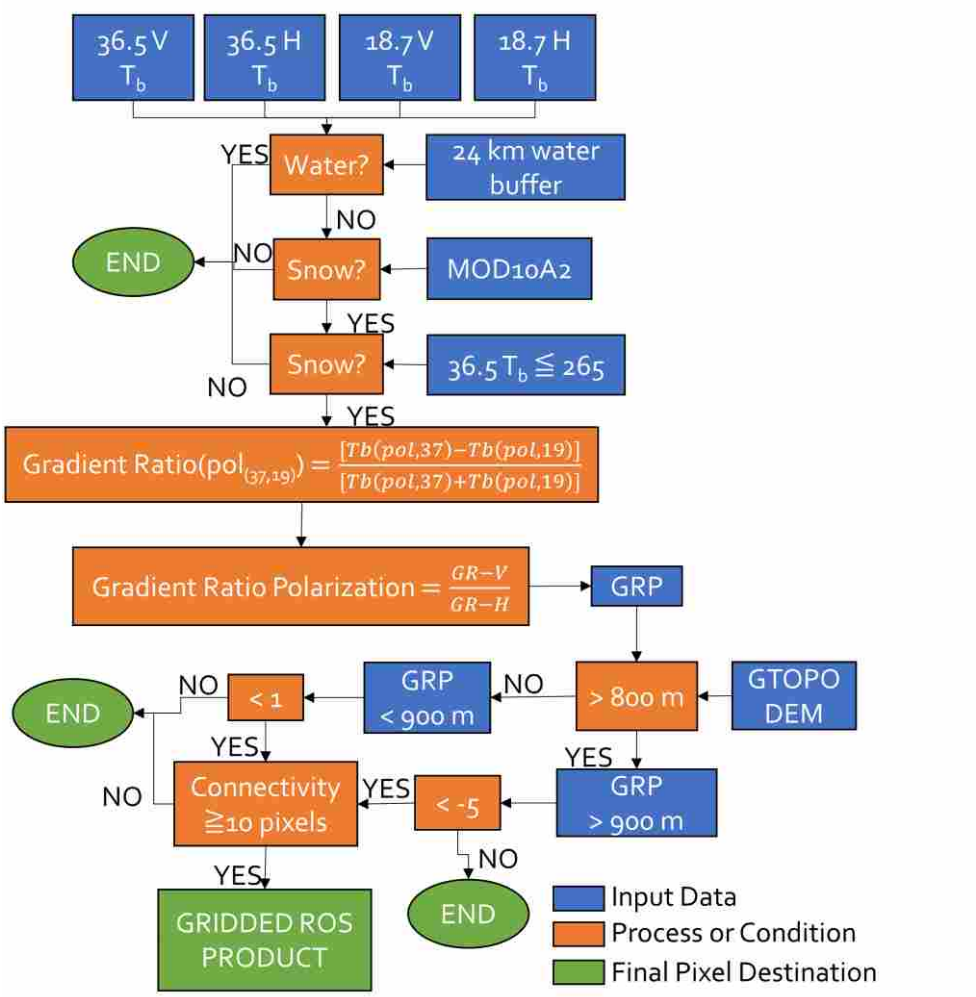

Figure S4.1 Schematic of workflow used to derive gridded daily PM ROS product.

Supplemental 1. GRP Threshold Selection

Algorithm outputs with a GRP threshold of 1, used to classify ROS events, were found to detect an anomalously high number of ROS events per year (i.e. >120 days) at higher elevations above 900 m (Figure S4.2). This apparent ROS overestimation at higher elevations was attributed to the strong GRP sensitivity to variations in snow density (Alford 1967; Pistocchi 2016), where the GRP threshold increases with decreasing snow density (Langlois et al. 2017). A discrete increase in apparent GRP overestimated ROS pixels at elevations between 900 - 2700 m is illustrated in figure S2. To address potential ROS classification errors we applied two different GRP thresholds for varying snow conditions at lower and higher elevations. We applied a GRP threshold of 1 (C. Dolant et

al. 2016) for elevations below 900 m and an alternate GRP threshold of -5 (Langlois et al. 2017) for elevations above 900 m. Figure S4.2 also portrays the apparent ROS overestimation at elevations between 0 and 200 m, addressed in section 4.2. Finally, ROS affected pixels below a minimum spatial connectivity threshold of 10 pixels at each daily time step were screened from the data record to spatially distinguish more extensive ROS occurrences from smaller isolated events. The resulting elevation threshold reduced anomalous ROS pixels above 900 m elevation by 100 %, while the spatial connectivity filter reduced the number of isolated locations with ROS below 900 m by 63 % (Figure S4.2).

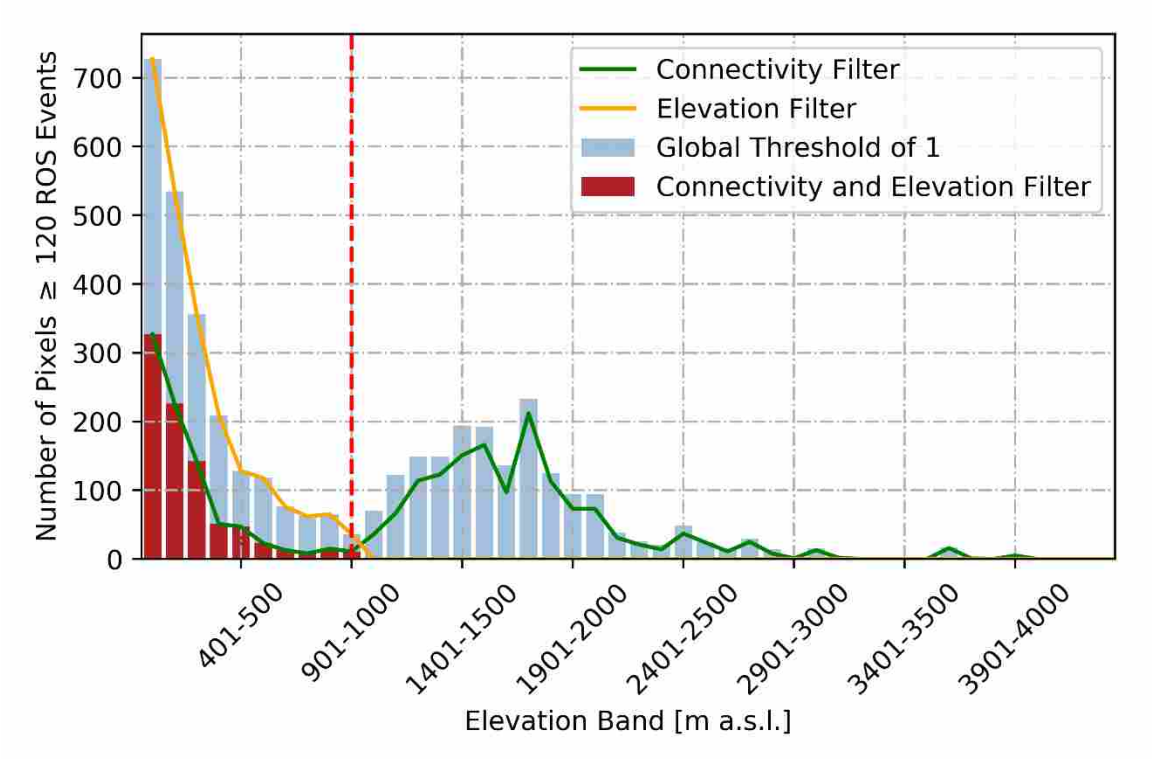

Figure S4.2. Distribution of ROS days per year by mean elevation band, vertical red line (900 m) denotes the minimum elevation where the GRP threshold of -5 was used.

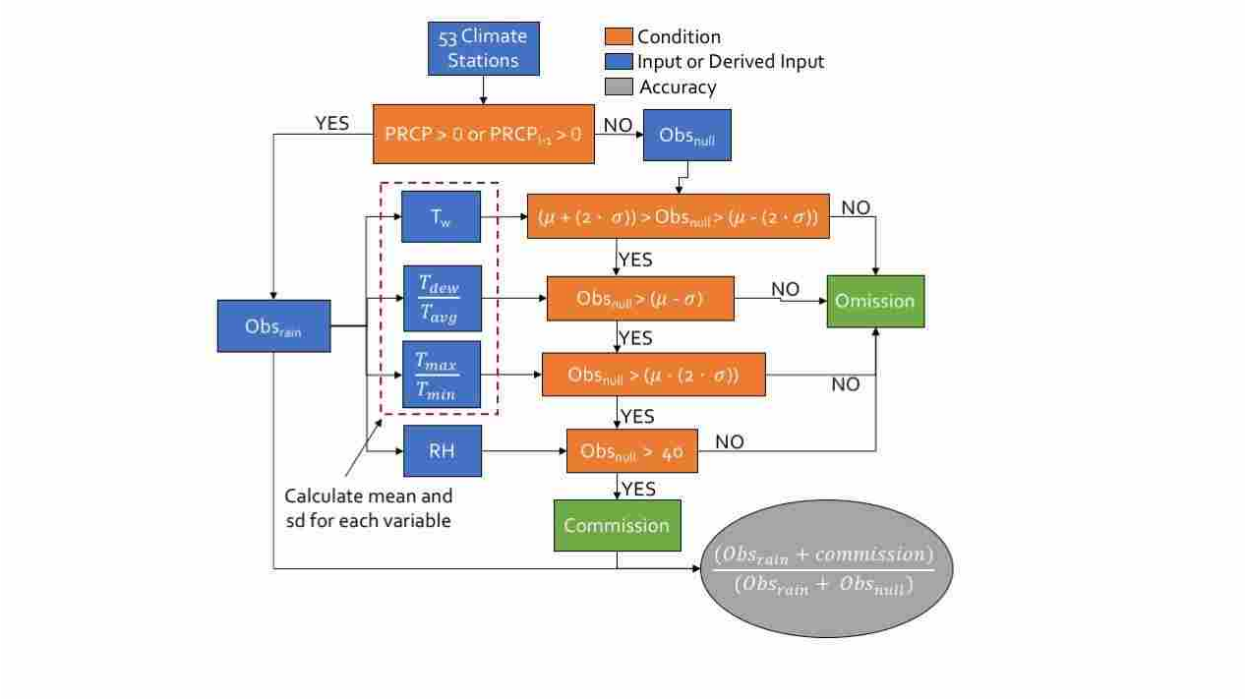

Figure S4.3. Workflow schematic for Tier 2 validation.

Supplemental 2. Description of Tier-2 temperature metrics

We created three temperature driven variables to be used as a proxy for rainfall conditions. These metrics included wet bulb temperature (T_w), the ratio between daily dew point temperature (T_{dew}) and average temperature (T_{dew}/T_{avg}) and the ratio between maximum temperature (T_{max}) and minimum temperature (T_{min}) (T_{max}/T_{min}). The precipitation proxies are used as indicators for atmospheric moisture and energy.

Because air temperature can be highly variable during ROS events (Caroline Dolant et al. 2017), we chose a more stable approach of T_w, where T_w is a proxy for precipitation and ROS occurrence. This served two purposes: 1) T_w constrained the feasibility that precipitation would fall as liquid and 2) T_w provided a better indicator of precipitation phase (Sims and Liu 2015). The derivation of T_w can be found in supplemental 3. The T_{dew}/T_{avg} metric was used to represent the dew point depression and the amount of moisture in the atmosphere (Feld, Cristea, and Lundquist 2013), providing a normalized value for the 'degree of saturation' in the atmosphere. The T_{max}/T_{min} metric was used as a proxy for cloudiness based on the assuming cloudier conditions decreased radiative heating and cooling of the land surface and the associated daily temperature amplitude

(Tomsett and Toumi 2000). Cloudiness was defined as a relative percentage from 0-100% ranging between clear sky conditions and complete cloud cover.

Using Obs_{rain}, the mean (μ) and standard deviation (σ) were created for each precipitation proxy to constrain Obs_{null}. If Obs_{null} met all of the requirements set by the precipitation proxies, the conditions were identified as feasible for precipitation. ROS days which met all of the constraining conditions set by Obs_{rain} were classified as commission whereas all Obs_{null} observations that did not meet the defined conditions were classified as omission. The final ROS accuracy was calculated as a percentage of the sum of Obs_{rain} and commission days divided by the total number of classified ROS days.

Supplemental 3. Derivation of wet bulb

To derive T_w, we first calculated vapor pressure [E] from T_{dew}:

$$E = 6.11 \cdot 10^{\frac{7.5 \cdot T_{dew}}{237.7 + T_{dew}}} \qquad \text{Eq. 1}$$

Using E, T_{dew}, T_{avg}, and station pressure [mb] (STP), Tw can then be derived by the following (Sullivan and Sanders 1977):

$$T_w = \left(0.00066 \cdot STP + T_{avg}\right) + \frac{\left[\frac{4098 \cdot E}{(T_{dew}+237.7)^2 \cdot T_{dew}}\right]}{\left[\frac{(0.00066 \cdot STP)+(4098 \cdot E)}{(T_{dew}+237.7)^2}\right]} \qquad \text{Eq. 2}$$

Figure S4. Time-series of mean annual temperature departures across the state of Alaska from 1949-2016; data are provided by the Alaska Climate Data Research Center.

Supplemental 4. Limitations in validating PM derived ROS

Validating satellite derived ROS is limited by the number and quality of in situ meteorological observations in boreal and arctic regions; a region with limited access, severe climate conditions and sparse weather station networks. The Tier-1 assessment included multiple precipitation observations and was the most inclusive and reliable form of validation used in this study, despite being limited to a single set of ground observations for a single location in central Alaska. The Tier-1 results also showed the limitation of in situ precipitation observations to exclusively validate ROS; this reflects uncertainty in precipitation measurements and reporting due to sensor limitations, wind

redistribution effects, blockage of gauges/sensors, biases introduced during post-thaw events, and human error (Merenti-Valimaki 2001, Martinaitis et al 2015, Grossi et al 2017). Discrepancies between the satellite retrievals and in situ precipitation measurements may also reflect differences in both the spatial footprint of observations and the physical phenomena being measured. For example, the PM derived ROS signal reflects changes in surface wetness that may be caused by either direct rainfall inputs or surface snowmelt driven by sensible, turbulent and or latent heat fluxes (Marks *et al.* 1998). The Tier-1 validation results indicated that the majority of ROS events occur in early November at the Fairbanks station location. This early occurrence and the large number of reported observations of fog suggests that latent and turbulent heat flux contribute to the ROS observations during periods with no measurable precipitation; these results also suggest that fog followed by wind may be a valid proxy for ROS occurrence. However, no attempt was made to differentiate between fog and freezing fog, as freezing fog would not contribute to wet snow conditions. Measured precipitation provided the highest omission error during each year of record, except for WY 2014, suggesting that a number of ROS events possessed only trace amounts of precipitation that were below the detection level of the PAFA station. Unfortunately, the Tier-1 validation was restricted to the PAFA station since it was the only record documented as a high-quality data set by human observers.

Tier-2 validation was applied across the Alaska domain, with only 19 % of the PM derived ROS days showing measured precipitation (Obs_{rain}). Two factors contribute to this lack of coincident observations. First, rain is not the singular factor determining wet snow surface conditions, which are frequently due to energy exchange processes that can occur before, during and after, and sometimes independently, of rain events. These processes include turbulent exchange and sensible and latent heat fluxes, which are the primary source of snowpack melt energy flux during the winter accumulation phase of high latitude snowpacks. The period for ROS detection in this study was constrained between Nov-Mar when solar insolation is relatively low, so that solar radiation is not the primary source of snowmelt energy. Second, measurement technologies and the arduous quality checking (QA and QC) process required to effectively discriminate between rain,

snow and mixed precipitation data are nearly nonexistent for Alaska climate records; the first observer data for the Fairbanks site used in the Tier-1 validation was the only record of this type we could find (Martinaitis et al. 2015; Grossi et al. 2017).

References

Alford, Donald. 1967. "Density Variations in Alpine Snow." *Journal of Glaciology* 6 (46).

Beniston, Martin, and Markus Stoffel. 2016. "Rain-on-Snow Events, Floods and Climate Change in the Alps: Events May Increase with Warming up to 4C and Decrease Thereafter." *Science of the Total Environment* 571 (May 1999). Elsevier B.V.: 228–36. https://doi.org/10.1016/j.scitotenv.2016.07.146.

Berger, J., C. Hartway, A. Gruzdev, and M. Johnson. 2018. "Climate Degradation and Extreme Icing Events Constrain Life in Cold-Adapted Mammals." *Scientific Reports* 8 (1). Springer US: 1156. https://doi.org/10.1038/s41598-018-19416-9.

Bieniek, Peter A., Uma S. Bhatt, Richard L. Thoman, Heather Angeloff, James Partain, John Papineau, Frederick Fritsch, et al. 2012. "Climate Divisions for Alaska Based on Objective Methods." *Journal of Applied Meteorology and Climatology* 51 (7): 1276–89. https://doi.org/10.1175/JAMC-D-11-0168.1.

Bieniek, Peter A., John E. Walsh, Richard L. Thoman, and Uma S. Bhatt. 2014. "Using Climate Divisions to Analyze Variations and Trends in Alaska Temperature and Precipitation." *Journal of Climate* 27 (8): 2800–2818. https://doi.org/10.1175/JCLI-D-13-00342.1.

Brodzik, Mary J, Brendan Billingsley, Terry Haran, Bruce Raup, and Matthew H Savoie. 2012. "EASE-Grid 2.0: Incremental but Significant Improvements for Earth-Gridded Data Sets." *ISPRS Int. J. Geo-Inf* 1: 32–45. https://doi.org/10.3390/ijgi1010032.

Callaghan, Terry V., Margareta Johansson, Ross D. Brown, Pavel Ya Groisman, Niklas Labba, Vladimir Radionov, Roger G. Barry, et al. 2011. "The Changing Face of Arctic Snow Cover: A Synthesis of Observed and Projected Changes." *Ambio* 40: 17–31. https://doi.org/10.1007/s13280-011-0212-y.

Cohen, Judah, Hengchun Ye, and Justin Jones. 2015. “Trends and Variability in Rain-on-Snow Events.” *Geophysical Research Letters* 42: 1–8. https://doi.org/10.1002/2015GL065320.Received.

Daly, Christopher, Michael Halbleib, Joseph I Smith, Wayne P Gibson, Matthew K Doggett, George H Taylor, and Phillip P Pasteris. 2008. “Physiographically Sensitive Mapping of Climatological Temperature and Precipitation across the Conterminous United States.” *International Journal of Climatology* 28: 2031–64. https://doi.org/10.1002/joc.

Derksen, C., and R. Brown. 2012. “Spring Snow Cover Extent Reductions in the 2008-2012 Period Exceeding Climate Model Projections.” *Geophysical Research Letters* 39 (19): 1–6. https://doi.org/10.1029/2012GL053387.

Derksen, C, P Toose, J Lemmetyinen, J Pulliainen, A Langlois, N Rutter, and M C Fuller. 2012. “Remote Sensing of Environment Evaluation of Passive Microwave Brightness Temperature Simulations and Snow Water Equivalent Retrievals through a Winter Season.” *Remote Sensing of Environment* 117. Elsevier B.V.: 236–48. https://doi.org/10.1016/j.rse.2011.09.021.

Dolant, C., A. Langlois, B. Montpetit, L. Brucker, A. Roy, and A. Royer. 2016. “Development of a Rain-on-Snow Detection Algorithm Using Passive Microwave Radiometry.” *Hydrological Processes* 30: 3184–96. https://doi.org/10.1002/hyp.10828.

Dolant, Caroline, A. Langlois, L. Brucker, A. Royer, A. Roy, and B. Montpetit. 2017. “Meteorological Inventory of Rain-on-Snow Events in the Canadian Arctic Archipelago and Satellite Detection Assessment Using Passive Microwave Data.” *Physical Geography* 3646. Taylor & Francis: 1–17. https://doi.org/10.1080/02723646.2017.1400339.

Du, Jinyang, J. S. Kimball, L. A. Jones, and J. D. Watts. 2016. “Implementation of Satellite Based Fractional Water Cover Indices in the Pan-Arctic Region Using AMSR-E and MODIS.” *Remote Sensing of Environment* 184. Elsevier Inc.: 469–81. https://doi.org/10.1016/j.rse.2016.07.029.

Du, Jinyang, John S. Kimball, Jiancheng Shi, Lucas A. Jones, Shengli Wu, Ruijing Sun, and Hu Yang. 2014. “Inter-Calibration of Satellite Passive Microwave Land Observations from AMSR-E and AMSR2 Using Overlapping FY3B-MWRI Sensor Measurements.” *Remote Sensing* 6 (9): 8594–8616. https://doi.org/10.3390/rs6098594.

Du, Jinyang, John S Kimball, Claude Duguay, Youngwook Kim, and Jennifer D Watts. 2017. “Satellite Microwave Assessment of Northern Hemisphere Lake Ice Phenology from 2002 to 2015.” *Cryosphere* 11: 47–63. https://doi.org/10.5194/tc-11-47-2017.

Feld, Shara I., Nicoleta C. Cristea, and Jessica D. Lundquist. 2013. “Representing Atmospheric Moisture Content along Mountain Slopes: Examination Using Distributed Sensors in the Sierra Nevada, California.” *Water Resources Research* 49 (7): 4424–41. https://doi.org/10.1002/wrcr.20318.

Frei, Allan, Marco Tedesco, Shihyan Lee, James Foster, Dorothy K. Hall, Richard Kelly, and David A. Robinson. 2012a. “A Review of Global Satellite-Derived Snow Products.” *Advances in Space Research* 50 (8). COSPAR: 1007–29. https://doi.org/10.1016/j.asr.2011.12.021.

———. 2012b. “A Review of Global Satellite-Derived Snow Products.” *Advances in Space Research* 50 (8). COSPAR: 1007–29. https://doi.org/10.1016/j.asr.2011.12.021.

Grenfell, T. C., and J. Putkonen. 2008. “A Method for the Detection of the Severe Rain-on-Snow Event on Banks Island, October 2003, Using Passive Microwave Remote Sensing.” *Water Resources Research* 44 (3): 1–9. https://doi.org/10.1029/2007WR005929.

Grossi, Giovanna, Amerigo Lendvai, Giovanni Peretti, and Roberto Ranzi. 2017. “Snow Precipitation Measured by Gauges: Systematic Error Estimation and Data Series Correction in the Central Italian Alps.” *Water (Switzerland)* 9 (7): 1–14. https://doi.org/10.3390/w9070461.

Guan, Bin, Duane E Waliser, F Martin Ralph, Eric J Fetzer, and Paul J Neiman. 2016. "Hydrometeorological Characteristics of Rain-on-Snow Events Associated with Atmospheric Rivers." *Geophysical Research Letters* 43: 2964–73. https://doi.org/10.1002/2016GL067978.Received.

Hall, Dorothy K, George A Riggs, Vincent V Salomonson, Nicolo E DiGirolamo, and Klaus J Bayr. 2002. "MODIS Snow-Cover Products." *Remote Sensing of Environment* 83 (1–2): 181–94. https://doi.org/http://dx.doi.org/10.1016/S0034-4257(02)00095-0.

Hall, Dorothy, and George Riggs. 2007. "Accuracy Assessment of the MODIS Snow Products." *Hydrological Processes* 21: 1534–47. https://doi.org/10.1002/hyp.6715.

Imaoka, K., M. Kachi, M. Kasahara, N. Ito, K. Nakagawa, and T. Oki. 2010. "Instrument Performance and Calibration of AMSR-E and AMSR2." *International Archives of the Photogrammetry, Remote Sensing and Spatial Information Sciences - ISPRS Archives* 38 (8): 13–18. http://www.scopus.com/inward/record.url?eid=2-s2.0-84907463202&partnerID=tZOtx3y1.

Jeong, Dae Il, and Laxmi Shushama. 2017. "Rain-on-Snow Events over North America Based on Two Canadian Regional Climate Models." *Climate Dynamics*. Springer Berlin Heidelberg. https://doi.org/10.1007/s00382-017-3609-x.

Kawanishi, Toneo, Toshihiro Sezai, Yasuyuki Ito, Keiji Imaoka, Toshiaki Takeshima, Yoshio Ishido, Akira Shibata, Masaharu Miura, Hiroyuki Inahata, and Roy W. Spencer. 2003. "The Advanced Microwave Scanning Radiometer for the Earth Observing System (AMSR-E), NASDA's Contribution to the EOS for Global Energy and Water Cycle Studies." *IEEE Transactions on Geoscience and Remote Sensing* 41 (2): 184–93. https://doi.org/10.1109/TGRS.2002.808331.

Kim, Youngwook, J S Kimball, D A Robinson, and C Derksen. 2015. "New Satellite Climate Data Records Indicate Strong Coupling between Recent Frozen Season Changes and Snow Cover over High Northern Latitudes." *Environmental Research Letters* 10 (084004). IOP Publishing: 1–10. https://doi.org/10.1088/1748-9326/10/8/084004.

Kim, Youngwook, John S Kimball, Joseph Glassy, and Jinyang Du. 2017. “An Extended Global Earth System Data Record on Daily Landscape Freeze – Thaw Status Determined from Satellite Passive Microwave Remote Sensing.” *Earch System Science Data* 9: 133–47. https://doi.org/10.5194/essd-9-133-2017.

Langlois, A., C. A. Johnson, B. Montpetit, A. Royer, E. A. Blukacz-Richards, E. Neave, C. Dolant, et al. 2017. “Detection of Rain-on-Snow (ROS) Events and Ice Layer Formation Using Passive Microwave Radiometry: A Context for Peary Caribou Habitat in the Canadian Arctic.” *Remote Sensing of Environment* 189. Elsevier B.V.: 84–95. https://doi.org/10.1016/j.rse.2016.11.006.

Loe, Leif Egil, Brage B. Hansen, Audun Stien, Steve D. Albon, Richard Bischof, Anja Carlsson, R. Justin Irvine, et al. 2016. “Behavioral Buffering of Extreme Weather Events in a High-Arctic Herbivore.” *Ecosphere* 7 (6): 1–13. https://doi.org/10.1002/ecs2.1374.

Marks, Danny, John Kimball, Dave Tingey, and Tim Link. 1998. “The Sensitivity of Snowmelt Processes to Climate Conditions and Forest Cover during Rain-on-Snow : A Case Study of the 1996 Pacific Northwest Flood.” *Hydrological Processes* 12: 1569–87.

Martinaitis, Steven M., Stephen B. Cocks, Youcun Qi, Brian T. Kaney, Jian Zhang, and Kenneth Howard. 2015. “Understanding Winter Precipitation Impacts on Automated Gauge Observations within a Real-Time System.” *Journal of Hydrometeorology* 16 (6): 2345–63. https://doi.org/10.1175/JHM-D-15-0020.1.

McCabe, Gregory, Martyn Clark, and Lauren Hay. 2007. “Rain-on-Snow Events in the Western United States.” *Bulletin of American Meteorological Society* March: 319–28. https://doi.org/10.1175/BAMS-88-3-319.

Merenti-Valimaki, Hanna-Leena. 2001. “Present Weather: Comparing Human Observations and One Type of Automated Sensor.” *Meteorological Applications* 8: 491–96. http://journals.ametsoc.org/doi/10.1175/JHM-D-15-0020.1.

O’Neel, Shad, Eran Hood, Allison L. Bidlack, Sean W. Fleming, Mayumi L. Arimitsu,

Anthony Arendt, Evan Burgess, et al. 2015. “Icefield-to-Ocean Linkages across the Northern Pacific Coastal Temperate Rainforest Ecosystem.” *BioScience* 65 (5): 499–512. https://doi.org/10.1093/biosci/biv027.

Oyler, Jared W, Ashley Ballantyne, Kelsey Jencso, and Steven W Running. 2015. “Creating a Topoclimatic Daily Air Temperature Dataset for the Conterminous United States Using Homogenized Station Data and Remotely Sensed Land Skin Temperature.” *International Journal of Climatology* 35: 2258–79. https://doi.org/10.1002/joc.4127.

Pistocchi, A. 2016. “Simple Estimation of Snow Density in an Alpine Region.” *Journal of Hydrology: Regional Studies* 6. Elsevier B.V.: 82–89. https://doi.org/10.1016/j.ejrh.2016.03.004.

Putkonen, J, and G Roe. 2003. “Rain-on-Snow Events Impact Soil Temperatures and Affect Ungulate Survival.” *Geophysical Research Letters* 30 (4): 1–4. https://doi.org/10.1029/2002GL016326.

Rees, Andrew, Juha Lemmetyinen, Chris Derksen, Jouni Pulliainen, and Michael English. 2010. “Remote Sensing of Environment Observed and Modelled Effects of Ice Lens Formation on Passive Microwave Brightness Temperatures over Snow Covered Tundra.” *Remote Sensing of Environment* 114 (1). Elsevier B.V.: 116–26. https://doi.org/10.1016/j.rse.2009.08.013.

Rennert, J. Kevin, Gerard Roe, Jaakko Putkonen, and M. Bitz, Cecilia. 2009. “Soil Thermal and Ecological Impacts of Rain on Snow Events in the Circumpolar Arctic.” *Journal of Climate* 22: 2302–15. https://doi.org/10.1175/2008JCLI2117.1.

Riseth, Jan Åge, Hans Tømmervik, Elina Helander-Renvall, Niklas Labba, Cecilia Johansson, Eirik Malnes, Jarle W. Bjerke, et al. 2011. “Sámi Traditional Ecological Knowledge as a Guide to Science: Snow, Ice and Reindeer Pasture Facing Climate Change.” *Polar Record* 47 (242): 202–17. https://doi.org/10.1017/S0032247410000434.

Serreze, Mark C, and Jennifer A Francis. 2006. “The Arctic Amplification Debate.”

Climatic Change 76: 241–64. https://doi.org/10.1007/s10584-005-9017-y.

Sims, H. Elizabeth, and Guosheng Liu. 2015. "A Parameterization of the Probability of Snow – Rain Transition." *Journal of Hydrometeorology* 16: 1466–77. https://doi.org/10.1175/JHM-D-14-0211.1.

Stafford, J. M., G. Wendler, and J. Curtis. 2000. "Temperature and Precipitation of Alaska: 50 Year Trend Analysis." *Theoretical and Applied Climatology* 67 (1–2): 33–44. https://doi.org/10.1007/s007040070014.

Sugg, Johnathan W., Christopher M. Fuhrmann, L. Baker Perry, Dorothy K. Hall, and Charles E. Konrad. 2017. "Sub-Regional Snow Cover Distribution across the Southern Appalachian Mountains." *Physical Geography* 38 (2). Taylor & Francis: 105–23. https://doi.org/10.1080/02723646.2016.1162020.

Thornton, P. E., S. W. Running, and M. A. White. 1997. "Generating Surfaces of Daily Meteorological Variables in Complex Terrain.Pdf." *Journal of Hydrology* 190: 214–51.

Tomsett, A. C., and R. Toumi. 2000. "Diurnal Temperature Range and Rainfall Probability over the United Kingdom." *Geophysical Research Letters* 27 (9): 1279–82. https://doi.org/10.1029/1999GL011335.

Vuyovich, Carrie M., Jennifer M. Jacobs, Christopher A. Hiemstra, and Elias J. Deeb. 2017. "Effect of Spatial Variability of Wet Snow on Modeled and Observed Microwave Emissions." *Remote Sensing of Environment* 198. Elsevier Inc.: 310–20. https://doi.org/10.1016/j.rse.2017.06.016.

Wang, Libo, Peter Toose, Ross Brown, and Chris Derksen. 2016. "Frequency and Distribution of Winter Melt Events from Passive Microwave Satellite Data in the Pan-Arctic, 1988-2013." *Cryosphere* 10 (6): 2589–2602. https://doi.org/10.5194/tc-10-2589-2016.

CHAPTER 5
Anomalous snowmelt events contribute to widespread livestock die-offs across Mongolia

Corresponding publication:

Pan, C. G., Kimball, J. S., Munkhjargal, M., Robinson, N. P., Tijdeman, E., Menzel, L., and Kirchner, P. B. (submitted). Anomalous snowmelt events contribute to widespread livestock die-offs across Mongolia. *Nature Scientific Reports*.

5.1 Abstract

Livestock production is a socio-economic linchpin in Mongolia that is affected by large-scale livestock die-offs. Colloquially known as dzuds, these die-offs are driven by anomalous climatic events, including extreme cold temperatures, extended snow cover duration (SCD) and drought. As temperatures across Mongolia have increased – we hypothesized that increasing cold season snow melt events associated with regional warming have become increasingly important drivers of dzud events as they can reduce pasture productivity and potentially inhibit access to grazing through subsequent icing events. Here, we use integrated satellite observations to determine the spatiotemporal variability in anomalous snowmelt events across Mongolia from 2003-2016 and their contribution to dzuds relative to other climatic drivers, including winter temperatures, SCD, and drought. We find a positive relationship between melt events and livestock mortality during the fall in southern Mongolia and during the spring in the central and western regions. Further, anomalous seasonal melt events explain 17-34% of the total variance in annual livestock mortality, with cold temperatures as the leading contributor of dzuds. Our results indicate that snowmelt events will become an increasingly important driver of dzuds as annual temperatures and livestock populations are projected to increase in Mongolia.

5.2 Introduction

Livestock production is a central part of Mongolia's economy (Fernández-Giménez 1999)and is exemplified by half of the regional human population's livelihoods connected to various forms of pastoralism(Johnson et al. 2006; T. Ã. Sternberg 2008). Mongolia's large livestock population and its role as a national economic driver, facilitates extreme vulnerabilities to small climatic fluctuations and can often result in large annual livestock die-offs. In Mongolia, these anomalous die-off events are known as dzuds, or wintertime disasters in the English language. Historically, dzud events played an important role in regulating livestock populations (Fernández-Giménez, Batkhishig, and Batbuyan 2012). However, the intensity and frequency of dzud events have increased with growing livestock populations, reduced rangeland management, and accelerated climate change(Batima et al. 2005). The largest recorded dzud event in the modern era occurred in 2010, where 8-10 million livestock perished in a single year (Hilker, Natsagdorj, and Waring 2014; Rao et al. 2015). Notably, these losses would likely have been greater had 10-20 million livestock not perished during the preceding dzuds of 1999-2002 (Pederson et al. 2014).

Through much of the 20th Century, Mongolia was influenced by the Soviet Union, during which the government subsidized key resources enabling herders to cope with challenging climatic conditions, including well maintenance(Sugita, Yoshizawa, and Byambakhuu 2015), and winter time hay and fodder storage(Fernández-Giménez 1999) - providing a necessary bridge for livestock to survive regional weather extremes and challenging climatic conditions. More recently, with the collapse of the Soviet Union and the privatization of livestock, livestock populations have precipitously increased whereas formerly provided vital services and subsidies have been reduced, increasing herder vulnerabilities to dzuds(T. Ã. Sternberg 2008). In 1990, there was a livestock population of approximately 25 million across Mongolia, and by 2016 this population increased over 200 % to 60 million (Mongolia Statistical Service, 2017) – straining Mongolian social and ecological systems near their tipping points (Fernández-giménez et al. 2016).

There are many different types of dzuds classified by different climatic and environmental conditions. The most studied dzuds include, but are not limited to, the *tsagaan dzud* (anomalously deep snow), *khar dzud* (extreme cold with snow), and

khavsarcan dzud (combination of deep snow and extreme cold)(Allison 2017). The most devastating dzud events often occur during winters that follow summertime drought, where limited summertime precipitation decreases pastoral productivity, which reduces available hay and fodder storage needed to sustain animal fitness during subsequent periods of extreme weather conditions including dzuds(Fernández-Giménez, Batkhishig, and Batbuyan 2012).

The magnitude of pastoral vulnerability to significant dzud events is a result of the interaction between climate, rangeland management, and governance, rather than just climatic events. However, perturbations in climatic conditions are the triggers of dzud events, manifested through or enhanced by multiple mechanisms, including: 1) summer time droughts (Rao et al. 2015; Pederson et al. 2014); 2) below average winter temperatures (T. Sternberg, Thomas, and Middleton 2011); and 3) above normal snowfall (a. L. C. Shinneman et al. 2010). However, few scientific efforts have examined the role and spatiotemporal heterogeneity of the *tumer dzud*, defined as a significant snowpack melt and subsequent icing event purported to be a major driver of livestock mortality in Mongolia(Hahn, Allison 2017). Much less is known regarding the frequency and regional extent of the *tumer dzud* due to challenges in detecting such events (Rennert et al. 2009; Pan et al. 2018). Moreover, as Mongolia's annual temperatures are warming at roughly twice the global average rate(Batima et al. 2005) and wintertime temperatures are also increasing (A. L. C. Shinneman et al. 2009), wintertime snowmelt events (J. Cohen, Ye, and Jones 2015) and the *tumer dzud* may become more common, leading to potentially greater risk of livestock die-offs within Mongolia.

Accumulated snowpack liquid water content (LWC) from melt events and/or rain-on-snow (ROS) can potentially freeze between the soil surface and overlying snowpack, forming a significant ice barrier to browsing wild and domestic ungulates - sometimes leading to large wintertime die-offs(Grenfell and Putkonen 2008; Riseth et al. 2011; Loe et al. 2016). Fall and spring melt events have also been found to reduce landscape productivity (Chen et al. 2015; Bokhorst et al. 2009), which can inhibit herder abilities to fatten animals to a critical weight (Fernández-Giménez, Batkhishig, and Batbuyan 2012) moving into and out of an extreme winter. However, both wild and domestic reindeer populations in the Eurasian Arctic have been found to offset the negative impacts of ROS

and icing events by adjusting movement and herding patterns to avoid impacted areas(Bartsch et al. 2010; Loe et al. 2016). But in Mongolia, livestock have less freedom of movement due to rangeland management (Johnson et al. 2006), limited herder preparedness and access to resources (Fernández-Giménez, Batkhishig, and Batbuyan 2012). Remote sensing observations from current operational passive microwave (PM) and optical satellites provide an opportunity to reduce the risk of livestock mortality through detection and monitoring of anomalous melt events from the *tumer dzud* in Mongolia.

In this paper we determine the spatiotemporal variability and trends in seasonal melt events across Mongolia using satellite daily brightness temperature (T_b) retrievals from the Advanced Microwave Scanning Radiometers (AMSR-E and AMSR2) and Special Sensor Microwave Imager/Sounder (SSMI/S)(Dolant et al. 2016; Grenfell and Putkonen 2008; Pan et al. 2018) from October through April for water years (WY) 2003-2016. As dzud events are a complex interaction of multiple climatic forces, we also examine the role of anomalous seasonal snowmelt events as a contributor to dzud events in addition to cold temperatures, SCD, and drought. This research clarifies the role of seasonal snow melt events and other climatic factors in influencing the occurrence, extent and severity of dzud events. Several international groups and non-governmental organizations (NGOs) including the World Bank, United Nations (UN), People in Need (PIN), and Save the Children, provide humanitarian aid during periods of severe dzuds – including cash, livestock feed, veterinary services, medical provisions, and other necessary resources. Thus, we aim to provide a resource available to the Mongolian government and international NGOs for identifying regions in Mongolia that are more prone to specific types of dzuds, to inform regional planning and risk mitigation.

5.3 Geographical Context

Mongolia is situated in the heart of the Asian landmass, centrally located between Russia and China, and spanning about 33° of longitude and 12° of latitude. The region has a strong continental climate with extreme seasonal temperature variations and limited precipitation. January is the coldest month, with average temperatures ranging from -15° C to -35° C. Average July temperatures are much warmer, ranging from 15°C in the

mountains of the northern and western regions to between 20-25°C at lower elevations(Batima et al. 2005). Winter precipitation in the region is limited by the Siberian High Pressure (SHP) zone (a. L. C. Shinneman et al. 2010; Gong and Ho 2002) while summer precipitation is associated with the westerlies bringing moisture from the Atlantic and Mediterranean regions (Blomdin et al. 2016). However, the majority of atmospheric moisture flow to Mongolia is blocked by surrounding mountain ranges, which creates strong regional gradients in annual precipitation ranging from 1000 mm yr^{-1} in the western and northern regions to 130-400 mm yr^{-1} in the central and southeastern areas (Rudaya et al. 2009; Lehmkuhl et al. 2016). Mongolia's ecoregions are dominated by arid deserts and shrublands (45%) and temperate grasslands (39%). The remaining 17% of Mongolia's landscape is comprised of temperate conifer forests (8%), montane grasslands (5%) and boreal forests (2%)(Olson et al. 2001) (Figure 5.1).

5.4 Results

The mean and coefficient of variation (C_v) of satellite detected melt events in each Mongolian aimag (provincial unit) during the fall (ON), winter (DJF), and spring (MA) months over the WY 2003-2016 period are shown in Figure 5.2. The number of anomalous melt events was relatively low in the fall, with a regional mean of 1.5 melt events yr^{-1} over Mongolia and a range from 0-3 melt events $aimag^{-1}$ yr^{-1}. The fall months had the highest mean C_V at 117%, indicating high inter-annual variability across all aimags relative to other seasons. Melt events were most common in the winter months, with a mean of 3 events yr^{-1} and range from 1 to 6 events $aimag^{-1}$ yr^{-1} with the greatest number of winter events occurring in the mountainous region of western Mongolia. Variability in wintertime melt events is moderately distributed across Mongolia, suggesting that anomalous melt events can occur in any aimag during the coldest months of the year. 45% of all annual melt events over the study period occurred during winter months, though March had the highest percentage (25%) of melt events congruent with the general onset of the spring snowmelt. Further, spring had a mean of 2.5 anomalous melt events yr^{-1} and range from 1 to 5 events $aimag^{-1}$ yr^{-1}, with the largest number of events occurring in the western and north central regions. There was also an increase in variability of spring melt events moving from the northwest to the southeast, where

higher variability in the southeast results from sporadic snowfall and lack of a persistent snowpack in the Gobi Desert.

We estimated the sign and strength of melt event trends and their rates of change for each aimag using Kendall's tau trend and regression analysis, with results summarized in Figure 5.3. The results show a weak to moderate increasing melt trend in the fall, which may inhibit the development of persistent snow cover until later in the fall or early winter. In contrast, the number of winter melt events show a general declining trend. Our results showed both positive and negative trends in the number of spring melt events, with positive trends predominately occurring in the western and central aimags characterized by more persistent winter snow cover. However, few of the seasonal trends were statistically significant ($p \leq 0.1$) due to the relatively short data record (13 years).

The correlations and associated statistical significance between the mortality index (MI) and anomalous melt events are presented in Figure 5.4 (a-c). The calculated MI were significantly and positively correlated with anomalous melt events across Mongolia, while the relative impact of melt events on mortality varied for different aimags and seasons. Four aimags showed strong to moderate relationships between the number of fall melt events and annual livestock losses, with a mean correlation of 0.35 ($p < 0.05$). These aimags were predominantly located in the Gobi Desert, except for Khovsgol in northern Mongolia. Winter melt events corresponded with higher mortality in only three aimags, with a mean correlation of 0.36 ($p < 0.05$). In contrast, spring melt events contributed directly and strongly to annual livestock losses in nine aimags, which represented 47% of the analyzed aimags and showed a mean correlation of 0.39 ($p < 0.05$). Six western and central aimags showed the strongest correlations between spring melt events and livestock mortality (mean correlation of 0.46, $p < 0.02$).

To clarify the role of seasonal melt events relative to other dzud climatic drivers, we present the correlations and significance of the relationships between MI and winter temperatures (f), summer NDVI (e), and SCD (f) in Figure 5.4 (d-f). The annual MI was generally inversely proportional to both winter temperature and summer NDVI (used as a proxy for rangeland productivity). Specifically, colder winter temperatures corresponded with a higher MI y (r = -0.39) while years with lower summer NDVI also coincided with

higher mortality (r = -0.55, $p < 0.05$) in 18 of the 19 aimags examined. The MI was also directly proportional to SCD in eight aimags across north-central and western Mongolia (r = 0.49, $p < 0.05$), whereby years with longer SCD coincide with greater livestock losses.

We next contextualized the role of melt events relative to other climatic dzud drivers by quantifying the relative contribution of each climatic driver to annual livestock mortality using a general linear model (GLM) regression framework. Due to collinearity between seasonal melt events, three separate GLM models were created, one for each respective season. Collinearity also existed between SCD and melt events, so we excluded SCD from all GLM models. The percent of total variance in the MI explained by each GLM and environmental factor is presented in Figure 5.5. Fall melt events explained 13-27% of the total variance in annual livestock losses in five aimags and were significant in ($p < 0.1$) Selenge and Uvs. Spring melt events explained 16-24% of the variance in annual MI in five aimags and were significant ($p < 0.1$) in Bulgan, Govi-Altai, Khentii, and Ovorkhanghai. Winter melt events had less explanatory power relative to fall and spring but were able to explain 23% ($p < 0.1$) of the variance in annual livestock losses in Sukhbaatar.

Winter temperatures and summer NDVI levels generally had greater influence on annual livestock mortality than seasonal melt events. However, in Selenge aimag fall melt events explained more variance in annual livestock losses than either winter temperatures or summer NDVI. Moreover, for each GLM, winter temperature consistently had the most significant results ($p < 0.05$) and accounted for 21 to 37 % of the total variance in annual MI. Summer NDVI was a significant ($p < 0.05$) predictor of annual mortality predominantly in the western regions, as well as the Sukhbaatar and Dundgovi aimags in eastern Mongolia. Summer NDVI also explained 26 to 47% of the total variance in annual livestock mortality in the spring melt model, with the strongest correspondence in Selenge and Zavkhan aimags of north central and western Mongolia, repectively.

The dzuds of 2010 were among the most devastating livestock mortality events in recent decades in which 10.2 million livestock perished across Mongolia (Mongolia Statistical Service 2017). The five environmental factors examined in this study and the

reported annual livestock losses are presented for the 2010 dzud as standardized anomalies from the long-term (2003-2016) record in Figure 5.6 (a-f). Here, the livestock mortality anomaly in 2010 for Sukhbaatar in eastern Mongolia is very low because of a dzud event in 2008 that elevated morality and resulted in a 25% decline in total livestock. Dornogovi to the south of Sukhbaatar, also shows a low livestock loss anomaly due to a large livestock die-off event in 2006 which contributed to a decline of 18% in total livestock. Regardless, these results show that the number of fall melt events in 2010 was anomalously high in the southern Gobi Desert and a few aimags in northern Mongolia. In addition, the number of spring melt events and SCD were anomalously high in the central and western aimags. Winter temperatures and summer NDVI were also anomalously low in 2010. Each of these factors alone promotes mortality, while their combined effects reinforce one another in contributing to the dramatic livestock losses in 2010. These results suggest that the most severe dzud events in Mongolia are a potent combination of cold winter temperatures, summer drought, and both enhanced snow duration and the number of anomalous melt events.

5.5 Discussion

Our results on the detection of melt events from satellite observations across Mongolia and the determination of their subsequent role in annual livestock mortality improves our understanding of the role that anomalous snowmelt events and other environmental factors have on dzud risk across the region. Our findings are consistent with other studies indicating anomalously cold winter temperatures are the leading contributor to dzuds (Nandintsetseg, Shinoda, and Erdenetsetseg 2017; Rao et al. 2015; Middleton et al. 2015; Tachiiri et al. 2008). However, our results also reveal that anomalous fall melt events contribute significantly to annual livestock mortality in the southern aimags of the Gobi Desert, while spring melt events are significant contributors to livestock mortality in the western and central aimags.

The impact future melt events have on livestock mortality will in large part be governed by climatic effects on seasonal snow cover. There has been an observed increase in Eurasian snow cover over the past two decades, largely attributed to a weakening of the polar vortex (J. L. Cohen et al. 2012). However, a weakening polar vortex has not

equated to enhanced snow cover in Mongolia, which agrees with our results indicating no significant positive trends in SCD (S5.1), and is also consistent with a recent study of snow cover trends over the Tibetan Plateau from 2000-2015 (Wang et al. 2017). In contrast to observed increased Eurasian snowcover, our results indicate increasing trends in anomalous fall snowmelt events, which likely inhibit the development of a persistent snowpack and extend the periods of intermittent regional snowcover. Hence, the duration of persistent or intermittent snow cover may be more suitable than the SCD metric for determining climatically driven modulations in snowcover characteristics in the semi-arid environments of Mongolia.

Climate warming in Mongolia(Batima et al. 2005) will likely increase the frequency of anomalous melt events (Pan et al. 2018). However, changes in precipitation mechanisms have shifted towards more convective activity during fall, winter, and spring across Eurasia due to warming (Ye et al. 2017). Warmer air temperatures and more frequent and intense convective activity under regional climate change is expected to enhance radiative melting and ROS events in the region; yet the impact of these changes on ecosystem processes and services, and livestock mortality risk in Mongolia remain uncertain.

Our GLMs and the results from other studies are not able to fully explain livestock mortality using only environmental variables (Nandintsetseg, Shinoda, and Erdenetsetseg 2017; Rao et al. 2015; Middleton et al. 2015; Tachiiri et al. 2008) because dzud events in Mongolia are caused by a combination of physical, biological, socio-economic and institutional factors (Fernández-Giménez, Batkhishig, and Batbuyan 2012; Murphy 2014). Hence, we suggest that improving herder capacities and preparedness during periods of extreme weather can greatly improve herder's resilience and reduce annual livestock mortality. Regardless, governance and socio-economic factors should be included through herder interviews and surveys in future studies to provide a more robust understanding of how snow melt and icing events influence livestock mortality at local scale.

The assumptions and simplifications used in our GLMs likely contributed to model uncertainty as described here. The derivation of melt events is acquired using a 50 km window around a long-term climate monitoring station located within a city center in

each aimag. Given that some aimags encompass over 60000 km^2 (Rao et al. 2015), the detection of melt events may not be representative of landscape heterogeneity within an aimag. However, during the winter months, herders often relocate to smaller aimag provincial units (soums) or city centers to increase access to resources(Murphy 2014) so that the local station may more closely represent environmental conditions that a greater number of livestock experienced. In addition, reported livestock losses are based on an annual census acquired in December that does not record the reason for mortality losses; this can lead to model uncertainty because we assume that the years with significant livestock losses reflect anomalous climate conditions rather than other factors including predation, isolated disease outbreaks, or inexperienced herders(Rao et al. 2015). Despite these uncertainties, our results indicate a seasonal and spatial pattern in the contribution of anomalous melt events to annual livestock mortality. Whether fall and spring melt events impact livestock through subsequent icing events (Berger et al. 2018; Grenfell and Putkonen 2008) or the degradation of landscape productivity (Chen et al. 2015; Bokhorst et al. 2009) remains undetermined. However, as temperatures and convective precipitation is predicted to increase into the future across Mongolia, seasonal melt events will also likely increase, placing greater demands on informed regional planning and governance to mitigate increased dzud and livestock mortality risk across Mongolia.

5.6 Methods

5.6.1 Satellite Datasets

Mongolia is at the southern boundary of consistent daily image retrievals from polar orbiting PM satellite sensors, which resulted in frequent gaps in daily T_b retrievals in the early portion of the satellite record used for this study due to diverging sensor orbital swath. The daily T_b coverage was improved after 2002 with the introduction of the AMSR and Special Sensor Microwave Imager/Sounder (SSMI/S) sensors. For this reason, we defined our study period from WY 2003-2016. The AMSR-E sensor was launched on-board the NASA Aqua satellite and operated until 2011 (Kawanishi et al. 2003). The AMSR-2 follow-on mission was successfully launched in 2012 on-board the JAXA GCOM-W satellite and continues normal operations (Imaoka et al. 2010; Du et al. 2014). We used similar T_b retrievals from SSMI/S on-board the Defense Meteorological

Satellite Program (DMSP) F18 satellite platform to fill an approximate nine-month data gap in 2012 between the effective end of AMSR-E and beginning of the AMSR2 T_b record. Daily AMSR-E (18.7 and 36.5 GHz) ascending retrievals (1:30 pm) and SSMI/S (19 and 37 GHz) evening retrievals (6:30 pm) were acquired from the NASA MEaSUREs calibrated enhanced-resolution PM daily EASE-GRID 2.0 ESDR V1 T_b record mapped to a consistent 25 km x 25 km global EASE-grid projection format (Brodzik et al. 2012). Daily AMSR2 (18.7 and 36.5 GHz) ascending retrievals (1:30 pm) were acquired through the JAXA G-portal as Level 3 (L3) T_b retrievals mapped to a similar 25 km x 25 km resolution global grid (www.gportal.jaxa.jp/gpr).

5.6.2 Ancillary Datasets

We used the Moderate Resolution Imaging Spectrometer (MODIS) derived Terra Daily MOD10A1 V6 daily 500 m Snow Cover product (Hall et al. 2010) to derive annual SCD. Pixels were first screened using the Quality Assurance (QA) band such that any pixel classified as 'Poor' was excluded. Daily MOD10A1 observations then were extracted from 19 WMO station locations across Mongolia (S5.2) using Google Earth Engine (GEE) for WY 2003-2016. The MOD10A1 snow cover timeseries were used to estimate annual SCD for each aimag using the following equation (Dietz et al. 2014) (Eq 1.):

$$SCD = \sum_{i=0}^{n}(S_i) \qquad \text{(Eq 1.)}$$

where n is the number of days in a given water year, and S_i is the extracted information from the binary snow cover information (0 no snow, 1 snow).

We extracted Landsat derived summer normalized difference vegetation index (NDVI) values for each aimag as a proxy for rangeland productivity (Hilker, Natsagdorj, and Waring 2014). We used mean NDVI values for August aggregated by aimag boundaries to represent summertime drought, such that, low NDVI values equate to limited water and as a result reduced above ground biomass (AGB) (Berner et al. 2018). Pasture productivity peaks in August in Mongolia and is followed by hay and fodder storage in September (Nandintsetseg, Shinoda, and Erdenetsetseg 2017; Johnson et al. 2006). The use of the NDVI is preferred over other (meteorological) drought proxies as it directly reflects anomalies in vegetation health associated with drought. Furthermore,

meteorological drought proxies do not always match with negative anomalies in vegetation health (Bachmair et al. 2018). Here, we used the NDVI of the preceding summer to represent the rangeland productivity of a given water year (e.g., the NDVI of August 2002 is used for WY 2003). With respect to dzuds, limited AGB in the late summer limits the amount of available hay and fodder available for winter storage (Nandintsetseg, Shinoda, and Erdenetsetseg 2017). A detailed explanation of our derivation of NDVI can be found in Robinson et al. (2017) (Robinson et al. 2017).

Annual livestock data were acquired from the Mongolia Statistical Service (www.1212.mn) and include the total number annual livestock losses and total livestock population. We represented annual livestock losses in the statistical analysis as a Mortality Index (MI), calculated by creating a normalized ratio between livestock losses and the previous year's total livestock population for each aimag (Hansen et al. 2014).

5.6.3 Climate Observations

Meteorological observations from 49 climate stations distributed across Mongolia were acquired from World Meteorological Organization (WMO) global weather station daily records archived at the National Climate Data Center (NCDC) (www.ncdc.noaa.gov). Station measurements included daily average, minimum, and maximum surface air temperature, total precipitation, snow depth, and precipitation type observations. Daily average temperature observations were used to create homogenized mean annual winter time temperatures for 19 of Mongolia's 21 aimags. We excluded the Govisumber and Darkhan Uul aimags from this study because they did not possess any WMO stations.

We selected one representative WMO station from each aimag (S5.2) and created a 50 km remote sensing sampling window around the station location. These windows were then used to extract and calculate daily mean T_b values from the PM satellite record and averaged August NDVI values. Station locations were determined by selecting stations with a consistent temporal record matching the study period and located near populated centers. Proximity to populated centers is important because herders often move their herds to these areas during the winter months to improve access to necessary

resources. Station site locations were also used to extract the MOD10A1 snow cover time series for each aimag.

In addition to the WMO stations, we also used a more comprehensive set of in situ meteorological measurements from a research station located approximately 100 km northwest of the Mongolian capital of Ulaanbaatar in the Sugnugur Valley. The station is located at the valley entrance at the transition zone between grasslands and boreal forest on a southern exposed slope at 1,193m elevation (a.s.l., 48°26'55" N, 107°11'41" E). The Sugnugur station has continuously collected measurements since spring 2012, including surface and air temperatures, precipitation, soil temperature, global and net radiation, wind velocity, and surface albedo (Minderlein and Menzel 2014). We performed the same remote sensing sampling window selection at the Sugnugur Valley site to compare the satellite retrievals and collected in situ measurements.

5.6.4 Detection of melt events

Our approach to detect melt events builds upon a ROS algorithm developed from gradient ratio polarization (GRP)(Dolant et al. 2016) and used in several other studies(Dolant et al. 2016; Langlois et al. 2017; Pan et al. 2018). The PM ROS algorithm is driven by the differential response in microwave emissions at 19 (V, H) GHz and 37 (V, H) GHz frequencies to changes in snow cover density and LWC within the snowpack surface. We first apply a spectral gradient ratio (GR)(Grenfell and Putkonen 2008), which identifies distinct differences in the dielectric response at 19 and 37 GHz to enhanced LWC in the surface snowpack; here, the LWC increase can result from either snowmelt or rainfall. The GR is derived separately for both V and H polarized (*pol*) T_b retrievals (Eq. 2).

$$GR\left(pol_{(37,19)}\right) = \frac{[T_b(pol,37) - T_b(pol,19)]}{[T_b(pol,37) + T_b(pol,19]} \quad (2)$$

During periods of enhanced snowpack LWC, the GR from H *pol* T_b frequencies (GR-h) returned negative values and the V *pol* GR returned positive values (GR-v)(Dolant et al. 2016). The inverse relationship between the polarizations contributed to the development of a GRP (Eq. 3).

$$GRP = \frac{GR-\mathrm{v}}{GR-h} \quad (3)$$

Previous research has applied the GRP to a variety of satellite PM sensors including SMMR, SSM/I, and AMSR to detect ROS events in Quebec, the Canadian Arctic Archipelago (CAA) , and Alaska (Dolant et al. 2016; Langlois et al. 2017; Pan et al. 2018). These studies applied a global GRP threshold, ranging from less than 1 to -10 to classify ROS and melt events.

Our preliminary research found that the GRP had discrete characteristics sensitive to both atmospheric and surface conditions. In regions of persistent snow cover, the GRP ranges from around zero during periods of no snow to 1 during periods of snow cover. Yet, we observe deviations from both zero and one at higher snowpack LWC levels associated with ROS or freeze-thaw events that can result in a range of GRP values from just under 1 to -10, depending on the magnitude of the such events (S5.3). In our melt detection algorithm, rather than applying a global threshold, we set a GRP condition such that the GRP must be greater than 1 the day before the GRP is observed to be less than 1. GRP values greater than 1 were assumed to coincide with snow-cover (S5.3). A detailed schematic for detecting melt events can be found in S5.4.

5.6.5 Statistical Analysis

The Kendall's tau statistic was used to quantify the sign and strength of annual and seasonal trends in melt and SCD at each station location. We also extracted the slope coefficient from the linear regressions to determine the rates of change in melt events and SCD.

Pearson's correlation coefficient (Pearson's r) was used to determine the sign and strength of the relationship between the derived *dzud* proxies (melt events, SCD, summer NDVI, and winter temperatures) and MI. Results from the correlation and trend analyses were ranked based on their significance, ranging from relatively strong ($p \leq 0.05$), to moderate ($0.05 \leq p < 0.1$) and weak ($p \geq 0.1$) relationship categories(Kim et al. 2015).

We employed a stepwise general linear model (GLM) regression approach and Analysis of Covariance (ANCOVA) to determine the influence of each dzud proxy on annual livestock mortality represented by the proportion of explained variance (SS). We first tested the correlations between each dzud proxy to reduce potential collinearity within the GLM. We found high collinearity between each seasonal melt event proxy as

well as between seasonal melt events and SCD ($r > 0.6$). For this reason, we created three separate GLM models, one for each respective melt season, and excluded SCD from all GLM models. We then ranked the models using a two-way stepwise approach using the Akaike information Criterion (AIC), such that the ranked model that produced the lowest AIC was selected (Tao et al. 2015; Rao et al. 2015). Lastly, ANCOVAs were performed on each seasonal model with lowest AIC to calculate the proportion of explained variance. The final models can be found in the supplementary section (S5.5).

5.7 References

Bachmair, S., M. Tanguy, J. Hannaford, and K. Stahl. 2018. "How Well Do Meteorological Indicators Represent Agricultural and Forest Drought across Europe?" *Environmental Research Letters* 13 (3). https://doi.org/10.1088/1748-9326/aaafda.

Bartsch, A, T Kumpula, B Forbes, and F Sammler. 2010. "Detection of Snow Surface Thawing and Refreezing in the Eurasian Arctic with QuikSCAT : Implications for Reindeer Herding." *Ecological Applications* 20 (8): 2346–58.

Batima, P, L Natsagdorj, P Gombluudev, and B Erdenetsetseg. 2005. "Observed Climate Change in Mongolia." *AIACC Working Paper*, no. 12: 25. https://doi.org/10.1890/08-0144.1.

Berger, J., C. Hartway, A. Gruzdev, and M. Johnson. 2018. "Climate Degradation and Extreme Icing Events Constrain Life in Cold-Adapted Mammals." *Scientific Reports* 8 (1). Springer US: 1156. https://doi.org/10.1038/s41598-018-19416-9.

Berner, Logan T, Patrick Jantz, Ken D Tape, and Scott Goetz. 2018. "Tundra Plant Aboveground Biomass and Shrub Dominance Mapped across the North Slope of Alaska." *Environmental Research Letters* 13: 035002. https://doi.org/10.1088/1748-9326/aaaa9a.

Blomdin, R., A. P. Stroeven, J. M. Harbor, N. A. Lifton, J. Heyman, N. Gribenski, D. A. Petrakov, et al. 2016. "Evaluating the Timing of Former Glacier Expansions in the Tian Shan: A Key Step towards Robust Spatial Correlations." *Quaternary Science Reviews* 153: 78–96. https://doi.org/10.1016/j.quascirev.2016.07.029.

Bokhorst, Stef F., Jarle W. Bjerke, Hans Tømmervik, Terry V. Callaghan, and Gareth K. Phoenix. 2009. "Winter Warming Events Damage Sub-Arctic Vegetation: Consistent Evidence from an Experimental Manipulation and a Natural Event." *Journal of Ecology* 97 (6): 1408–15. https://doi.org/10.1111/j.1365-2745.2009.01554.x.

Brodzik, Mary J, Brendan Billingsley, Terry Haran, Bruce Raup, and Matthew H Savoie. 2012. "EASE-Grid 2.0: Incremental but Significant Improvements for Earth-

Gridded Data Sets." *ISPRS Int. J. Geo-Inf* 1: 32–45. https://doi.org/10.3390/ijgi1010032.

Chen, Xiaona, Shunlin Liang, Yunfeng Cao, Tao He, and Dongdong Wang. 2015. "Observed Contrast Changes in Snow Cover Phenology in Northern Middle and High Latitudes from 2001-2014." *Scientific Reports* 5 (November). Nature Publishing Group: 1–9. https://doi.org/10.1038/srep16820.

Cohen, Judah L, Jason C Furtado, Mathew A Barlow, Vladimir A Alexeev, and Jessica E Cherry. 2012. "Arctic Warming, Increasing Snow Cover and Widespread Boreal Winter Cooling." *Environmental Research Letters* 7 (1): 014007. https://doi.org/10.1088/1748-9326/7/1/014007.

Cohen, Judah, Hengchun Ye, and Justin Jones. 2015. "Trends and Variability in Rain-on-Snow Events." *Geophysical Research Letters* 42: 1–8. https://doi.org/10.1002/2015GL065320.Received.

Dietz, Andreas J., Christopher Conrad, Claudia Kuenzer, Gerhard Gesell, and Stefan Dech. 2014. "Identifying Changing Snow Cover Characteristics in Central Asia between 1986 and 2014 from Remote Sensing Data." *Remote Sensing* 6 (12): 12752–75. https://doi.org/10.3390/rs61212752.

Dolant, C., A. Langlois, B. Montpetit, L. Brucker, A. Roy, and A. Royer. 2016. "Development of a Rain-on-Snow Detection Algorithm Using Passive Microwave Radiometry." *Hydrological Processes* 30: 3184–96. https://doi.org/10.1002/hyp.10828.

Du, Jinyang, John S. Kimball, Jiancheng Shi, Lucas A. Jones, Shengli Wu, Ruijing Sun, and Hu Yang. 2014. "Inter-Calibration of Satellite Passive Microwave Land Observations from AMSR-E and AMSR2 Using Overlapping FY3B-MWRI Sensor Measurements." *Remote Sensing* 6 (9): 8594–8616. https://doi.org/10.3390/rs6098594.

Fernández-Giménez, María E. 1999. "Sustaining the Steppes: A Geographical History of Pastoral Land Use in Mongolia." *The Geographical Review1* 89 (3): 267–90. https://doi.org/10.1038/126199a0.

Fernández-Giménez, María E., B. Batkhishig, and B. Batbuyan. 2012. “Cross-Boundary and Cross-Level Dynamics Increase Vulnerability to Severe Winter Disasters (Dzud) in Mongolia.” *Global Environmental Change* 22 (4): 836–51. https://doi.org/10.1016/j.gloenvcha.2012.07.001.

Fernández-giménez, María E, Niah H Venable, Jay Angerer, Steven R Fassnacht, Robin S Reid, and J Khishigbayar. 2016. “Exploring Linked Ecological and Cultural Tipping Points in Mongolia.” *Anthropocene* 17. Elsevier B.V.: 46–69. https://doi.org/10.1016/j.ancene.2017.01.003.

Freudiger, Daphné, Irene Kohn, Jan Seibert, Kerstin Stahl, and Markus Weiler. 2017. “Snow Redistribution for the Hydrological Modeling of Alpine Catchments.” *Wiley Interdisciplinary Reviews: Water* 4 (October): e1232. https://doi.org/10.1002/wat2.1232.

Gong, D.-Y., and C.-H. Ho. 2002. “The Siberian High and Climate Change over Middle to High Latitude Asia.” *Theoretical and Applied Climatology* 72 (1–2): 1–9. https://doi.org/10.1007/s007040200008.

Grenfell, T. C., and J. Putkonen. 2008. “A Method for the Detection of the Severe Rain-on-Snow Event on Banks Island, October 2003, Using Passive Microwave Remote Sensing.” *Water Resources Research* 44 (3): 1–9. https://doi.org/10.1029/2007WR005929.

Hahn, Allison, H. 2017. “Mongolian Dzud: Threats to and Protection of Mongolia’s Herding Communities.” *Association for Asian Studies* 22 (2).

Hall, Dorothy K., George A. Riggs, James L. Foster, and Sujay V. Kumar. 2010. “Development and Evaluation of a Cloud-Gap-Filled MODIS Daily Snow-Cover Product.” *Remote Sensing of Environment* 114 (3). Elsevier Inc.: 496–503. https://doi.org/10.1016/j.rse.2009.10.007.

Hansen, Brage B., Ketil Isaksen, Rasmus E. Benestad, Jack Kohler, Åshild Pedersen, Leif E. Loe, Stephen J. Coulson, Jan Otto Larsen, and Øystein Varpe. 2014. “Warmer and Wetter Winters: Characteristics and Implications of an Extreme Weather Event in the High Arctic.” *Environmental Research Letters* 9 (11). IOP Publishing:

114021. https://doi.org/10.1088/1748-9326/9/11/114021.

Hilker, Thomas, Enkhjargal Natsagdorj, and Richard H Waring. 2014. “Satellite Observed Widespread Decline in Mongolian Grasslands Largely Due to Overgrazing.” *Global Change Biology* 20: 418–28. https://doi.org/10.1111/gcb.12365.

Imaoka, K., M. Kachi, M. Kasahara, N. Ito, K. Nakagawa, and T. Oki. 2010. “Instrument Performance and Calibration of AMSR-E and AMSR2.” *International Archives of the Photogrammetry, Remote Sensing and Spatial Information Sciences - ISPRS Archives* 38 (8): 13–18. http://www.scopus.com/inward/record.url?eid=2-s2.0-84907463202&partnerID=tZOtx3y1.

Johnson, Da, Dp Sheehy, Daniel Miller, and Daalkhaijav Damiran. 2006. “Mongolian Rangelands in Transition.” *Secheresse* 17: 133–41. http://www.jle.com/e-docs/00/04/1F/0D/telecharger.phtml?code_langue=en&format=application/pdf&titre=Version PDF.

Kawanishi, Toneo, Toshihiro Sezai, Yasuyuki Ito, Keiji Imaoka, Toshiaki Takeshima, Yoshio Ishido, Akira Shibata, Masaharu Miura, Hiroyuki Inahata, and Roy W. Spencer. 2003. “The Advanced Microwave Scanning Radiometer for the Earth Observing System (AMSR-E), NASDA’s Contribution to the EOS for Global Energy and Water Cycle Studies.” *IEEE Transactions on Geoscience and Remote Sensing* 41 (2): 184–93. https://doi.org/10.1109/TGRS.2002.808331.

Kim, Youngwook, J S Kimball, Jinyang Du, Crystal Schaaf, and P Kirchner. 2018. “Quantifying the Effects of Freeze-Thaw Transitions and Snowpack Melt on Land Surface Albedo and Energy Exchange over Alaska and Western Canada.” *Environmental Research Letters*, 1–35. https://doi.org/10.1088/1748-9326/aacf72.

Kim, Youngwook, J S Kimball, D A Robinson, and C Derksen. 2015. “New Satellite Climate Data Records Indicate Strong Coupling between Recent Frozen Season Changes and Snow Cover over High Northern Latitudes.” *Environmental Research Letters* 10 (084004). IOP Publishing: 1–10. https://doi.org/10.1088/1748-9326/10/8/084004.

Langlois, A., C. A. Johnson, B. Montpetit, A. Royer, E. A. Blukacz-Richards, E. Neave, C. Dolant, et al. 2017. “Detection of Rain-on-Snow (ROS) Events and Ice Layer Formation Using Passive Microwave Radiometry: A Context for Peary Caribou Habitat in the Canadian Arctic.” *Remote Sensing of Environment* 189. Elsevier B.V.: 84–95. https://doi.org/10.1016/j.rse.2016.11.006.

Lehmkuhl, Frank, Michael Klinge, Henrik Rother, and Daniela Hülle. 2016. “Distribution and Timing of Holocene and Late Pleistocene Glacier Fluctuations in Western Mongolia.” *Annals of Glaciology* 57 (1): 1–10. https://doi.org/10.3189/2016AoG71A030.

Loe, Leif Egil, Brage B. Hansen, Audun Stien, Steve D. Albon, Richard Bischof, Anja Carlsson, R. Justin Irvine, et al. 2016. “Behavioral Buffering of Extreme Weather Events in a High-Arctic Herbivore.” *Ecosphere* 7 (6): 1–13. https://doi.org/10.1002/ecs2.1374.

Meinander, O., S. Kazadzis, A. Arola, A. Riihelä, P. Räisänen, R. Kivi, A. Kontu, et al. 2013. “Spectral Albedo of Seasonal Snow during Intensive Melt Period at Sodankylä, beyond the Arctic Circle.” *Atmospheric Chemistry and Physics* 13 (7): 3793–3810. https://doi.org/10.5194/acp-13-3793-2013.

Middleton, Nick, Henri Rueff, Troy Sternberg, Batjav Batbuyan, and David Thomas. 2015. “Explaining Spatial Variations in Climate Hazard Impacts in Western Mongolia.” *Landscape Ecology* 30 (1): 91–107. https://doi.org/10.1007/s10980-014-0091-2.

Minderlein, Stefanie, and Lucas Menzel. 2014. “Evapotranspiration and Energy Balance Dynamics of a Semi-Arid Mountainous Steppe and Shrubland Site in Northern Mongolia.” *Environmental Earth Sciences* 73 (2): 593–609. https://doi.org/10.1007/s12665-014-3335-1.

Murphy, Daniel J. 2014. “Booms and Busts: Asset Dynamics, Disaster, and the Politics of Wealth in Rural Mongolia.” *Economic Anthropology* 1: 104–23. https://doi.org/10.1111/sea2.12007.

Nandintsetseg, Banzragch, Masato Shinoda, and Baasandai Erdenetsetseg. 2017.

"Contributions of Multiple Climate Hazards and Overgrazing to the 2009/2010 Winter Disaster in Mongolia." *Natural Hazards*. Springer Netherlands, 1–18. https://doi.org/10.1007/s11069-017-2954-8.

Olson, David M., Eric Dinerstein, Eric D. Wikramanayake, Neil D. Burgess, George V. N. Powell, Emma C. Underwood, Jennifer A. D'amico, et al. 2001. "Terrestrial Ecoregions of the World: A New Map of Life on Earth." *BioScience* 51 (11): 933. https://doi.org/10.1641/0006-3568(2001)051[0933:TEOTWA]2.0.CO;2.

Pan, Caleb G, Peter Kirchner, John S Kimball, Youngwook Kim, and Jinyang Du. 2018. "Rain-on-Snow Events in Alaska, and Their Frequency and Distribution from Satellite Observations." *Environmental Research Letters*. https://doi.org/10.1088/1748-9326/aac9d3.

Pederson, Neil, Amy E Hessl, Nachin Baatarbileg, Kevin J Anchukaitis, and Nicola Di Cosmo. 2014. "Pluvials, Droughts, the Mongol Empire, and Modern Mongolia." *Proceedings of the National Academy of Sciences of the United States of America* 111 (12). National Academy of Sciences: 4375–79. https://doi.org/10.1073/pnas.1318677111.

Rao, Mukund Palat, Nicole K Davi, Rosanne D D 'arrigo, Jerry Skees, Baatarbileg Nachin, Caroline Leland, Bradfield Lyon, Shih-Yu Wang, and Oyunsanaa Byambasuren. 2015. "Dzuds, Droughts, and Livestock Mortality in Mongolia." *Environ. Res. Lett. Environ. Res. Lett* 10 (10): 74012–74012. https://doi.org/10.1088/1748-9326/10/7/074012.

Rennert, J. Kevin, Gerard Roe, Jaakko Putkonen, and M. Bitz, Cecilia. 2009. "Soil Thermal and Ecological Impacts of Rain on Snow Events in the Circumpolar Arctic." *Journal of Climate* 22: 2302–15. https://doi.org/10.1175/2008JCLI2117.1.

Riseth, Jan Åge, Hans Tømmervik, Elina Helander-Renvall, Niklas Labba, Cecilia Johansson, Eirik Malnes, Jarle W. Bjerke, et al. 2011. "Sámi Traditional Ecological Knowledge as a Guide to Science: Snow, Ice and Reindeer Pasture Facing Climate Change." *Polar Record* 47 (242): 202–17. https://doi.org/10.1017/S0032247410000434.

Robinson, Nathaniel P, Brady W Allred, Matthew O Jones, Alvaro Moreno, John S Kimball, David E Naugle, Tyler A Erickson, and Andrew D Richardson. 2017. “A Dynamic Landsat Derived Normalized Difference Vegetation Index (NDVI) Product for the Conterminous United States.” *Remote Sensing* 9 (863): 1–14. https://doi.org/10.3390/rs9080863.

Rudaya, Natalia, Pavel Tarasov, Nadezhda Dorofeyuk, Nadia Solovieva, Ivan Kalugin, Andrei Andreev, Andrei Daryin, et al. 2009. “Holocene Environments and Climate in the Mongolian Altai Reconstructed from the Hoton-Nur Pollen and Diatom Records: A Step towards Better Understanding Climate Dynamics in Central Asia.” *Quaternary Science Reviews* 28 (5–6). Elsevier Ltd: 540–54. https://doi.org/10.1016/j.quascirev.2008.10.013.

Shinneman, a. L.C., C. E. Umbanhowar, M. B. Edlund, and N. Soninkhishig. 2010. “Late-Holocene Moisture Balance Inferred from Diatom and Lake Sediment Records in Western Mongolia.” *The Holocene* 20 (1): 123–38. https://doi.org/10.1177/0959683609348861.

Shinneman, Avery L C, James E. Almendinger, Charles E. Umbanhowar, Mark B. Edlund, and Soninkhishig Nergui. 2009. “Paleolimnologic Evidence for Recent Eutrophication in the Valley of the Great Lakes (Mongolia).” *Ecosystems* 12 (6): 944–60. https://doi.org/10.1007/s10021-009-9269-x.

Sternberg, T Ã. 2008. “Environmental Challenges in Mongolia ’ s Dryland Pastoral Landscape.” *Journal of Arid Environments* 72. https://doi.org/10.1016/j.jaridenv.2007.12.016.

Sternberg, Troy, David Thomas, and Nick Middleton. 2011. “Short Communication Drought Dynamics on the Mongolian Steppe , 1970 – 2006” 1830 (July 2010): 1823–30. https://doi.org/10.1002/joc.2195.

Sugita, Michiaki, Shintaroh Yoshizawa, and Ishgaldan Byambakhuu. 2015. “Limiting Factors for Nomadic Pastoralism in Mongolian Steppe: A Hydrologic Perspective.” *Journal of Hydrology* 524. Elsevier B.V.: 455–67. https://doi.org/10.1016/j.jhydrol.2015.02.050.

Tachiiri, K., M. Shinoda, B. Klinkenberg, and Y. Morinaga. 2008. “Assessing Mongolian Snow Disaster Risk Using Livestock and Satellite Data.” *Journal of Arid Environments* 72 (12): 2251–63. https://doi.org/10.1016/j.jaridenv.2008.06.015.

Tao, Shengli, Jingyun Fang, Xia Zhao, Shuqing Zhao, Haihua Shen, Huifeng Hu, Zhiyao Tang, Zhiheng Wang, and Qinghua Guo. 2015. “Rapid Loss of Lakes on the Mongolian Plateau.” *Proceedings of the National Academy of Sciences of the United States of America* 112 (7): 2281–86. https://doi.org/10.1073/pnas.1411748112.

Wang, Xiaoyue, Chaoyang Wu, Huanjiong Wang, Alemu Gonsamo, and Zhengjia Liu. 2017. “No Evidence of Widespread Decline of Snow Cover on the Tibetan Plateau over 2000-2015.” *Scientific Reports* 7 (1). Springer US: 1–10. https://doi.org/10.1038/s41598-017-15208-9.

Wilson, Ryan R., Annett Bartsch, Kyle Joly, Joel H. Reynolds, Anne Orlando, and Wendy M. Loya. 2013. “Frequency, Timing, Extent, and Size of Winter Thaw-Refreeze Events in Alaska 2001-2008 Detected by Remotely Sensed Microwave Backscatter Data.” *Polar Biology* 36 (3): 419–26. https://doi.org/10.1007/s00300-012-1272-6.

Ye, Hengchun, Eric J. Fetzer, Sun Wong, and Bjorn H. Lambrigtsen. 2017. “Rapid Decadal Convective Precipitation Increase over Eurasia during the Last Three Decades of the 20th Century.” *Science Advances* 3 (1): 1–8. https://doi.org/10.1126/sciadv.1600944.

Zhang, Yinsheng, M Ishikawa, T Ohata, and D Oyunbaatar. 2008. “Sublimation Form Thin Snow Cover at the Edge of the Eurasian Cryosphere of Mongolia.” *Hydrological Processes* 22: 3564–75. https://doi.org/10.1002/hyp.6960.

Figures

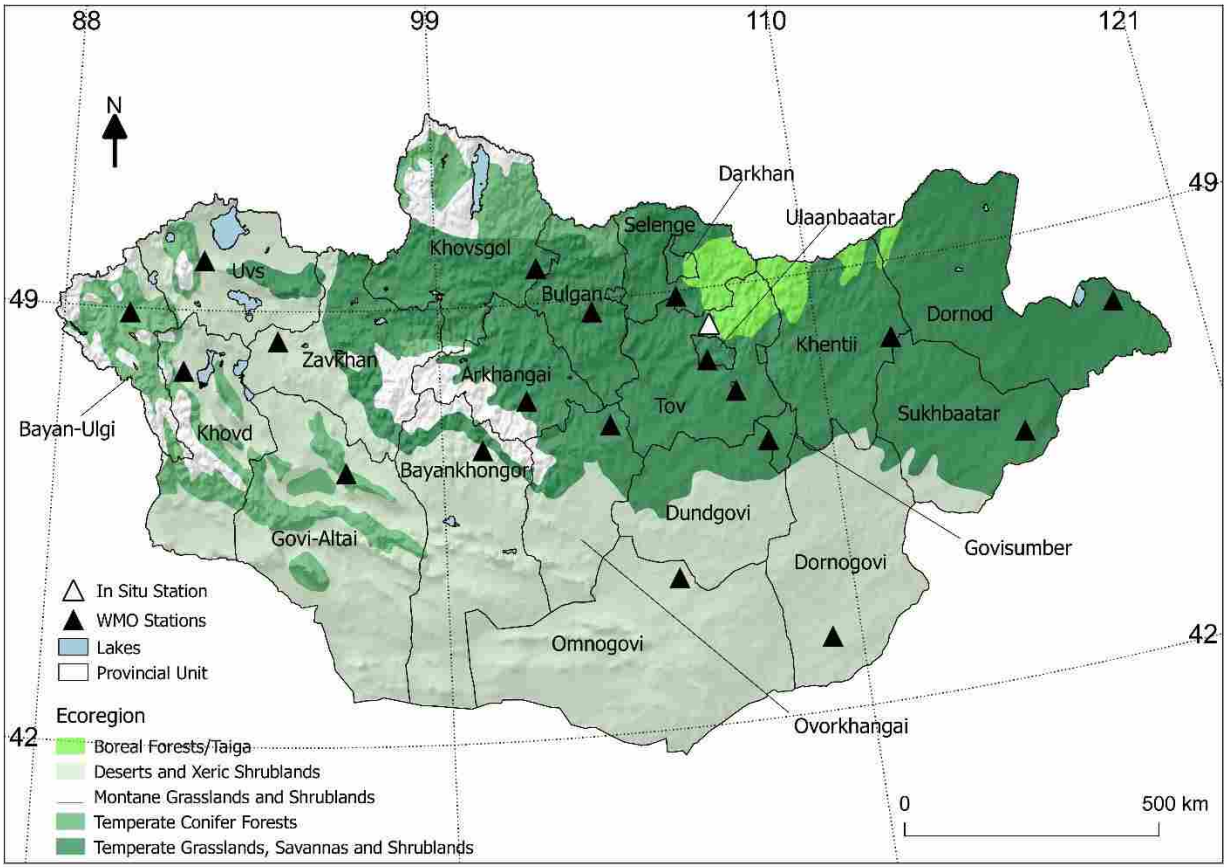

Figure 5.1 Reference map of Mongolia including the in situ climate station at Sugnugur Valley and other surface weather (WMO) stations. WWF ecoregions and the boundaries of provincial units (i.e. aimags) are also shown.

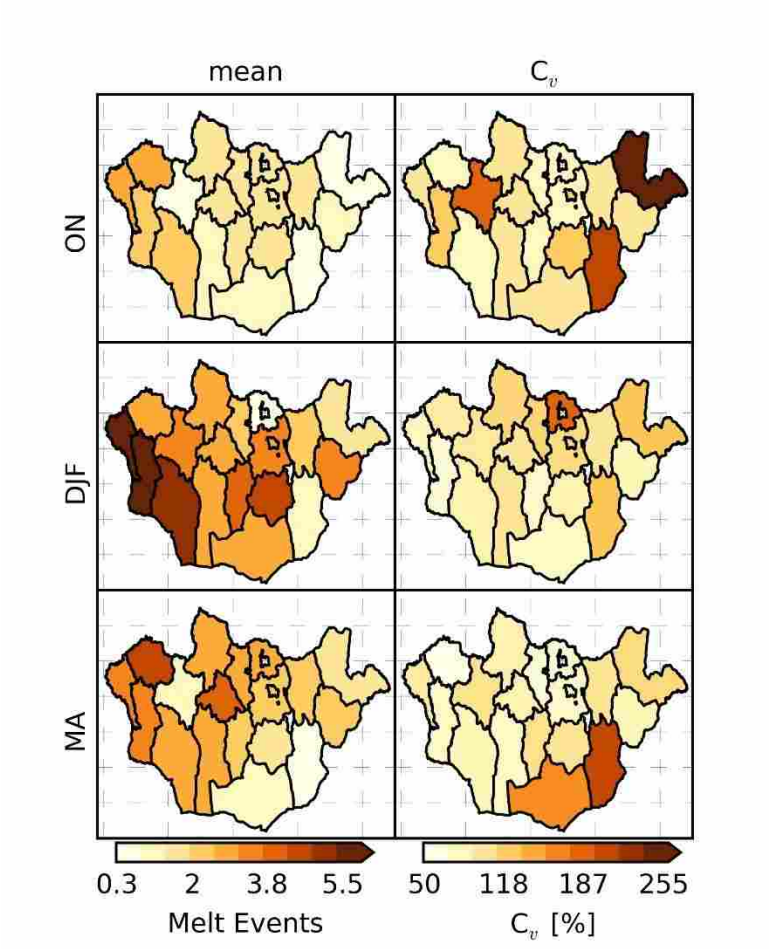

Figure 5.2 The mean and coefficient of variation (C_v) in the number of anomalous melt events for each aimag and season during WY 2003-2016 in Mongolia; the images represent aggregated monthly results for fall (ON), winter (DJF) and spring (MA).

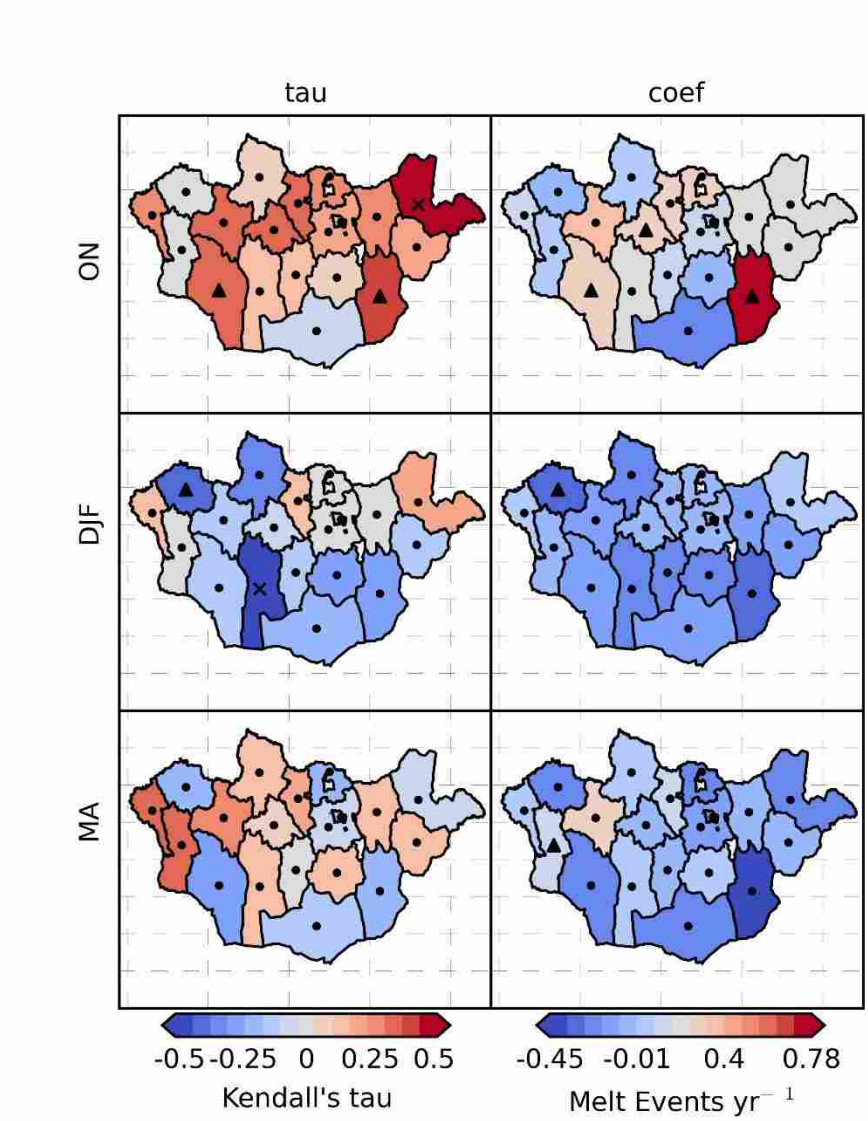

Figure 5.3 The Kendall's tau and slope coefficient for melt events across Mongolia for WY 2003-2016. The black dots indicate weak correlations ($p > 0.1$), black triangles indicate moderate correlations ($0.05 \leq p < 0.1$) and the black 'x' symbols indicate strong correlations ($p < 0.05$).

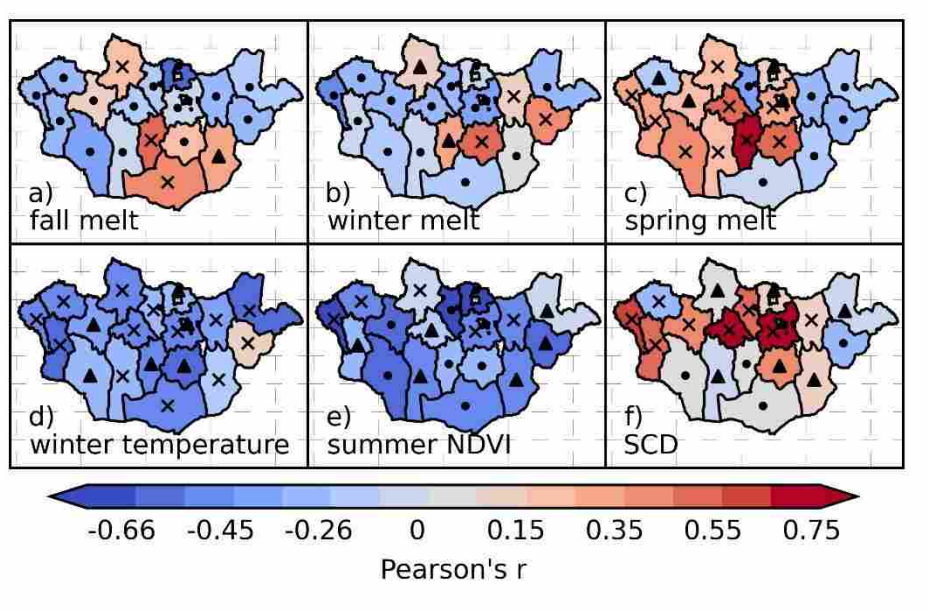

Figure 5.4 Correlations between dzud climate proxies and MI for WY 2003-2016. The black dots indicate weak correlations ($p > 0.1$), black triangles indicate moderate correlations ($0.05 \leq p < 0.1$) and the black 'x' symbols indicate strong correlations ($p < 0.05$).

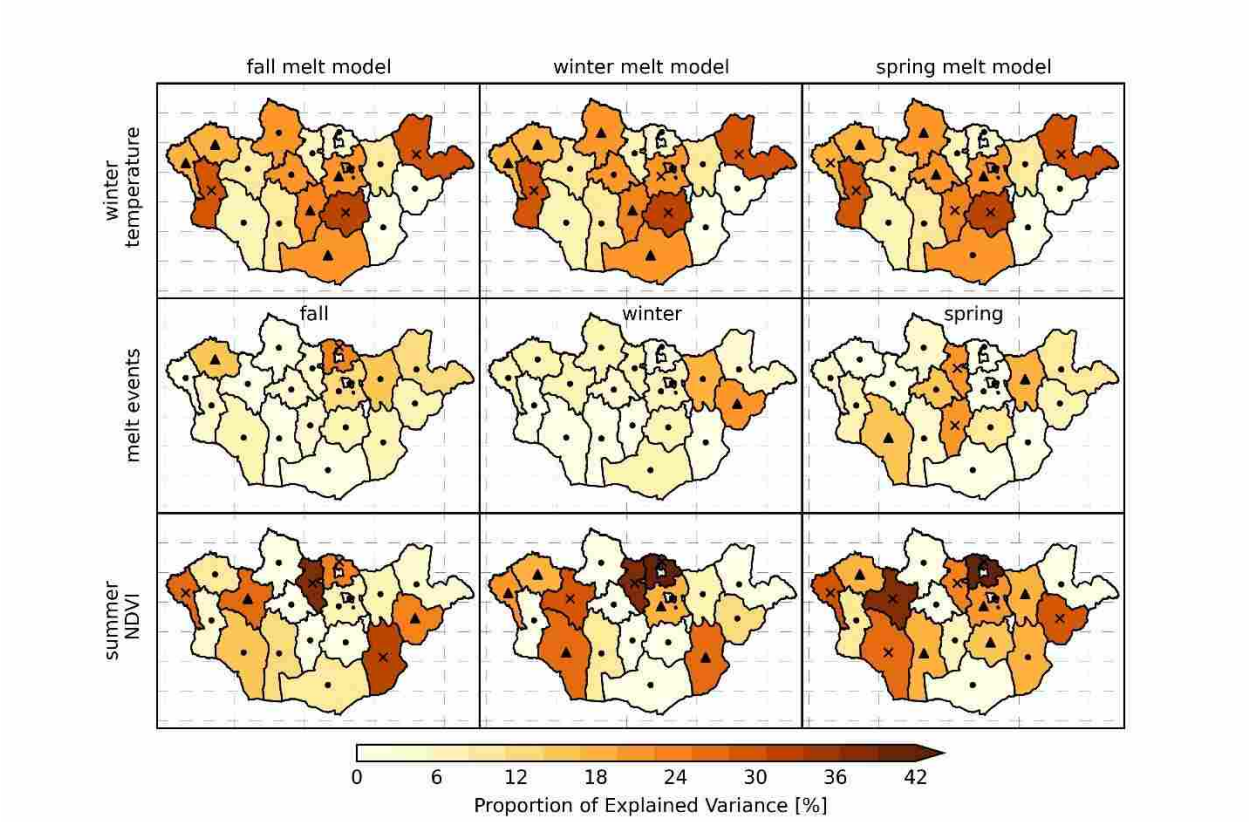

Figure 5.5 GLM results for the fall, winter, and spring. For each model, the proportion of total variance in annual MI explained by each environmental factor is represented. Black dots indicate weak correlations ($p > 0.1$), black triangles indicate moderate correlations ($0.05 \leq p < 0.1$) and the black 'x' symbols indicate strong correlations ($p < 0.05$).

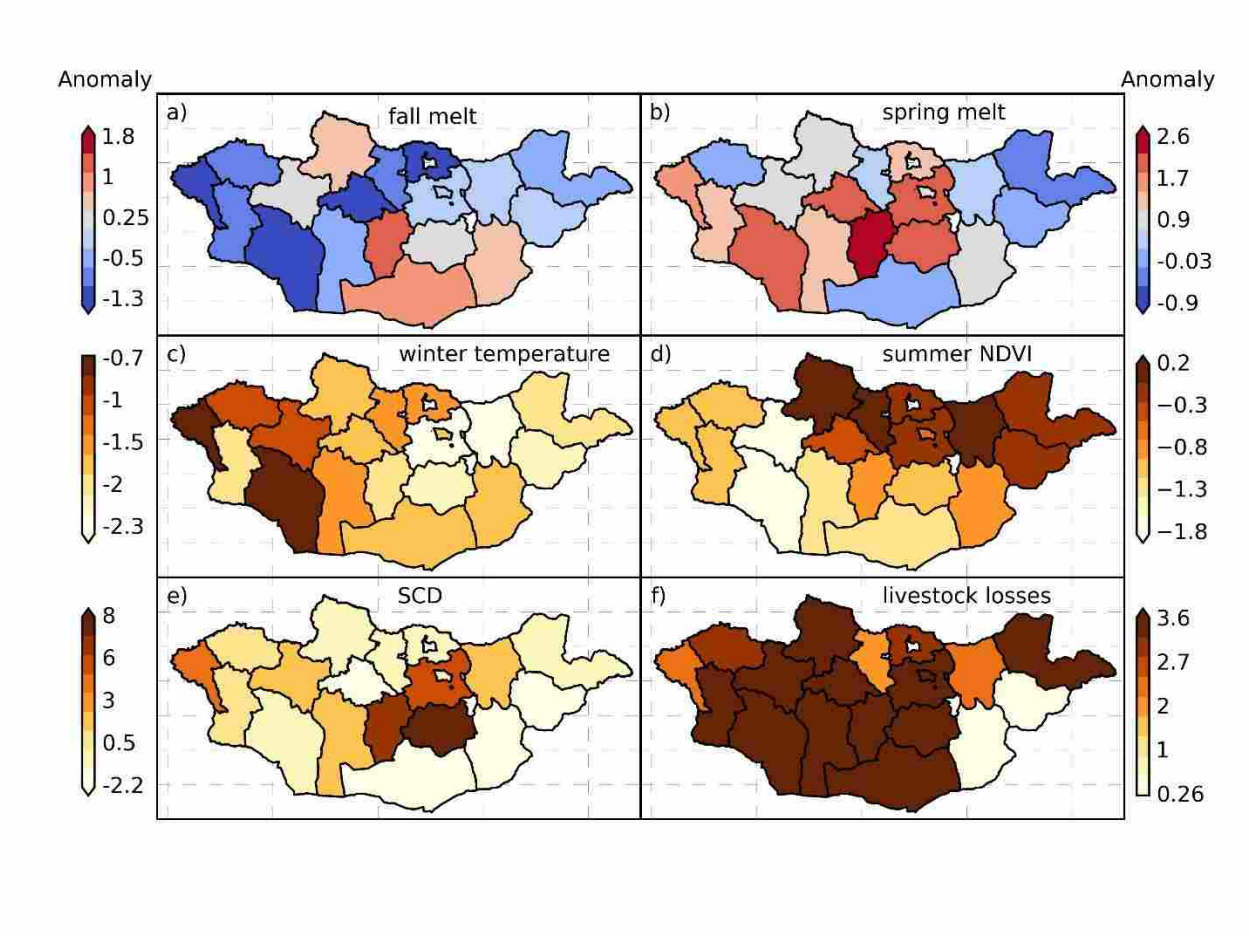

Figure 5.6 Standardized anomalies for fall melt events (a), spring melt events (b), winter temperature (c), summer NDVI (d), SCD (e), and livestock losses (f) during the dzud of 2010. Note winter melt events were not included due to the limited number of significant correlations with livestock losses.

Supplemental

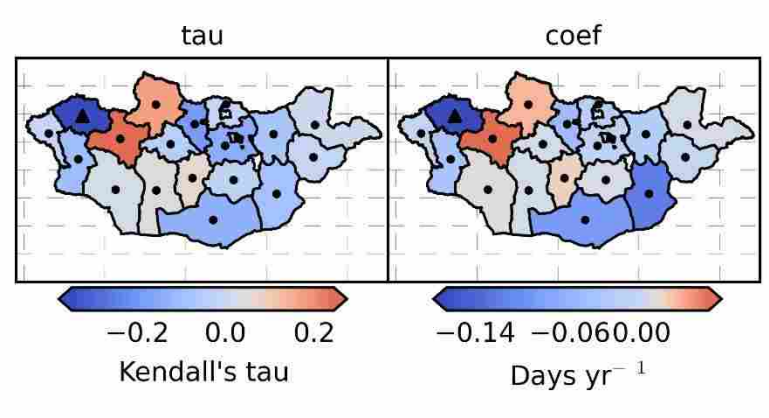

Supplementary 5.1 (S5.1). The Kendall's tau and slope coefficient for MODIS derived SCD across Mongolia for WY 2003-2016. The black dots indicate weak correlations ($p > 0.1$), black triangles indicate moderate correlations ($0.05 \leq p < 0.1$) and the black 'x' symbols indicate strong correlations ($p < 0.05$).

Supplementary 5.2 (S5.2). The selected WMO stations used to extract Tb retrievals and validate melt events and SCD.

Aimag	Station	Lat [dd]	Long [dd]	Elev [m]	Start [YYYYMMDD]	End [YYYYMMDD]
Arkhangai	TSETSERLEG	47.5	101.5	1691	19560803	20171230
Bayankhongor	GALUUT	46.7	100.1	2126	19570725	20171230
Bayan-Ulgi	ULGI	48.9	89.9	1715	19590101	20171230
Bulgan	BULGAN	48.8	103.6	1208	19560805	20171230
Dornod	KHALKH-GOL	47.6	118.6	688	19831011	20171230
Dornogovi	UNKNOWN MNG	43.2	109.2	213	19730102	20171230
Dundgovi	CHOIR	46.5	108.2	1286	19560802	20171230
Govi-Altai	ALTAI	46.4	96.3	2181	19560802	20171230
Khentii	BAYAN-OVOO	47.8	112.1	926	19690101	20171230
Khovd	HOVD	48.0	91.6	1405	19561016	20171230
Khovsgol	TARIALAN	49.6	102.0	1235	19830112	20171230
Omnogovi	TSOGT-OVOO	44.4	105.3	1298	19690101	20171230
Ovorkhangai	BAT OLDZIY BUND	47.0	103.8	1358	19730103	20171230
Selenge	BARUUNHARAA	48.9	106.1	807	19560802	20171230
Sukhbaatar	ERDENETSAGAAN	45.9	115.4	1076	19730101	20171230
Tov	MAANTI	47.3	107.5	1430	19560821	20171230
Ulaanbaatar	CHINGGIS KHAAN INT	47.8	106.8	1330.1	19560802	20171230
Uvs	ULAANGOM	49.8	92.1	939	19570701	20171230
Zavkhan	URGAMAL	48.5	94.3	1263	19750109	20171230

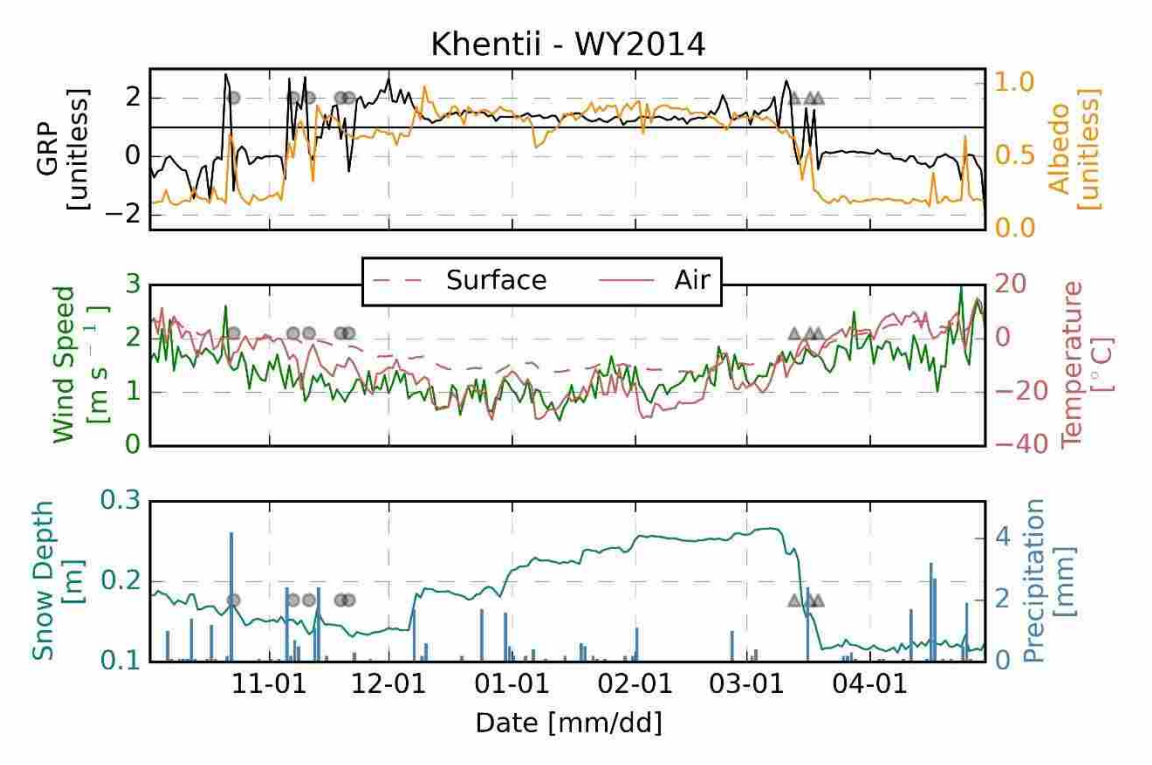

Supplementary 5.3 (S5.3). GRP timeseries plotted with in situ atmospheric and climatic parameters during selected WY 2014 from the Sugnugur valley (Khentii) site. The gray circles indicate melt event that were classed as commissions and the gray triangles indicate melt events that were classed as omission.

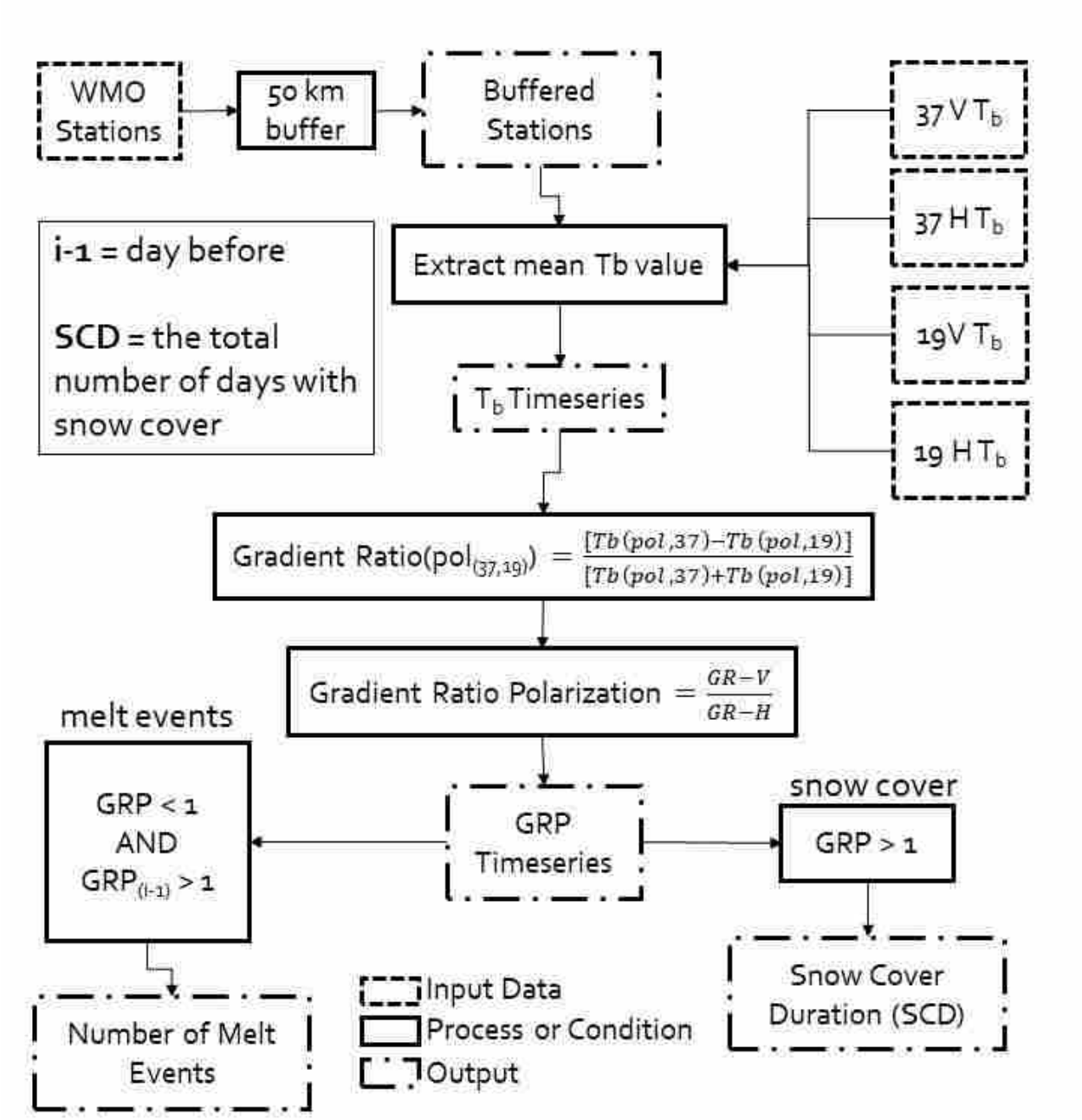

Supplementary 5.4 (S5.4). Workflow chart to illustrate the steps required to detect melt events from PM retrievals. Each frequency (37, 19) and polarization (v, h) are averaged and processed separately before calculating the gradient ratio.

Supplementary 5.5 (a-c) (S5.5). GLM model outputs for the fall (a), winter (b), and spring (c) models. Each table includes the p-value and the proportion of variance each predictor explains (SS).

(a)

Aimag	Winter Temperature		Fall Melt		Summer NDVI	
	p	*SS%*	*p*	*SS%*	*p*	*SS%*
Arkhangai	0.11	22.43	0.49	3.73	0.72	0.96
Bayan-Ulgi	0.06	21.11	0.57	1.65	0.03	29.92
Bayankhongor	0.26	10.80	0.87	0.22	0.20	14.08
Bulgan	0.18	9.04	0.29	5.43	0.01	42.97
Dornod	0.03	32.50	0.14	13.02	0.45	3.17
Dornogovi	0.53	2.23	0.27	7.29	0.03	36.90
Dundgovi	0.03	36.67	0.27	7.67	0.97	0.01
Govi-Altai	0.29	8.30	0.31	7.66	0.13	17.96
Khentii	0.21	11.22	0.14	16.21	0.26	8.99
Khovd	0.04	33.62	0.44	3.86	0.44	3.76
Khovsgol	0.11	23.90	0.99	0.00	0.95	0.03
Omnogovi	0.09	22.63	0.63	1.61	0.23	10.70
Ovorkhangai	0.08	25.86	0.43	4.56	0.61	1.92
Selenge	0.26	5.82	0.03	27.22	0.03	26.39
Sukhbaatar	0.77	0.59	0.29	8.20	0.07	26.22
Tov	0.05	25.11	0.12	14.66	0.21	9.09
Ulaanbaatar	0.11	22.53	0.60	2.24	0.85	0.27
Uvs	0.07	21.04	0.09	17.88	0.19	10.11
Zavkhan	0.19	11.82	0.82	0.33	0.05	28.88

(b)

Aimag	Winter Temperature		Winter Melt		Summer NDVI	
	p	*SS %*	*p*	*SS %*	*p*	*SS %*
Arkhangai	0.1	22.4	0.41	5.3	0.55	2.7
Bayan-Ulgi	0.06	21.1	0.2	9.0	0.05	23.1
Bayankhongor	0.27	10.8	0.81	0.5	0.29	10.0
Bulgan	0.17	9.0	0.22	6.9	0.01	43.6
Dornod	0.04	32.5	0.36	5.7	0.65	1.4
Dornogovi	0.58	2.2	0.67	1.3	0.06	29.8
Dundgovi	0.03	36.7	0.31	6.5	0.6	1.6
Govi-Altai	0.27	8.3	0.59	1.9	0.05	29.6
Khentii	0.21	11.2	0.11	19.2	0.33	6.5
Khovd	0.04	33.6	0.77	0.6	0.5	3.0
Khovsgol	0.09	23.9	0.35	6.6	0.88	0.2
Omnogovi	0.1	22.6	0.31	7.9	0.67	1.3
Ovorkhangai	0.09	25.9	0.6	2.1	0.73	0.9
Selenge	0.29	5.8	0.57	1.6	0.01	45.8
Sukhbaatar	0.77	0.6	0.08	23.3	0.18	12.9
Tov	0.05	25.1	0.25	7.1	0.07	19.4
Ulaanbaatar	0.12	22.5	0.75	0.8	0.75	0.8
Uvs	0.07	21.0	0.22	8.7	0.08	19.5
Zavkhan	0.14	11.8	0.19	9.3	0.03	32.0

(c)

Aimag	Winter Temperature		Spring Melt		Summer NDVI	
	p	*SS %*	*p*	*SS %*	*p*	*SS %*
Arkhangai	0.08	22.4	0.14	15.9	0.65	1.4
Bayan-Ulgi	0.04	21.1	0.28	5.2	0.02	33.8
Bayankhongor	0.22	10.8	0.42	4.5	0.1	21.3
Bulgan	0.17	9.0	0.04	22.3	0.03	28.0
Dornod	0.04	32.5	0.22	9.9	0.7	0.9
Dornogovi	0.59	2.2	0.57	2.6	0.12	21.3
Dundgovi	0.01	36.7	0.13	10.0	0.05	17.1
Govi-Altai	0.21	8.3	0.08	17.1	0.03	29.0
Khentii	0.16	11.2	0.07	19.8	0.06	21.3
Khovd	0.02	33.6	0.22	8.4	0.19	9.8
Khovsgol	0.1	23.9	0.42	5.1	0.96	0.0
Omnogovi	0.11	22.6	0.66	1.5	0.6	2.2
Ovorkhangai	0.03	25.9	0.04	24.3	0.22	7.2
Selenge	0.29	5.8	0.8	0.3	0.01	47.4
Sukhbaatar	0.76	0.6	0.24	9.1	0.04	31.6
Tov	0.05	25.1	0.64	1.2	0.06	23.0
Ulaanbaatar	0.12	22.5	0.88	0.2	0.79	0.6
Uvs	0.09	21.0	0.8	0.4	0.09	20.3
Zavkhan	0.13	11.8	0.93	0.0	0.01	43.5

Supplementary 5.6 (S5.6) Validation of GRP derived melt events

GRP timeseries extracted over the Sugnuguur Valley climate station correlated well with the in situ surface albedo ($r = 0.73$, $p < 0.001$) and air temperature ($r = -0.60$, $p < 0.001$) measurements. These two parameters were therefore used to evaluate the GRP effectiveness in detecting melt events. In the Sugnuguur Valley, the GRP detected 17 melt events from WY 2013-2016. Under the assumption that snow albedo decreased with enhanced LWC we found that 11 of the GRP detected melt events corresponded with a decrease in albedo from the previous day whilst the albedo was at least greater than 0.5 (Meinander et al. 2013) and resulted in an agreement of 65%. Further, since during the winter months and a persistent snow cover, we observed 235 days that met our surface albedo however no GRP melt event was detected. However, during there were no days

during the fall and spring that met our albedo conditions that did not coincide with a GPR melt event.

In contrast, the GRP melt events occurred across a broad range of air temperatures at the Sugnuguur Valley site. For example, temperatures coincident with GRP melt events ranged up to 9 °C and as low as -20 °C, with strong diurnal variation. Overall, the melt events occurred when mean temperatures were approximately -5.8 ± 4.5 °C. These results are consistent with other studies documenting large air temperature variability during snowmelt events, including temperatures extending well below freezing (Dolant et al. 2016; Kim et al. 2018; Wilson et al. 2013). However, the apparent temperature discrepancy may also reflect spatial scale differences between the in situ station measurement and coarser satellite footprint. For this reason, we next evaluated the GRP algorithm and associated melt events using other WMO station air temperature records within each aimag. We stratified GRP detected melt events by daily maximum temperature [°C] including; $T > 0$, $0 \geq T > -4$, $-4 \geq T > -8$, and $T \leq -8$ (S5.7). The results showed that during the fall and spring, 82.5% of all GRP melt events occurred during days with a maximum surface air temperature greater than 0°C. However, during December and January 76.1% of the GRP melt events occurred on days when the maximum temperature was below -8 °C; these results suggest that changes in snowpack properties, including grain size, depth, and density, are being influenced through mechanisms other than surface air temperature such as snow redistribution, sublimation, and enhanced solar radiation (Freudiger *et al* 2017, Zhang *et al* 2008, Komatsu *et al.* 2011)

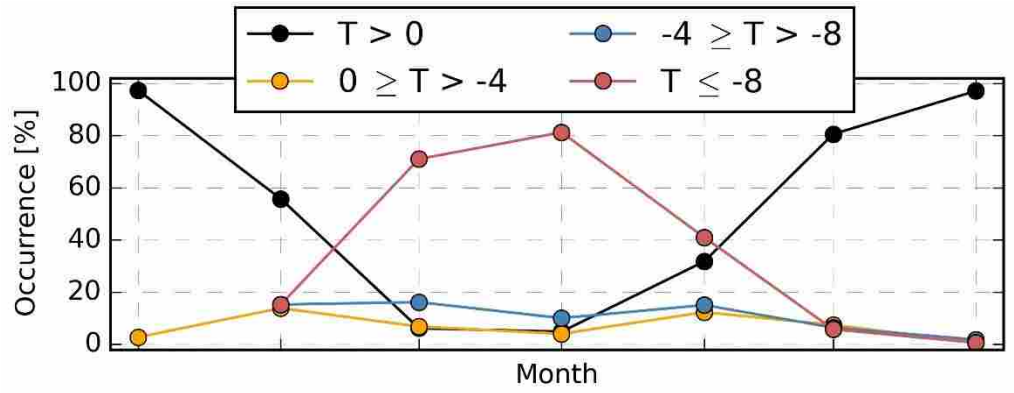

Supplementary 5.7 (S5.7). The percent occurrence of melt event for each month stratified by the daily maximum temperature for when the melt event occurred.

References

Dolant C, Langlois A, Montpetit B, Brucker L, Roy A and Royer A 2016 Development of a rain-on-snow detection algorithm using passive microwave radiometry *Hydrol. Process.* **30** 3184–96 Online: http://doi.wiley.com/10.1002/hyp.10828

Freudiger D, Kohn I, Seibert J, Stahl K and Weiler M 2017 Snow redistribution for the hydrological modeling of alpine catchments *Wiley Interdiscip. Rev. Water* **4** e1232 Online: http://doi.wiley.com/10.1002/wat2.1232

Kim Y, Kimball J S, Du J, Schaaf C and Kirchner P 2018 Quantifying the effects of freeze-thaw transitions and snowpack melt on land surface albedo and energy exchange over Alaska and Western Canada *Environ. Res. Lett.* 1–35

Komatsu, Y, Shinoda, M, and Ueda, H 2011 Snowmelt and atmospheric heating processes over eastern Mongolia *SOLA* **7** 001-004

Meinander O, Kazadzis S, Arola A, Riihelä A, Räisänen P, Kivi R, Kontu A, Kouznetsov R, Sofiev M, Svensson J, Suokanerva H, Aaltonen V, Manninen T, Roujean J L and Hautecoeur O 2013 Spectral albedo of seasonal snow during intensive melt period at Sodankylä, beyond the Arctic Circle *Atmos. Chem. Phys.* **13** 3793–810

Wilson R R, Bartsch A, Joly K, Reynolds J H, Orlando A and Loya W M 2013 Frequency, timing, extent, and size of winter thaw-refreeze events in Alaska 2001-2008 detected by remotely sensed microwave backscatter data *Polar Biol.* **36** 419–26

Zhang Y, Ishikawa M, Ohata T and Oyunbaatar D 2008 Sublimation form thin snow cover at the edge of the Eurasian cryosphere of Mongolia *Hydrol. Process.* **22** 3564–75

Chapter 6: Conclusions future research directions

6.1 Glacier recession in Mongolia

A glacier inventory was created for the Altai Mountains in western Mongolia derived from optical satellite sensors including multiple Landsat missions and Sentinel 2-A for 1990, 2000, 2010, and 2016; providing one of the most comprehensive temporal glacier records in the HMA. In 2016 there were 627 debris-free glaciers covering an area of 334.0 ± 42.3 km^2. The trend analysis revealed that from 1990-2016, glaciers receded at a rate of 6.4 ± 0.4 km^2 yr^{-1} and resulted in an overall decrease in area of 43%. Glacier recession in Mongolia's Altai Mountains compares well with other mountain ranges in the region. For example, glacier recession in the Kodar Mountains of Siberia observed a decrease in glacier area of 40% from 1995 to 2011 (Stokes *et al* 2013). From 2000 to 2016 the glaciers in Mongolia receded by 29% , similar to a reduction of 24% from 2000 to 2014 in the Kamchatka Peninsula (Lynch *et al* 2016) and a reduction of 27% from 2001/02 to 2006/11 in the east Sayan of southeast Siberia (Osipov and Osipova 2014). Relative to glacier recession in regions governed by maritime climate influences (e.g. Paul and Mölg 2014, Bolch *et al* 2010, Gardent *et al* 2014), the rates of glacier recession are higher in mountain environments of continental climates. However, no extensive comparison exists within the literature that explicitly compares rates of recession across globally discrete climatic zones.

Regardless, optically stimulated luminescence (OSL) dating (Blomdin *et al* 2016) and ice cores acquired from Tsambagarav in western Mongolia (Herren *et al* 2013) have identified competing climatic influences on glacier mass balance in Mongolia's continental climate. It has been largely believed that Mongolia's modern glaciers are remnants of the late Pleistocene (Lehmkuhl *et al* 2016). However, recent work suggests Mongolia's glaciers are a result of a neoglaciation that occurred during the mid-Holocene (6k BP), facilitated by a transition from a dry-westerly influence to a cool-wet climatic influence from the Asian monsoons (Herren *et al.* 2013). The transition between hot-dry to cool-wet during the time of the mid-Holocene is also in agreement with lake sediment cores collected at Hoton Nuur (Rudaya *et al* 2009). However, this period of enhanced regional moisture began to weaken later in the Holocene (5k BP) and equated to the end of the regional neoglaciation – further emphasizing the importance of precipitation to

glacier mass balance within the continental regions. In addition, we can anticipate the recession of Mongolia's glaciers to continue recession in the future, unless the Asian monsoon replaces the westerlies as the regional mechanism of moisture delivery to the region.

As the glaciers of Mongolia continue to recede, future glaciological research in the region should be directed at contributing to a better understanding of the spatial and temporal variability of glacier recession, and the forces that govern it. In chapter 2, I presented a new satellite-derived glacier inventory of Mongolia and described potential drivers of recession. However, temporal integrity is the most critical component of glacier monitoring, while the anticipated launch of Landsat 9 in 2020 (Wulder *et al* 2012) and continuity of the European Space Agency's (ESA) Sentinel series (Berger *et al* 2012) offer better capabilities for regional monitoring and longer-term trend analysis to distinguish both annual and decadal variations in glacier recession. These new data sources will allow for a more robust modelling of glacier mass balance as these 'water towers' (Viviroli *et al* 2007) recede in the already water restricted country (Batima 2005).

6.2 Water availability and land use in western Mongolia

Colloquially, alpine glaciers are often referred to as regional 'water towers' because during the summer months, glacier melt from the high mountains is often the major contributing source of freshwater, particularly in [semi] arid landscapes (Viviroli *et al* 2007). Accordingly we found that glaciers are an important contribution to the regional hydrology of the Upper Khovd River Basin in western Mongolia despite their relatively small area. Temporally, our analysis showed that during 2000 and 2010, glacier melt contributions were consistent but decreased in 2016. These results indicated that from 2010 to 2016 glacier accumulation zones have reduced in area and nearly disappeared, resulting in a decreasing trend in glacier melt contributions (Bury *et al* 2013).

The disappearance of Mongolia's glaciers in the mid-Holocene (Herren *et al.* 2013) was of little importance with respect to water resources and availability, since water-dependent livelihoods did not exist. Today, the decrease in annual glacier melt contributions in western Mongolia is significant because Mongolia's dominant economic drivers are water-intensive industries. In addition to the observed glacier recession, other sources of surface water have been observed to decrease as well. Recent work identified

that from the 1970s to the 2000s, lakes across Mongolia have decreased by about 18% a^{-1} (Tao *et al* 2015) and several lakes have disappeared in the western region (Szumińska 2016). Similar to the glacier recession, climate change in Mongolia is an important driver for decreasing lake area, such that the observed decrease in precipitation coupled with increasing temperatures enhances atmospheric evaporation potential (Tao *et al* 2015, Szumińska 2016, Zhang *et al* 2017). However, the dominant causative factor for decreasing lake levels across Mongolia are unsustainable land use practices including mining, livestock, and agriculture (Tao *et al.* 2015).

As Mongolia's climate becomes more arid and the glaciers and lakes of western Mongolia decrease in area – action should be taken to accommodate economic development as water availability decreases into the future. Some initiatives have already begun, namely the joint Mongolian-German projects: Integrated Water Resources Management in Central Asia, and Model Region Mongolia (MoMo). MoMo's goal is to develop sustainable management strategies in the Kharaa river basin in north central Mongolia (Priess *et al* 2011). However, in the more remote and data scarce regions of western Mongolia, very few such initiatives exist. In lieu of water management initiatives, attempts are being made to improve data richness in western Mongolia to contribute to our knowledge of relationships between glaciers, lakes, climate, and land use. Efforts have included the installation of high-elevation climate stations in the Altai Mountains, bathymetric mapping, and glacier ablation measurements (Walther *et al* 2017). These observations will provide the foundation for future research that will focus on quantifying water availability in western Mongolia under different climate scenarios and hopefully contribute to a transition towards more sustainable economic development.

6.3 Remote sensing of rain-on-snow and melt events and their role on livestock mortality

Several methods have been developed to detect rain-on-snow (ROS) and melt events from passive microwave (PM) satellite remote sensing, often drawing from either 37 GHz or both 37 and 19 GHz frequencies. The diurnal amplitude variation (DAV) is one technique that effectively teases out diurnal fluctuations of surface snowpack liquid water content (LWC) and is often a thresholding technique utilizing differences in the daytime and nighttime dielectric properties at 37 GHz frequency (Tedesco *et al* 2009,

Ramage and Isacks 2002). However, the DAV is limited in that it only utilizes one sensor frequency, whilst other methods can extrapolate more information by including multiple frequencies and polarizations to examine snow surface properties. The difference between brightness temperatures (Tb) at 19v and 37v have been used to assess global changes in surface snowpack properties including melt events and main melt onset dates (MMOD) (Wang *et al* 2008, 2016, Takala *et al* 2011). The Tb differencing approach exploits the varying sensitivities and interactions of both 19 and 37 GHz frequencies in relation to the snow pack LWC. Specifically, as LWC increases, the Tb will increase in both 19 and 37 GHz channels but to a greater magnitude at 37 GHz. Hence, if the difference between 19v and 37v GHz exceeds a threshold, a ROS or melt event can be classified. The Tb differencing approach is limited by high seasonal variability, including large variability during relatively stable (dry snow) conditions which can decrease retrieval accuracies.

In chapters 4 and 5, I employed the recently developed Gradient Ratio Polarization (GRP) algorithm to detect ROS and melt events across both Alaska and Mongolia. An Alaska regional domain was selected for ROS algorithm development and validation because of the high density of polar orbiting satellite data and a sufficient density of in situ weather observations form the region, used for ROS algorithm development and validation. In contrast, Mongolia has an extremely sparse and inconsistent weather station network. The GRP improves upon the DAV and Tb differencing approaches in that it utilizes both 19 and 37 GHz frequencies, and vertical and horizontal polarizations. The GRP algorithm was first used at single pixel locations across Canada and the Canadian Arctic Archipelago (CAA) using a thresholding technique to detect ROS events (Langlois *et al* 2017, Dolant *et al* 2016). In chapter 4, I applied the GRP algorithm across the state of Alaska to create the first gridded ROS product using the GRP (Pan *et al* 2018), drawing from similar combined satellite observational records from the Advanced Microwave Scanning Radiometers (AMSR-E/2) for water years (WY) 2003-2016. In chapter 5, I elaborated on the use of the AMSR-E/2 derived GRP to detect snow melt events at single pixel locations across Mongolia using a dynamic time-series approach.

In chapter 5, I tested seasonal snowmelt events with livestock mortality to determine if snowmelt events exert any control on annual livestock mortality. My results showed that fall melt events were significantly correlated to livestock mortality in the southern Gobi Desert, but spring melt events were significantly correlated to livestock mortality in the central and western regions of Mongolia. These results document the importance of understanding the spatio-temporal variability in seasonal snowmelt events in Mongolia because they are important contributors to annual livestock mortality. Further, the application of the GRP coupled with a time-series detection technique was effective in detecting anomalous snow melt events.

Future work can improve upon our understanding of snow melt events and livestock mortality in Mongolia with two distinct contributions. First, extending the satellite passive microwave based ROS record to earlier years by incorporating Tb retrievals from the Special Sensor Microwave Imager/Sounder (SSMI/S) on-board the Defense Meteorological Satellite Program (DMSP). The extended Tb record will allow for a longer snowmelt record that extends from 1988 to the present and facilitates more robust statistical analysis. Furthermore, the addition of qualitative interviews and surveys would also contribute to this work. Because snowmelt events are only validated using climate variables (i.e. temperature), in situ observations will provide the most concrete form of validation. Interviews and surveys will also provide a rich source of information as to how herders in Mongolia react to and are affected by snowmelt events, providing an opportunity to create well-planned hazard-mitigation strategies.

6.4 References

Batima P, Natsagdorj L, Gombluudev P, Erdenetsetseg B. 2005. *Observed Climate Change in Mongolia*. Assessments of Impacts and Adaptations to Climate Change (AIACC) Project, Working Papers, **13**, Nairobi.

Berger M, Moreno J, Johannessen J A, Levelt P F and Hanssen R F 2012 ESA's sentinel missions in support of Earth system science *Remote Sens. Environ.* **120** 84–90 Online: http://dx.doi.org/10.1016/j.rse.2011.07.023

Blomdin R, Heyman J, Stroeven A P, Haettestrand C, Harbor J M, Gribenski N, Jansson K N, Petrakov D A, Ivanov M N, Alexander O, Rudoy A N and Walther M 2016 Glacial geomorphology of the Altai and Western Sayan Mountains, Central Asia *J. Maps* **12** 123–36

Bolch T, Menounos B and Wheate R 2010 Landsat-based inventory of glaciers in western Canada , 1985 – 2005 *Remote Sens. Environ.* **114** 127–37

Bury J, Mark B G, Carey M, Young K R, McKenzie J M, Baraer M, French A and Polk M H 2013 New Geographies of Water and Climate Change in Peru: Coupled Natural and Social Transformations in the Santa River Watershed *Ann. Assoc. Am. Geogr.* **103** 363–74 Online: http://www.tandfonline.com/doi/abs/10.1080/00045608.2013.754665

Dolant C, Langlois A, Montpetit B, Brucker L, Roy A and Royer A 2016 Development of a rain-on-snow detection algorithm using passive microwave radiometry *Hydrol. Process.* **30** 3184–96 Online: http://doi.wiley.com/10.1002/hyp.10828

Gardent M, Rabatel A, Dedieu J and Deline P 2014 Multitemporal glacier inventory of the French Alps from the late 1960s to the late 2000s *Glob. Planet. Change* **120** 24–37 Online: http://dx.doi.org/10.1016/j.gloplacha.2014.05.004

Herren P A, Eichler A, Machguth H, Papina T, Tobler L, Zapf A and Schwikowski M 2013 The onset of Neoglaciation 6000 years ago in western Mongolia revealed by an ice core from the Tsambagarav mountain range *Quat. Sci. Rev.* **69** 59–68 Online: http://dx.doi.org/10.1016/j.quascirev.2013.02.025

Langlois A, Johnson C A, Montpetit B, Royer A, Blukacz-Richards E A, Neave E, Dolant C, Roy A, Arhonditsis G, Kim D K, Kaluskar S and Brucker L 2017 Detection of rain-on-snow (ROS) events and ice layer formation using passive microwave radiometry: A context for Peary caribou habitat in the Canadian Arctic *Remote Sens. Environ.* **189** 84–95 Online: http://dx.doi.org/10.1016/j.rse.2016.11.006

Lehmkuhl F, Klinge M, Rother H and Hülle D 2016 Distribution and timing of Holocene and late Pleistocene glacier fluctuations in western Mongolia *Ann. Glaciol.* **57** 1–10 Online: http://www.ingentaconnect.com/content/igsoc/agl/pre-prints/content-a71A030

Lynch C M, Barr I D, Mullan D and Ruffell A 2016 Rapid glacial retreat on the Kamchatka Peninsula during the early 21st century *Cryosphere* **10** 1809–21

Osipov E Y and Osipova O P 2014 Mountain glaciers of southeast Siberia : current state and changes since the Little Ice Age *Ann. Glaciol.* **55** 167–76

Pan C G, Kirchner P, Kimball J S, Kim Y and Du J 2018 Rain-on-snow events in Alaska, and their frequency and distribution from satellite observations *Environ. Res. Lett.*

Paul F and Mölg N 2014 Hasty retreat of glaciers in northern Patagonia from 1985 to 2011 *J. Glaciol.* **60** 1033–43

Priess J A, Schweitzer C, Wimmer F, Batkhishig O and Mimler M 2011 The consequences of land-use change and water demands in Central Mongolia *Land use policy* **28** 4–10 Online: http://dx.doi.org/10.1016/j.landusepol.2010.03.002

Ramage J M and Isacks B L 2002 Determination of melt-onset and refreeze timing on southeast Alaskan icefields using SSM/I diurnal amplitude variations *Ann. Glaciol.* **34** 391–8

Rudaya N, Tarasov P, Dorofeyuk N, Solovieva N, Kalugin I, Andreev A, Daryin A, Diekmann B, Riedel F, Tserendash N and Wagner M 2009 Holocene environments and climate in the Mongolian Altai reconstructed from the Hoton-Nur pollen and diatom records: a step towards better understanding climate dynamics in Central Asia *Quat. Sci. Rev.* **28** 540–54 Online: http://dx.doi.org/10.1016/j.quascirev.2008.10.013

Stokes C R, Shahgedanova M, Evans I S and Popovnin V V. 2013 Accelerated loss of alpine glaciers in the Kodar Mountains, south-eastern Siberia *Glob. Planet. Change* **101** 82–96 Online: http://dx.doi.org/10.1016/j.gloplacha.2012.12.010

Szumińska D 2016 Changes in surface area of the Böön Tsagaan and Orog lakes (Mongolia, Valley of the Lakes, 1974–2013) compared to climate and permafrost changes *Sediment. Geol.* **340** 62–73

Takala M, Luojus K, Pulliainen J, Derksen C, Lemmetyinen J, Kärnä J P, Koskinen J and Bojkov B 2011 Estimating northern hemisphere snow water equivalent for climate research through assimilation of space-borne radiometer data and ground-based measurements *Remote Sens. Environ.* **115** 3517–29 Online: http://dx.doi.org/10.1016/j.rse.2011.08.014

Tao S, Fang J, Zhao X, Zhao S, Shen H, Hu H, Tang Z, Wang Z and Guo Q 2015 Rapid loss of lakes on the Mongolian Plateau. *Proc. Natl. Acad. Sci. U. S. A.* **112** 2281–6 Online: http://www.pnas.org/content/112/7/2281.short

Tedesco M, Brodzik M, Armstrong R, Savoie M and Ramage J 2009 Pan arctic terrestrial snowmelt trends (1979-2008) from spaceborne passive microwave data and correlation with the Arctic Oscillation *Geophys. Res. Lett.* **36** 1–6

Viviroli D, Dürr H H, Messerli B, Meybeck M and Weingartner R 2007 Mountains of the world, water towers for humanity: Typology, mapping, and global significance *Water Resour. Res.* **43** 1–13

Walther M, Dashtseren A, Kamp U, Temujin K, Meixner F, Pan C G and Gansukh Y 2017 Glaciers , Permafrost and Lake Levels at the Tsengel Khairkhan Massif ,

Mongolian Altai , During the Late Pleistocene and Holocene *Geosciences* **7** 1–20

Wang L, Derksen C and Brown R 2008 Detection of pan-Arctic terrestrial snowmelt from QuikSCAT, 2000-2005 *Remote Sens. Environ.* **112** 3794–805

Wang L, Toose P, Brown R and Derksen C 2016 Frequency and distribution of winter melt events from passive microwave satellite data in the pan-Arctic, 1988-2013 *Cryosphere* **10** 2589–602

Wulder M A, Masek J G, Cohen W B, Loveland T R and Woodcock C E 2012 Remote Sensing of Environment Opening the archive : How free data has enabled the science and monitoring promise of Landsat *Remote Sens. Environ.* **122** 2–10 Online: http://dx.doi.org/10.1016/j.rse.2012.01.010

Zhang G, Yao T, Piao S, Bolch T, Xie H, Chen D, Gao Y, O'Reilly C M, Shum C K, Yang K, Yi S, Lei Y, Wang W, He Y, Shang K, Yang X and Zhang H 2017 Extensive and drastically different alpine lake changes on Asia's high plateaus during the past four decades *Geophys. Res. Lett.* **44** 252–60